

IN

DOE/OR/00033--T691

**ANALYSIS of STRAY RADIATION PRODUCED by
THE ADVANCED LIGHT SOURCE
(1.9 GeV Synchrotron Radiation Source)
at LAWRENCE BERKELEY LABORATORY**

by

RECEIVED

MAY 22 1997

Robert C. Ajemian

OSTI

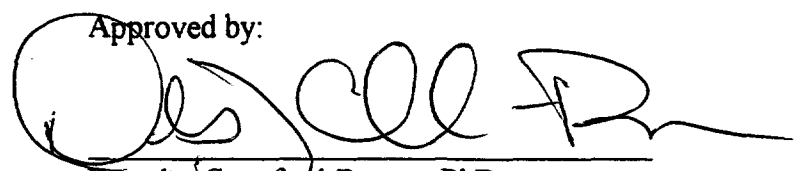
A thesis submitted to the Faculty of the University of North Carolina at Chapel Hill
in partial fulfillment of the requirements for the degree of Master of Science in Public
Health in the Department of Environmental Sciences and Engineering

Chapel Hill

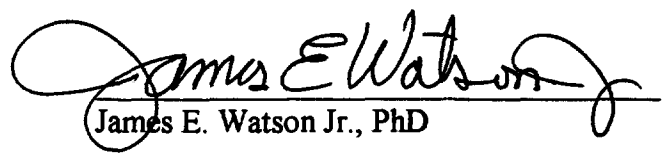
1995

MASTER

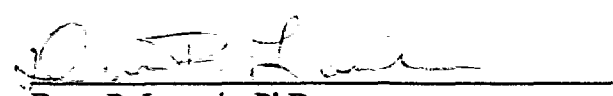
Approved by:



Douglas Crawford-Brown, PhD



James E. Watson Jr., PhD



Dana P. Loomis, PhD

DISTRIBUTION OF THIS DOCUMENT IS UNLIMITED



DISCLAIMER

Portions of this document may be illegible in electronic image products. Images are produced from the best available original document.

[Handwritten signature]
12/1/85

ROBERT C. AJEMIAN, Analysis of Stray Radiation Produced by the Advanced Light Source (1.9 GeV Synchrotron Radiation Source) at Lawrence Berkeley Laboratory

The yearly environmental dose equivalent likely to result at the closest site boundary from the Advanced Light Source was determined by generating multiple linear regressions. The independent variables comprised quantified accelerator operating parameters and measurements from synchronized, in-close (outside shielding prior to significant atmospheric scattering), state-of-the-art neutron remmeters and photon G-M tubes. Neutron regression models were more successful than photon models due to lower relative background radiation and redundant detectors at the site boundary. As expected, Storage Ring Beam Fill and Beam Crashes produced radiation at a higher rate than gradual Beam Decay; however, only the latter did not include zero in its 95% confidence interval. By summing for all three accelerator operating modes, a combined yearly DE of 4.3 mRem/yr with a 90% CI of (0.04 - 8.63) was obtained. These results fall below the DOE reporting level of 10 mRem/year and suggest repeating the study with improved experimental conditions.

DISCLAIMER

This report was prepared as an account of work sponsored by an agency of the United States Government. Neither the United States Government nor any agency thereof, nor any of their employees, makes any warranty, express or implied, or assumes any legal liability or responsibility for the accuracy, completeness, or usefulness of any information, apparatus, product, or process disclosed, or represents that its use would not infringe privately owned rights. Reference herein to any specific commercial product, process, or service by trade name, trademark, manufacturer, or otherwise does not necessarily constitute or imply its endorsement, recommendation, or favoring by the United States Government or any agency thereof. The views and opinions of authors expressed herein do not necessarily state or reflect those of the United States Government or any agency thereof.

TABLE OF CONTENTS

Title	Page
Introduction	1
Background	3
The Advanced Light Source	3
Radiation Generation	7
-Photons	8
-Neutrons	11
Dose Calculations for the ALS	12
-Radiation Shielding	13
-Skyshine	20
Radiation Field Measurement	24
Procedure	30
Instrument Calibration	30
Placement and Movement of Detectors	33
Control Room Data Mapping	37
Synchronization of Dataloggers	37
Data Processing: Spreadsheet and Regression Work	38
Results and Discussion	44
Corrections for Background (Cosmic) Radiation	44
Comparison of Detector Measurements for Accelerator Functions.....	49
Determination of Mezzanine "Hot Spots"	57
First Set of Multiple Regressions	59
Further Consolidation of Mezzanine Positions to Continuous Variables ..	64
Second Set of Multiple Regressions	67
Summary of Regression Results	77
Regression Models to Predict Yearly Mezzanine Dose Equivalents	81
Comparison of Regression Results with Previous Estimation of DE.....	84
Recommendations	86
Conclusion	89
References	91
Appendices	94
appendix i (synopsis of on-off averaging report)	94

ACKNOWLEDGMENTS

I would like to thank Mr. Henry Collins for offering me this project and supporting my drive to complete the data gathering phase in (almost) a summer, Mr. Ted De Castro for providing a wealth of assistance and knowledge pertaining to accelerator health physics and instrumentation, Dr. Hiroshi Nishimura for the customized computer code he wrote for me and numerous, other employees at the ALS who offered me everything from information to cable, all served with good amounts of patience.

I thank Milton Constantine and Mary Kinney at the DOE - ORISE, who through two and a half years of have shown me every kindness and support. The research was performed under appointment to the U.S. Department of Energy, Industrial Hygiene Graduate Fellowship Program, administered by Oak Ridge Institute for Science and Education.

Chapel Hill provided a fruitful learning environment, albeit somewhat unsupportive, for three years. I thank my committee members for their participation and suggestions. Also, I am indebted to Dr. Mike Symons who, in a show of Christian charity, guided my statistical journey, despite my lack of success in his course. Thanks to Randy Marx for logistical support (including defense shoes) and friendship for the nine month "sprint" to complete this thesis.

I thank my mother for covering my financial shortcomings, an inevitable result of an "older" student going back to school, and her unfailing love.

Most of all, I thank God, who not only strengthened me with a persevering spirit to complete this work, but also created light to begin with. Truly He is omniscient.

ANALYSIS of STRAY RADIATION PRODUCED by THE ADVANCED LIGHT SOURCE at LAWRENCE BERKELEY LABORATORY

By Robert C. Ajemian

INTRODUCTION

The measurement of stray radiation fields (those exiting protective shielding) produced by high energy particle accelerators and the evaluation of the radiation hazard posed to humans present a well-documented, historical challenge that accelerator health physicists have grappled with to varying degrees of success. Ideally, knowledge of the radiation fields produced by accelerator and time and space resolution of the energy spectrum would be available for designing shielding, detection instrumentation and personnel dosimetry programs. Generally, this type of detailed information is not available and estimates of radiation types and strengths are used. Fortunately and confidently, it can be stated that conservative radiation shielding designs have diminished any chance of harmful occupational or community exposures. One 6 GeV electron accelerator, located within 15 feet of a busy city street reported no exceedances of even 1/5 of the (then) allowable dose to the public of 100 mrem¹. Over a ten year period of personal dosimetry monitoring at Cern, the percentage of radiation workers exposed to > 5 rem/year never exceeded 0.3%, with the large majority (52-92%) receiving ≤ 0.5 rem/year². Nevertheless, precise, quantifiable knowledge of these stray radiation fields or their production as a function of accelerator operating parameters remains difficult to precisely quantify. Sophisticated mathematical modelling can predict source terms (particle yields per accelerated particle)³ and thus total stray radiation fields; however, the effective energy range of extant models do not coincide with the dramatic range of particles found at high energy accelerators (7 or 8 orders of magnitude in the case of neutrons). Thus they are subject to error. By reason of the same vast energy range, it is difficult to verify the results from these mathematical models due to the instrumentation limitations. One study, using several coincidental detector systems, did show there was relatively good agreement on the levels of radiation found outside of shielding⁴. However, this success was in large part attributed to compensating errors amongst the detector systems. Again, the hazard to humans was demonstrated to be minimal, but the precision and accuracy of characterizing the radiation field was subject to considerable uncertainty.

The intent of this report is to investigate the radiation leakage at The Advanced Light Source (ALS). The ALS is a recently completed (1993), third generation electron synchrotron accelerator located at the University of California - Lawrence Berkeley Laboratory. It accelerates electrons to near speed of light and with resulting energies of 1.9 GeV. Specifically designed to accommodate up to eleven insertion devices, it is the brightest source of far ultraviolet and soft x-rays available for research. The stray radiation produced by the ALS is comprised primarily of photons and neutrons. Extensive modelling and analytical calculations of the radiation produced were undertaken as part of the shielding design. The success and efficacy of the shielding is verified by the lack of triggering any of the twelve radiation detector alarms (set at 10 mrem/hour) located at various points around the accelerator. In addition to these alarms, personal dosimetry programs and continuous site boundary monitors are present.

This research received impetus after an attempt to generate a monthly environmental radiation report based on data from the environmental monitoring shed which is located at the LBL site boundary nearest to the ALS⁵. By averaging 24 hour periods, representing days when the accelerator was operating or not, a negative net environmental dose was calculated. This is not a logical outcome. Statistical treatment to eliminate outliers from the data "improved" the results to calculate a net yearly dose of ~0.5 mrem/year. Most of the monthly doses still included a zero dose within the 95% confidence interval (see appendix i for a synopsis of these results).

The principal objective of this work is to attempt to more accurately assess the radiation produced by the accelerator at this site boundary location. All of the radiation reaching the environmental monitors (at the site boundary) is assumed to result from "skyshine" or radiation scattered by the atmosphere. The strategy for this project was to use detectors to measure the directly emitted radiation in close to the accelerator and see if these measurements correlated with the site boundary detectors. To accomplish the above goals two additional sets of state-of-the-art neutron remmeters and large volume Geiger-Muller counters were calibrated and synchronized to within a few seconds with the site detectors and the control room data loggers. One set was placed in the cupola of the dome over the

accelerator (where normal planes to the electron beam intersect). The other was moved periodically around the periphery of the mezzanine (to measure forward scattered radiation in a 10-20 degree angle). The radiation produced at the three locations were compared for the different accelerator operating modes.

A number of questions framed the strategy for pursuing this work. By answering them, additional insight into operational health physics at the ALS was obtained. They are listed below:

- 1) Are background radiation levels, due to cosmic radiation, the same for monitoring locations in the environmental shed, the cupola of the ALS dome, and for mezzanine positions? If not, how should background corrections be performed?
- 2) How does radiation measured in the cupola compare with that on the mezzanine during different accelerator operating modes?
- 3) Are mezzanine or cupola detector values correlated with the the shed detector values for specific accelerator operation modes?
- 4) Do "hotspots" exist on the mezzanine for specific beam operation functions?
- 5) Can measurement data from cupola and/or particular mezzanine detector positions (perhaps those in line with the shed direction) be used to generate logical, well-fitting regression models that predict radiation at the shed or any mezzanine "hotspots"?
- 6) If predictive models can be generated, how do the results compare with the radiation shielding calculations (analytical method), the Morse Code Skyshine modelled results, and the original on-off monthly average technique for obtaining yearly dose equivalents?

I hope to show that both the upward directed radiation and the radiation directed towards the shed from the mezzanine are predictive of what is detected at the shed. Further, by inputing accelerator operating conditions (fill, decay, dump) and parameters (starting current, duration, rate), I hope to utilize a regression model that will predict the yearly dose equivalent expected at the site boundary. It may be possible that, with sufficient model predictive power, the need for site detectors could be eliminated.

BACKGROUND

THE ADVANCED LIGHT SOURCE

The Advanced Light Source (ALS) of the UC-DOE Lawrence Berkeley Laboratory is a "third generation" electron synchrotron accelerator designed to produce the greatest spectral flux of controlled photons in the ultraviolet to soft x-ray (few eV to a few KeV) energy range. The designation third generation is because it is the first time that an accelerator was constructed to optimally accommodate advanced magnetic field insertion devices, which in turn generate the brilliant light. The qualitative and quantitative parameters of this light will lead to scientific breakthrough in the pure scientific fields of atomic and molecular physics and molecular biology and applied science such as advanced materials and catalysis and advanced lithography for computer chip design, to name a few. The ALS was completed on time at a cost of approximately \$100 million. It was commissioned in 1992 with a break in period lasting into 1993.

DESIGN AND OPERATION

The basic layout of the ALS is shown (diagram 1a). It consists of a linear accelerator, booster ring and storage ring with insertion devices (diagram 1b). For detailed description of the physical equipment and theory of operation, the reader is referred to the Conceptual Design Report⁶. A greatly simplified description of its operation follows. Free electrons are produced from an $h\nu$ gun at the entrance to the linear accelerator (Linac) and accelerated to 50 MeV (by imparting kinetic energy) by the Linac. Upon leaving the Linac, the 50 MeV electron beam can be directed to either the booster or a "beam test facility". The electrons

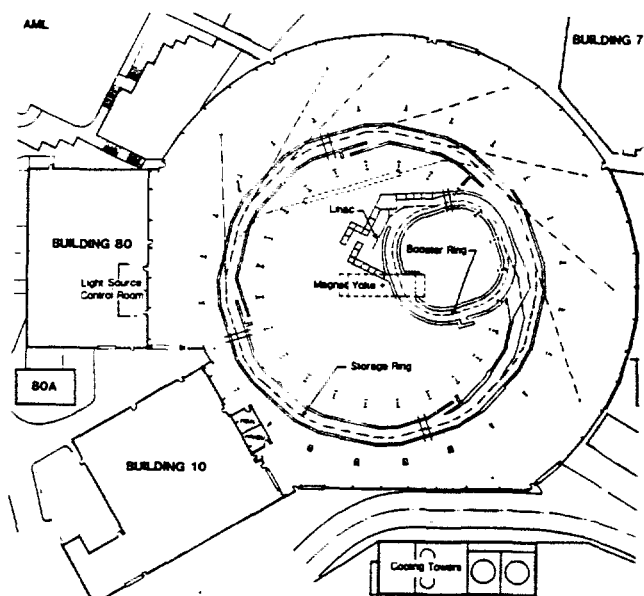


diagram 1a

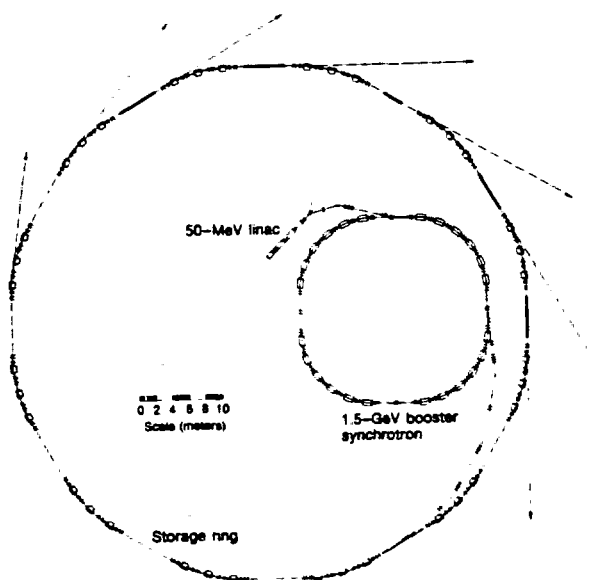


diagram 1b

are chopped into "bunches" which then enter the booster ring. In the booster, the electron bunches (following a predetermined number and fill pattern) are ramped up to 1.5 GeV with 1 Hz frequency. These energized bunches may then be directed either to the storage ring (via the BTS line) or deliberately sent to a beam dump (during experimental physics work). The bunches directed towards the storage ring pass through a series of septum magnets and are introduced into the storage ring, where the orbit of any pre-existing current has been bumped to allow a phase melding of the two electron streams. The storage ring beam electrons are monoenergetic at 1.9 GeV. Though possible to operate the storage ring according to any range of energies from 0.75 to 1.9 GeV and beam currents from 10 - 400 mA, it is usually operated at peak values. Exceptions occur when longer pulse spacing is required for time resolution spectroscopy.

The storage ring comprises 12 curved and 12 straight sections. No less than six types of sophisticated magnets are utilized to focus, steer, separate and bump the electron beam. The synchrotron radiation is bremsstrahlung produced when the electron paths are bent into circular orbit (specifically 10 degrees by each of 36 bending magnets). The energy lost in

producing this bremsstrahlung must be resupplied to the electrons, which occurs in the RF acceleration cavities immediately following one of the straight sections. In addition to the photons produced at the bending magnets (and the reason this is a third generation electron synchrotron) light is produced when the electron beam passes through insertion devices. These insertion devices (wigglers and undulators) are hybrid permanent and induced magnets that manipulate the path of the electrons to generate not only intense light of narrow spectral lines with minimal divergence, but also light that is nearly coherent. As of this writing, five of the straight sections have insertion devices (four undulators and one wiggler). Seven beam lines are operational from these five devices; up to 60 beam lines could ultimately be functional if all the bending magnets were developed. The entire beam network must be operated at high vacuum of approximately 1 nTorr. If a vacuum leak occurs the beam interacts with the fugitive molecules and crashes immediately. (This is a possible worst case scenario considered for protective shielding design.). The optimal vacuum is not, however, the lowest achievable one. This is because at too low a pressure, molecules adsorbed to the accelerator walls can desorb and interact with the beam.

The operational control of the accelerator is accomplished by a complex, multitiered system. The first level of control is approximately 600 Intelligent Local Controllers (ILCs) which interface directly to the individual device instrumentation. A global database (data pool) of all the ILC real-time databases is kept in the Collector Micro Module (CMM) which polls the ILCs using a fiber optic network. The CMM shares this global database with the display Micro Module (DMM) via a Multibus I to Multibus II bus converter. Each CPU in the DMM is connected to a Personal Computer, the majority of which are located in the Control Room⁷. Numerous beam operational parameters are monitored, both in real time and stored to data files for future analysis. Useful parameters for this work were Storage Ring DCCT (DC Current Transformer), BTS (beam-to-storage ring line) magnets 1 and 2 voltages, booster ring voltages (at beginning and end of pulse), BTF (beam test facility line) magnet voltage and hv gun voltage. Thus the status of the Linac, Booster and Storage Ring could be summarized on a minute by minute basis. Time resolution on a seconds scale was possible, but would have produced unwieldy amounts of data and required excessive cpu time.

The standard operating schedule, which did not vary during the course of this study except for the shortened week of Labor Day, was the conduction of physics experiments from accelerator startup (around 4 PM Monday afternoons) through late Tuesday evening. These experiments often featured numerous fillings of the ring, though seldom did they exceed 50 mA. Generally, by Tuesday midnight the storage ring had been filled to capacity (320 bunches- 400 mA) and was kept this way by refilling about two or three times a day. The accelerator was shut down every Friday night at 11:00 PM and remained down every weekend.

RADIATION GENERATION

Radiation produced by the electron beam at the ALS is the basis for its functioning as well as the need for protective shielding. The useful synchrotron radiation is produced by magnetic deflection of the electrons in a circular orbit; the fugitive radiation by the interaction of the electron beam with the physical structures of the accelerator. For radiation protection from the latter, the radiation field is classified as either prompt or remanent. The prompt field is a direct result of the operation of the accelerator and ceases upon terminating operation. It is the radiation that this study is concerned with. The remanent field is the result of activation of accelerator components. Due to additional shielding of known beam dumping sites and short half-life of the activated radiolnuclide, the remanent field is unlikely to contribute to the stray radiation field.

The radiation field produced by the electron beam is characterized as pulsed (due to the periodic nature of the circulating electron bunches) and mixed (comprised primarily of photons, neutrons and muons). In general, the higher the energy of the accelerated particles, the more complex the radiation field. At 1.9 GeV, a very complex field is produced, though the muon contribution to dose may be neglected because they have a very small cross section for interacting with matter). The particle fluences have broad energy spectra from thermal

to the highest energies possible (equivalent to beam energy). Due to cascade processes, primarily electromagnetic, but also hadronic (nuclear), the lower energy components dominate the prompt radiation field. The stray radiation field, however, is dominated by more energetic particles that can penetrate the shielding. To state a much used quotation⁸, "A general rule that has emerged from our studies is that fast neutrons (0.1 to 10 MeV) dominate the biological hazard of the radiation field existing near a well shielded particle accelerator by contributing more than half the total rem dose. Gamma rays and low energy neutrons contribute 10% to 20% and high-energy neutrons (>20 MeV) make up the balance". The fundamental processes for each of the types of radiation are briefly discussed below.

Photons

Energetic electrons lose energy upon interacting with matter in one of two mechanisms described as collision and radiation losses. The radiative loss process is by the production of bremsstrahlung, German for "braking radiation" and occurs as high energy electrons pass near a nucleus or other electromagnetic deflecting source. Due to their light mass, the accelerating force changes the path of the electron, producing a photon of energy equivalent to the energy loss of the electron.

The balance between these two mechanisms is a function of the energy of the electron beam. The critical energy E_c of the electron beam is defined as the initial electron energy for which the average energy loss rates due to radiation and collision are equal. The empirical formula is given as

$$E_c = 800/(z + 1.2) \quad E_c \text{ in MeV}$$

For stainless steel, z is taken for iron = 56, and $E_c = 13.4$ MeV.

Bremsstrahlung production occurs via an electromagnetic cascade or shower, which consists of high energy photons interacting with matter to form electron and positron pairs.

The electrons then generate photons via bremsstrahlung and the positron recombine with electrons to form two 0.51 MeV photons. Thus a chain reaction is propagated. The showering effect reaches its maximum at the Compton minimum, which is defined as the photon energy at which the minimum attenuation coefficient occurs in that material. Typically, the Compton minimum is $1/2$ to $1/3 E_c$ according to the reference⁹. Below this energy the probability of photon energy loss via Compton scattering becomes greater than for pair production (diagram 2) and the chain terminates. The resultant radiation field from this cascade comprises essentially all energies from thermal to the maximum allowable energy. Both empirically derived formulae and Monte Carlo calculations have been developed to predict the photon yields with good success and are available.

Photon Interactions with Matter as a Function of (Z, E)

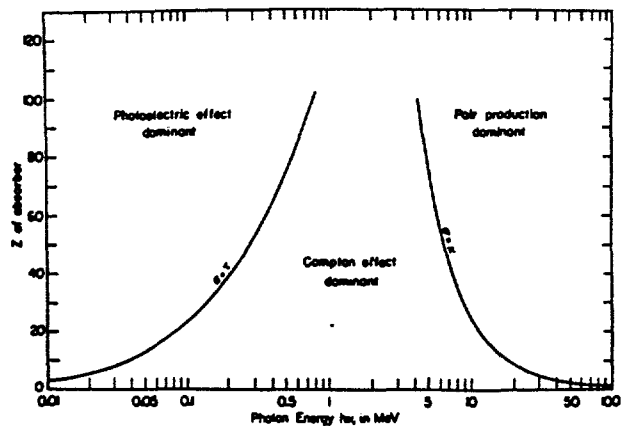


diagram 2

Bremsstrahlung production is also a function of target thickness. In diagram 3 below this effect is demonstrated for 17 MeV electrons on a gold target.¹⁰ For target thickness greater than 0.2 radiation length

Dependence of Forward Photon Intensity on Target Thickness

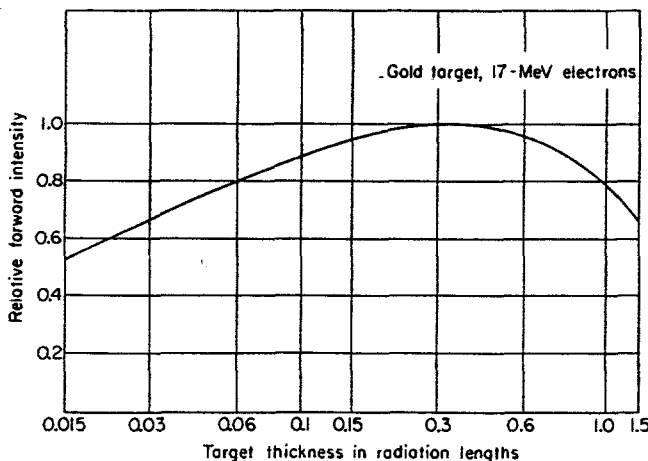


diagram 3

(defined as the thickness in a given material through which the photon energy is reduced by $1/e$ when only radiative losses are considered), so called "thick targets", the efficiency of radiation production is proportional to z and increases as electron energy goes up.

There is also angular variation in the production of bremsstrahlung. The resultant photon field for thick targets is characterized by a broad forward peak with a very sharp, forward spike containing photons of the highest energy possible. Diagram 4 shows the angular dependence of photon dose rate¹¹. A detailed study by Dinter and Tesch found that absorbed doses declined with detector angle for all configurations of target thickness and beam energies they studied¹². Swanson³ suggests rules of thumb for scaling photon doses at zero and 90 degrees. For forward directed bremsstrahlung he uses a formula scaled as a higher power of primary beam energy. 90° bremsstrahlung is scaled linearly to primary beam energy. Backscattering (angles $\geq 90^\circ$) is less than less than 5% of the forward intensity.

Dependence of Photon Dose Rate on Scattering Angle for Different Radiation Types and Target Materials

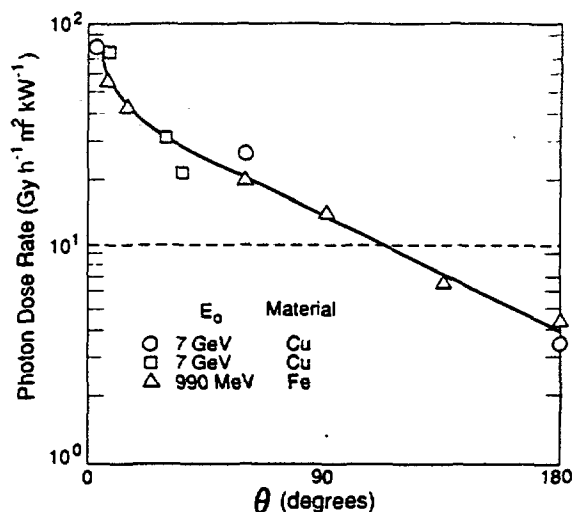


Diagram 4

An important consideration for this work is that the stray radiation is not produced by directing the beam onto a target (with the exceptions of the booster beam dump and storage ring scraper). Rather the beam interacts with the accelerator wall at a random position in an unpredictable grazing angle. Thus, the definition of scattering angle is sorely complicated. It is known that for shallow glancing angles, the largest doses of ionizing radiation are in the direction of the open face of the target. For this work, the assumption is made that all forward biased radiation (both high energy photons and neutrons) is biased in the primary beam direction. Accordingly, the detectors located on the mezzanine receive may only receive radiation from one half of the accelerator ring sectors, starting at the ring position diametrically opposed to the detector location.

NEUTRONS

The production of secondary neutrons proceeds by 3 photonuclear mechanisms which are activated with increasing primary beam energy. The three mechanisms are shown in diagram 5. All neutrons are produced as a result of photon interactions with the accelerator materials and shielding and thus are intimately associated with the electromagnetic cascade. It is important to recall that photon energies range up to the primary beam energy. High energy neutrons ($\sim > 20$ MeV) participate in the hadronic (nuclear) cascade. These two cascade processes are closely intertwined.

Neutron Formation Mechanisms Showing Cross Sections vs. Incident Photon Energies

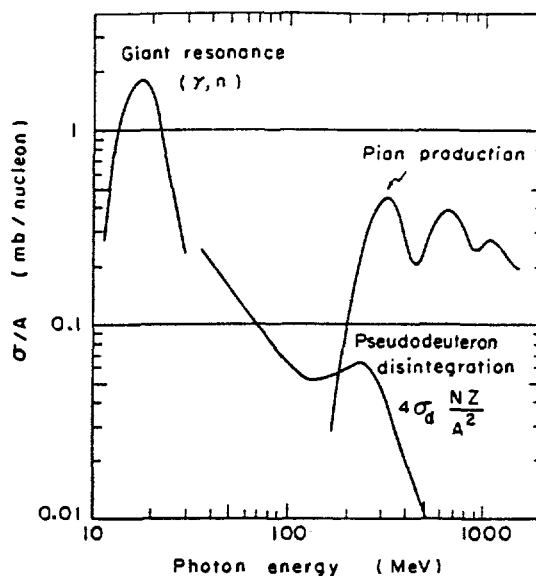


diagram 5

Giant resonance neutrons are produced with photon energies in the 10 - 30 MeV range. The energy of the electric field of the photon is transferred to the nucleus of a target atom where it creates an oscillation between the protons and neutrons. Neutrons are subsequently ejected. These giant resonance neutrons are isotropic and dominate the neutron spectra measurements (though this changes outside of protective shielding). Their energies are described by a Maxwellian distribution⁹. The equation describing this distribution is:

$$\frac{d\phi}{dE_n} = \frac{E_n}{T^2} \exp(-E_n/T)$$

which is normalized to unit fluence. For this distribution, the peak and average energies lie in the range $E_p = T \approx 0.5 - 1.5$ MeV and $E_n = 2T \approx 1 - 3$ MeV, respectively.

For photons in the energy range 20 - 100 MeV a second mechanism is present called the "quasi-deuteron" mechanism. This mechanism is so called because rather than interacting with the nucleus as a whole, the photon interacts with a neutron-proton pair. The cross section for this mechanism (probability of neutrons interacting with the target material) is about an order of magnitude below the giant resonance peak¹³. The relatively smaller cross section combined with the rapid decrease with energy in the number of neutrons produced result in a small contribution to the neutron spectrum. They are, however, more penetrating and thus likely to contribute to the neutron yield outside of the shielding.

The third mechanism is called photopion production and is comprised of a series of decreasing resonance peaks referred to as pion, dipion and tripion. These neutrons are produced by nucleon isobar formation. These peaks are only a fraction of the cross section of the giant resonance peaks, but the resultant neutrons are much more penetrating. Thus we may expect these high energy neutrons to contribute significantly to the dose outside of well shielded accelerators. In a study at DESY, it was found that high energy neutrons contribute 30-70% of the total dose, though the paper argues for disregarding neutrons with energies >40 MeV¹⁴. Detailed neutron yield calculations are provided in the literature^{15,16}.

The hadronic cascade is propagated as high energy neutrons, which are devoid of charge, undergo both inelastic and elastic scattering. Inelastic scattering plays a dominant role in neutron attenuation at energies as low as 20 MeV. Below that, elastic scattering is the only mechanism for energy reduction. The latter is dependent on the hydrogen content of the medium (via proton recoil nuclei formation). The angular distribution of photoneutrons is isotropic for energies below 50 MeV. With increasing energies, the more forward peaked is the elastic scattering. For energies greater than 150 MeV neutrons are essentially all forward scattered. One author¹⁷ has demonstrated the angular dependence on neutron production by electrons on copper in diagram 6.

Dependence of Neutron Production Rate as a Function of Incident Electron Energy and Measurement Angle

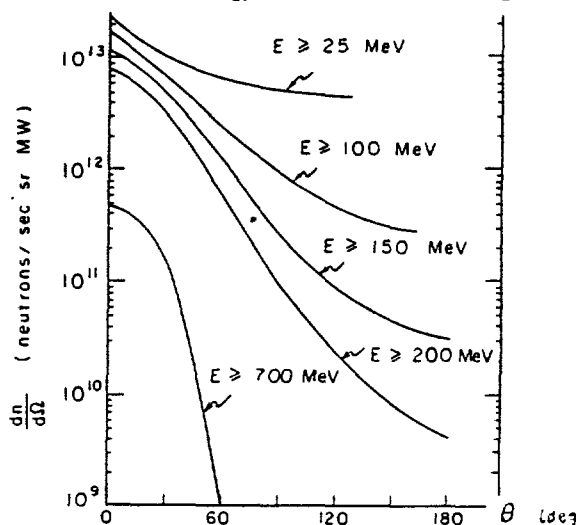


diagram 6

DOSE CALCULATIONS FOR THE ALS

Calculating dose equivalents from the ALS has been performed by two methods, namely an analytical method and a computer modelling method. Both methods utilize an energy balance approach to calculate the initial particle yield. The types and energies of particles escaping the shielding are determined and their transport through air is modelled. The difference between the two methods is that the former utilizes empirically determined photon yields, whereas the latter models the cascade processes. Results from the two methods are shown below:

LOCATION	EXPOSURE GROUP	MORSE CODE MODEL	ANALYTIC METHOD
Mezzanine	Occupational	1.56 mrem/yr. (ave.)	
Shed	Environmental	0.36 mrem/yr.	11 mrem/yr.

Since the protective shielding and skyshine phenomena are central to determining the radiation reaching the site boundary for both methods, it is appropriate to discuss both subjects in detail. The following two sections discuss these two phenomena, the equations developed to handle them and the specific parameters utilized by the health physicists to obtain the above dose equivalents.

RADIATION SHIELDING

The basic shielding approach of determining yields and energies of radiation particles and then utilizing mass range and attenuation coefficients to calculate shielding thicknesses is greatly complicated for accelerators. This is because of the incomplete understanding of particle yields, particularly in the case of high energy neutrons, and the variability in both the angle of incidence of the beam on the "target" and the time scale of beam loss (gradual or

abrupt). Nonetheless, considerable progress has been made both in empirical formulae for calculating particle yields and in Monte Carlo computer simulation codes. A detailed comparison of these two approaches with actual measured dose equivalent rates was studied at Stanford and is presented in the reference¹⁸.

Much of the theoretical work for calculating radiation fields through shielding was based on cosmic ray studies. For the earth's atmosphere, an average attenuation value of 120 g cm⁻¹ was determined. In a nuclear sense, air is quite similar to the concrete used for shielding.

The shielding specifications can be designed to address each type of radiation separately and in practice is broken down into high energy neutrons, low energy neutrons and photons. As mentioned before, these are produced by cascade processes (electromagnetic and nuclear) that are intertwined at these high energies. Typically, the radiation field before the target is dominated by bremsstrahlung and outside the shielding by neutrons.

For predicting the shielding requirements for the neutron field, Moyer working at LBL in the 1960's developed what became known as the Moyer Model for predicting the shielding requirements for the Bevatron at LBL¹⁹. In his formulation, he made several assumptions:

- 1) The neutron inelastic cross section is essentially constant above 150 MeV. He also assumed that flux of low energy neutrons to be zero for $E < 150$ MeV. This is a valid assumption due to the considerably larger cross section of these neutrons (including an absorption cross section for $E < 20$ MeV).
- 2) The neutron DE for $E > 150$ MeV was assumed constant per unit dose fluence.
- 3) A simplifying mathematical substitution for multiplying angular distribution of neutrons by a multiplicity factor to simplify the final equation form.

This model was latter generalized to a line source (such as a beam line interacting with accelerator structures). This model proved robust and showed agreement with measurements to within a factor of 2. Confirmatory shielding experiment studies were conducted at CERN(1960-63), Berkeley (1964) and Brookhaven (1965). The experimental data obtained from the CERN experiments gave an approximation for the angular distribution of neutrons for 0 - 90°. This in turn led to the "Moyer Integral" which is a function of the angular distribution coefficient and the number of mean free paths in the shield²⁰:

$$M(\beta, I) = \int_0^{\pi} \exp(-\beta\theta) \exp(-I \operatorname{cosec}\theta) d\theta$$

which is a function of the angular distribution coefficient β and the number of mean free paths in the shield I , where $I = d/\lambda$. Values of these integrals and mathematical derivations are provided in the excellent textbook referenced in the above two references. These integrals may also be used to calculate the dose equivalent rate for uniform loss at proton accelerators, an issue not of concern at the ALS.

When considering the shielding for the electromagnetic cascade both collisional and radiative losses must be considered as discussed previously under radiation production. Although the basic interactions of electrons and photons are well understood, the solution of the transport equations that describe the development of the cascade is very difficult. The longitudinal behaviour may be best represented by an attenuation length, one formula of which follows.

With this background, the radiation shielding calculations for the ALS were conducted by McCaslin²¹. Two dose equivalent rate (rem) equations were used.

For photons:

$$H_{\gamma} = 10^{-11} E_0 \left(\frac{\sin\theta}{R} \right)^2 \left[\frac{133 \exp\left(-\frac{\mu}{\rho} \frac{\rho d}{\sin\theta}\right)}{(1-0.98 \cos\theta)^{1.2}} + \frac{0.27 \exp\left(-\frac{\rho d}{\lambda_1 \sin\theta}\right)}{(1-0.72 \cos\theta)^2} \right] \text{rem cm}^2 \text{ GeV}^{-1}$$

where H_{γ} = the dose equivalent(rem) due to photons, per GeV-electron, normalized to 1 cm distance

E_0 = electron energy in GeV,

R = distance normal to the beam line to the outer shield surface (cm),

μ/ρ = $0.024 \text{ cm}^2 \text{ g}^{-1}$, mass attenuation coefficient for the Compton minimum in the target material (8 MeV for iron),

d = shield thickness at 90° to beam direction (cm),

λ_1 = 120 g/cm^2 , the attenuation length of high-energy neutrons in concrete,

ρ = density of ordinary concrete, 2.25 g/cm^3 used in these calculations, and

θ = angle with respect to beam direction.

For neutrons (accounting for the DE from G-R, mid-energy and high-energy neutrons):

$$H_n = 10^{-11} E_0 \left(\frac{\sin\theta}{R} \right)^2 \left[\frac{13.7 \exp\left(-\frac{\rho d}{\lambda_1 \sin\theta}\right)}{A^{0.65} (1-0.72 \cos\theta)^2} + \frac{10 \exp\left(-\frac{\rho d}{\lambda_2 \sin\theta}\right)}{(1-0.75 \cos\theta)} + 4.94 Z^{0.66} \exp\left(-\frac{\rho d}{\lambda_3 \sin\theta}\right) \right] \text{rem cm}^2 \text{ GeV}^{-1}$$

where λ_2 = 55 g/cm^2 for the mid-energy neutrons (1 tenth-value layer = 53 cm). and

λ_3 = 30 g/cm^2 for giant-resonance neutrons (1 tenth-value layer = 29 cm).

A, Z refer to the atomic weight and number, respectively of the target material.

In using these equations, it must be borne in mind that the angle with respect to the beam direction θ at which the dose equivalent is the maximum, θ_{\max} , is not the same for neutrons as for photons. For the purpose of calculating the dose equivalent outside of the shielding for point losses, the photon dose at θ_{\max} is added to the neutron dose equivalent at that same angle (θ for neutrons, θ_{\max} for photons).

The following table lists the values used for some of the variables in the preceding equations used by McCaslin. Where appropriate the conservative values used follow the actual working values (not known at the time of his work) in parentheses. Beam dumps and time factors are indicated.

COMPONENT	E_0	CURRENT	CIRCUM-FERENCE	BEAM DUMP	TIME FACTOR
STORAGE RING	1.9 GeV	800 mA (twice actual) = 3.3×10^{12} electrons stored(1KJ) x 125% (electrons lost uniformly during fill)	197 m	separate dump not required	estimated at two fills/ shift (non standard modes) conducted at much lower beam intensities
BOOSTER RING	1.5 GeV	pulse rate 4 Hz (conservative since normally run at 1 Hz)	75 m	well -shielded beam dump provided	for each filling cycle 1 hour at 1/4 intensity; followed by 15 min at full intensity
INJECTOR LINAC	50 MeV	8×10^{10} electrons per cycle (0.64 J / cycle)	n/a	provided and shielded	4 Hz (conservative assumption)

The actual shielding for the accelerator consists of outer and inner concrete walls for the three accelerator components, half inch iron plates lining the storage ring outer wall and a 2 x 12 inch iron bar at beam level along the storage ring outer wall.

The following table lists concrete thicknesses (standard density) used for McCaslin's calculations. When final thicknesses are different from those used in the calculation, the are included in parenthesis. MCCaslin did not consider the iron plates or bars (thus his final results will be made more conservative):

COMPONENT	OUTER WALL	INNER WALL	ROOF
Storage Ring	1.5 feet (2 ft.*)	1.5 feet (2 ft.*)	1.0 feet (1.5 ft.*)
Booster Ring	2.5 feet	2.5 feet	2.5 feet
Linac (nearest dump)	3.0 feet	3.0 feet	2.0 feet
Linac (10 ft or more from dump)	2.5 feet	2.5 feet	2.0 feet

* actual final concrete thicknesses

His final results using the empirical method resulted in dose equivalents as follows:

LOCATION	SCENARIO	PER SHIFT DOSE EQUIVALENT	PER 2000 HOUR WORKER YEAR DE
Storage Ring	Beam Crash	40 mrem*	
	Uniform Loss	0.8 mrem	200 mrem
Booster Ring	Point Loss	0.8 mrem*	
	Uniform Loss	1.6 mrem	400 mrem
Linac		40 mrem	
Mezzanine*	Uniform Loss		330 mrem
Environment#	Photons		1 mrem
	Neutrons		10 mrem

* calculated for a point determined to be a maximum based on distances from ring centers assuming

using a single scattering approximation- fence-line distance not specified

These calculated values are likely to overestimate the actual dose equivalence due to four reasons:

- 1) They fail to account for the lead lining placed throughout the outer walls of the storage ring, the two inch thick lead bar located at beam level, lead lined shielding walls and additional concrete thickness in the storage ring shielding.

- 2) They do not account for administrative restrictions on limited access during beam operation; they assume a worker is located directly outside of the shielding, except for the mezzanine and site boundary.

- 3) The conservative assumptions for operating parameters were not actually realized (storage ring at 400 mA, not 800 mA; Booster at 1 Hz, not 4 Hz)

- 4) They fail to consider the actual work schedule of only running the accelerator 3 days/ week at full current (first two days of week are for physics experiments and tuning < 100 mA).

Nevertheless, the calculations serve several useful purposes, including shielding expense reduction and estimates for DE which serve for comparison with this work. Limits for the general public were taken as 100 mrem/yr with an administrative action level at 25 mrem/yr and a shielding design goal to result in a dose < 10 mrem/year to the general public (site boundary). For occupational exposure the corresponding limits are 5 rem/yr, an administrative action level at 0.25 rem/ 2000-hr year and design goals for occupational exposure of 1 rem/ 9000-hr yr or 0.25 rem/ 2000-hr year, and. Three figures from the original paper are included to illustrate the results of the calculations. Diagrams 7 and 8 illustrate percentages and amount of energy lost per machine cycle (1 filling cycle).

Diagram Demonstrating Injection Losses as Fractions of Total Electrons Lost at Each Loss Location

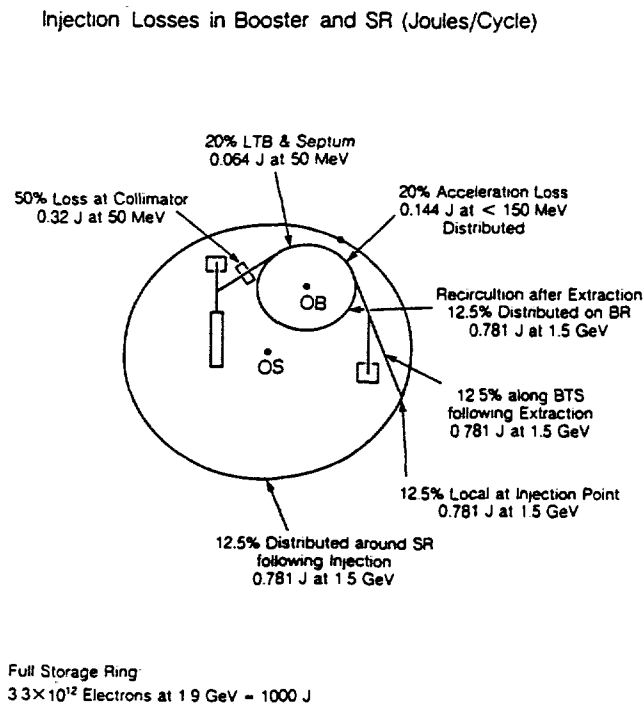


diagram 7

Diagram Demonstrating Energy Losses Based On Number and Energy of Electrons at Each Loss Location

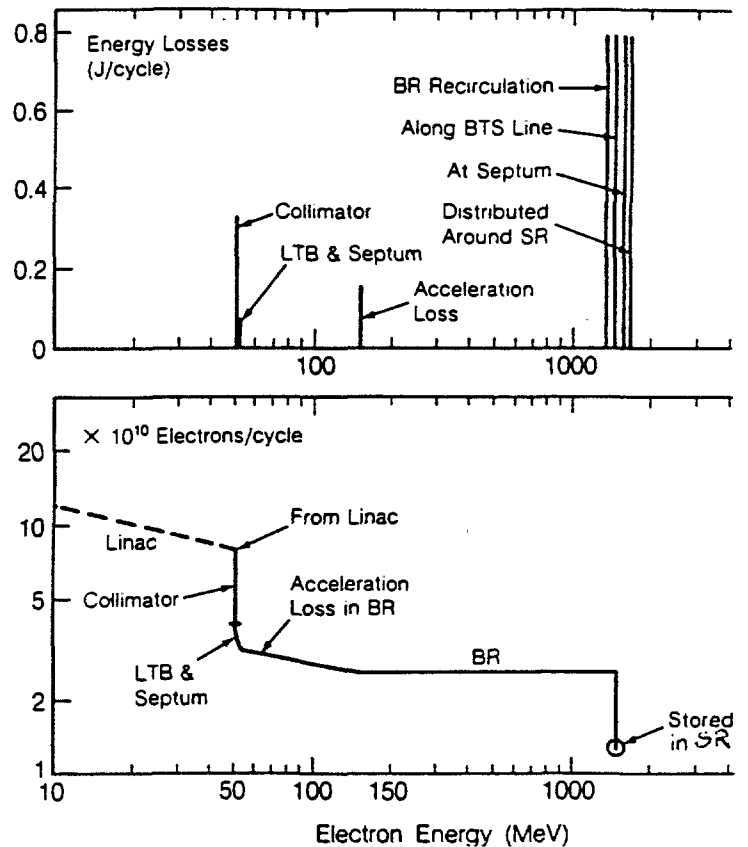


diagram 8

SKYSHINE

Skyshine is a term generally applying the radiation that reaches a point distant from an accelerator through atmospheric scattering. Neither a comprehensive theoretical treatment of the phenomena, nor ideal, precise experimental data exists for its quantification. Nevertheless, laudable attempts have been made at both and empirical formulae provide accurate estimates of skyshine to within a factor of two. Both of the estimation techniques for the ALS used equations that model this phenomena and thus it is appropriate to discuss it here.

It is known that the principal component of the radiation field penetrating appropriately shielded accelerators is due to the neutrons. Depending upon their energy spectrum, they have a characteristic mean free path length ranging from 250 up to 850 meters (one author reports 1300 meters). The mean free path is the distance a particle can travel without interacting with another molecule and is proportional to the attenuation length in the medium.

The predecessor of all theoretical treatments is the Lindenbaum²² equation, which is an expression for the neutron flux produced by a point source in an infinite isotropic scattering medium. It in turn is a variation of an equation derived by Case²³ using diffusion theory. The equation for the scalar neutron flux density $\phi(r)$ is :

$$\phi(r) = \frac{Qe^{-\Sigma_t r}}{4\pi r^2} \epsilon(c,r) + \frac{Qk(c)e^{-k_0 r}}{4\pi D r}$$

- where Q = neutron source strength (neutrons sec^{-1}),
 Σ_t = macroscopic total cross section,
 Σ_s = scattering cross section,
 D = Diffusion coefficient,
 $1/k_0$ = diffusion length
 c = Σ_s / Σ_t , the ration of the scattering to the total cross section;
 $\epsilon(c,r)$ = function of c
 $k(c)$ = function of c .

The first term is a result of direct path flux accounting for scattering out and absorption to the point in question. The second term, or skyshine component, is the scattering radiation to the point from all directions. It includes scattered radiation from the ground, but this is insignificant compared to that of the atmosphere. A key assumption in this equation derivation was that the neutron spectrum that emerged from the shielding was dominated by neutrons in a narrow energy band of 1 to 5 MeV. Since there is a significant and likely dominant contribution to the spectrum by high energy neutrons, great accuracy can not be expected from this equation. However, it has been demonstrated that Lindenbaum's equation can predict neutron flux densities within a factor of three at distances out to ~200 m. Both experimental observation and Monte Carlo analyses conducted by other scientists have confirmed the robustness of this theory²⁴.

Studies on skyshine from the Bevatron at LBL conducted by Dakin²⁵ indicated the rate of decrease in radiation was greater than an inverse square law at distances >500 meters. He suggested the following empirical formula for skyshine:

$$\phi(r) = \frac{a}{4\pi r^2} e^{-r/\lambda}$$

where a = source strength (dimensionally consistent with $r^2 \phi(r)$)
 r = distance from source
 λ = effective absorption length

In this equation the exponential term is represented as neutron attenuation in the atmosphere. A further modification to this equation to include a buildup component was used to fit experimental data obtained at Berkeley, Harwell and Saclay²⁶:

$$\phi(r) = \frac{aQ}{4\pi r^2} (1 - e^{-r/\mu}) e^{-r/\lambda}$$

where the symbols are the same as immediately above and,
 a = an empirical "buildup" factor
 μ = "buildup" relaxation length.

This equation is most correct for distances large compared with the source dimensions (not the case for this work). The selection of values for λ and Q can be a formidable endeavor. The former varies from 250 and 990 meters, depending on the neutron energy spectrum. By choosing a lower value, a greater neutron interaction cross section corresponding to a lower neutron energy range is assumed and vice versa. The higher value can be thought of as a continuation of the high energy cascade occurring in the shielding into the air, giving rise to a diffuse source of evaporation neutrons. By making the simplifying assumption that the neutron spectrum emerging from the shielding has the form of $1/E$ up to a neutron energy equal to the maximum energy (for proton accelerators, analogous to electron accelerators), Stevenson and Thomas²⁷ published the adjacent curve for calculating effective absorption length as shown in diagram 9.

Atmospheric Absorption Length vs Neutron Energy

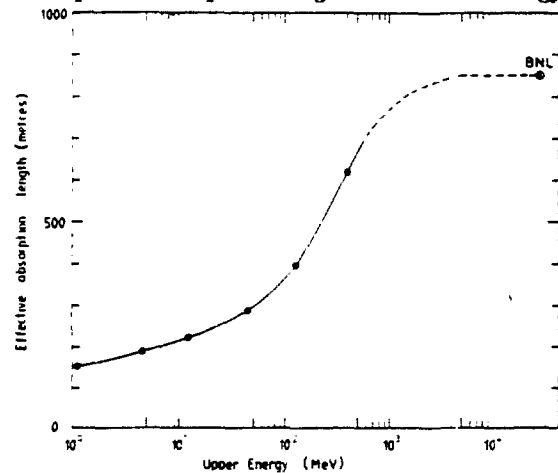


diagram 9

In perhaps the only systematic study of skyshine²⁸, a 50 MeV proton accelerator at Rutherford Lab was used. The main findings were that increasing the shielding wall height from 12 to 19 feet (in effect decreasing the subtended angle) decreased the dose rate due to skyshine by 50% and the dose rate maximum shifted from four to 16 meters. It was also found that increasing the thickness of the concrete from three to five feet, for the 12 foot high shield wall, slightly decreased the dose up to 16 meters away, then actually increased it.

Moin-Vasiri²⁹ in his graduate work, used Morse code to model the dose equivalent received at different locations from the center of the storage ring (treated as a point source) of the ALS. The modelling was performed for giant resonance neutrons. High energy neutrons and photons were not included.

His modelling parameters were:

- ▶ 45 cm lateral shielding and 30 cm roof shielding
(except for site modelling - 45 cm roof)
- ▶ continuous beam loss (corresponding to the decay period of this work)
of 312 J/hr (1.9 GeV, current 0.8 mA, cir.= 197 m, 2 fill cycles per 8 hr shift)
- the same conditions used for shielding calculations discussed earlier
- ▶ The detector locations were as follows:
 - 1) MEZZANINE -39 m from center of ring and 5 meters above ground
(good approximation)
 - 2) CUPOLA -50 m from ring center and 20 meters above ground
(fair approximation) -a better location would be 50 m from both ring
center above ground (i.e. the dome radius)
 - 3) SITE BOUNDARY(SHED) -104 m. away and 289 cm above ground
(fair approximation) - the actual detector height is 15 feet below
the ring. There is no direct line of sight to shed.

A contour map with the location and the elevation of the shed indicated is shown below:

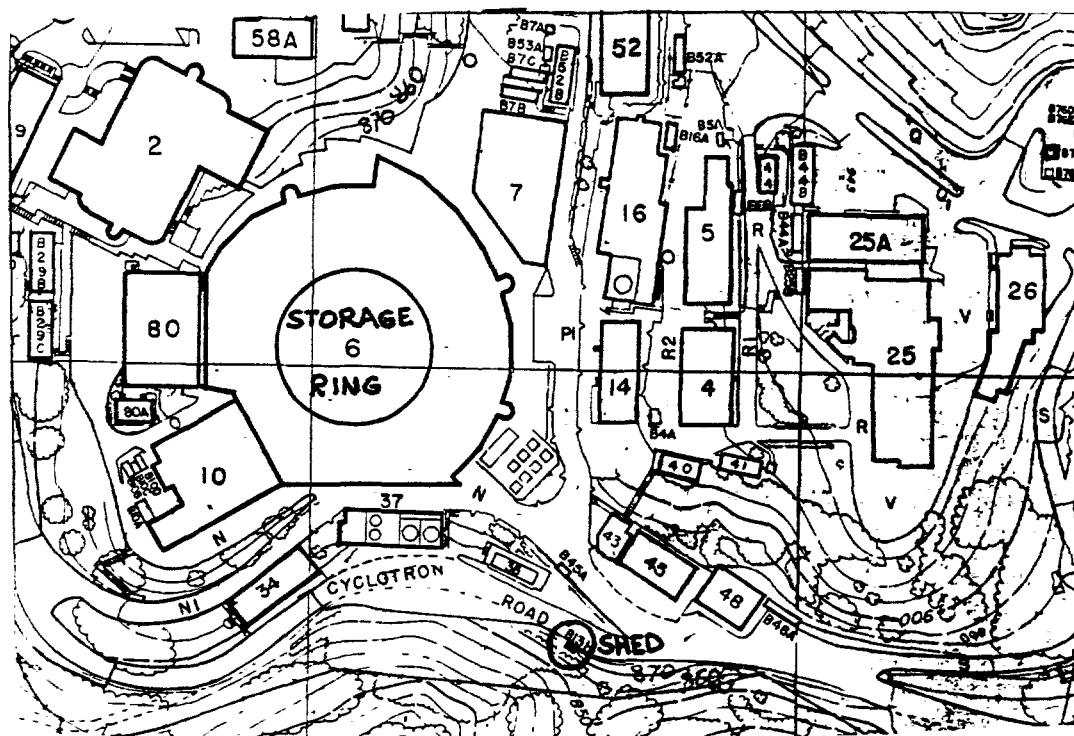


diagram 10

The approach used in this modelling technique is an energy balance. The total energy lost from a fill to 800 mA to zero current is calculated to be 1000 Joules, giving an hourly energy loss of 250 Joules. This number is multiplied by 1.25 to account for the inefficiency of filling the ring. These numbers are then plugged into neutron yield equation. The neutron yields in turn are put into a skyshine equation and dose equivalents are produced for specified "detector" locations.

Based on these assumptions, the dose equivalents were calculated as follows:

Location	Neutron DE Rate per Joule lost (mrem/J)	Neutron DE rate (mrem/hr) @ 312 J/hr	Occupational Neutron DE (mrem/2000 hr)	Environmental Neutron DE (mrem/6000hr)
mezzanine	2.5×10^{-6}	7.80×10^{-4}	1.56	
cupola	1.5×10^{-6}	4.68×10^{-4}	0.936	2.81
shed	2.0×10^{-7}	6.14×10^{-5}		0.36

These are conservative estimates since the operational current is one half the value at 400 mA and the shielding is thicker. However, these estimates do not include high energy neutrons, photons or contributions from the electron gun or booster ring.

RADIATION FIELD MEASUREMENT

The development of radiation field measurement techniques at accelerators has been hampered by a number of obstacles, both in the definition of quantities and in instrumentation. This is particularly so for neutron field measurements where a lively debate continues through this day. The great difficulty lies in the fact that apart from measuring the spatial and temporal distributions for neutrons of all energies, these neutrons have different efficacies for causing radiation damage to human tissues. Further, the damage caused is a function of type of tissue, depth in tissue and number of particles (fluence). This difficulty is compounded in accelerator environments due to the pulsed nature of the radiation, the large range of particle energies and the coincidental presence of other particles (photons and muons in our case).

There are two general approaches to evaluating the dose equivalent from accelerators. The first is to measure the neutron field and then multiply the absorbed energy over specified ranges by a "quality factor". This requires the use of a number of different type of detectors to cover the wide range of neutron energies present. This method was strongly recommended by McCaslin and Thomas³⁰. They reasoned that the high number of qualified physicists and appropriate instrumentation typically found at accelerators enable this more challenging approach. They pointed out that typically this method was not chosen (1 out of 23 accelerator facilities surveyed) and cited reasons of procedural difficulty, time requirements and lack of interest. They also described the lack of importance assigned by academic physics departments to the accurate characterization of radiation fields from high energy accelerators and state that, since the fifties, interest has diminished in accelerator health physics research. This excellent review article lists the types of instrumentation required to perform neutron spectra measurements and summarizes six projects where different instrument clusters simultaneously measured radiation fields at different accelerators. There are, however, limits on the usefulness of multidetector systems. These are due to problems associated with overlapping of instrument responses, pile-up phenomena in pulsed radiation fields, lack of sensitivity of ionization chambers, environmental sensitivity (to relative humidity and temperature) and the limited energy ranges and resolution of Bonner sphere neutron spectroscopy. Furthermore, the basis for assigning values to quality factors have changed rather dramatically over time. The uncertainty of these latter "administrative" changes has added to the difficulty in evaluating dose equivalence.

The alternative approach involves using a "remmeter" or an instrument which is constructed to respond to a flux of mixed energy neutrons with an output of units of dose equivalence. It does this by having a scaled sensitivity to neutrons of differing energies in accordance with dose equivalent conversion factors given in ICRP 51 (1987). These are a very complex set of calculations that take into account the location in a body that is irradiated and the depth at which each neutron energy has the maximum energy transfer to the tissue. In the remmeter these sensitivities are closely approximated by surrounding a thermal neutron detector with a moderating material (generally polyethylene) machined to precise dimensions.

The main advantage to using this approach is the elimination of the need to directly measure the energy spectrum. Additional advantages of using this approach are: covering the largest energy range, high sensitivity, almost insensitive to other kinds of radiation and simple operation. One author argues³¹ that this wide ranging accuracy is more than adequate given the uncertainty associated with the "administrative" quality factors. This latter approach to measuring the neutron dose equivalent was used in this study. A brief history of the development of the remmeter and specific modifications for the instrument used in this study are appropriate at this time.

The prototype of all rem responsive meters was the instrument described in a 1964 article by Andersson and Braun³². Their detector consisted of a BF_3 proportional counter surrounded by a moderator (comprised of an inner and outer polyethylene cylinders separated by a boron-doped sleeve- 200 mg /cm² of boron). Their instrument design showed good rem response for up to about 13 MeV. Noted shortcomings were a direction dependence of the detector response (maximum at normal angle to the moderating cylinder decreasing to 40% at the end), an oversensitivity to midrange neutrons (1-100 KeV), and an undersensitivity to thermal neutrons to about 1 eV. Hankins³³ performed a series of modifications to address these shortcomings. By rounding the end of the base of the cylinder and sealing the top of the instrument where the electronics package is, he greatly diminished the directional dependence of the remmeter, particularly through the southern "hemisphere" of the instrument (i.e. the lower hemisphere formed by a plane traversing the center of the remmeter and parallel to the ground.). He also increased the hole size in the boron impregnated sleeve and repositioned the BF_3 tube. These changes increased the thermal neutron sensitivity threefold to equal the sensitivity to the fast neutrons which also increased 15%.

Starting in 1990, an Italian team under the leadership of C. Birattari began to publish their findings on an attempt to increase the Andersson-Braun remmeter neutron energy range from the low teens to 400 MeV. This was an important advance, since it was known that higher energy neutrons contributed to and probably dominated the dose outside of concrete shielding. The first publication³⁴ utilized Monte Carlo calculations to demonstrate that an

internal, 1 centimeter lead collar would serve as a perfect additional moderating component to "capture" neutrons with energies up to 400 MeV. Lead was chosen because it has a medium high atomic number for which the elastic scattering processes do not affect the energy region where present rem counters already respond correctly, but at the same time inelastic processes produce enough low energy neutrons that are detected by the BF_3 counter. The group then constructed the modified detector and performed a calibration in the energy range from thermal to 19 MeV³⁵. Its response was 40 % higher at 14 MeV and 55% higher at 19 MeV, compared to the lead-free predecessor. Preliminary analyses of a calibration with roughly monoenergetic neutrons at 45, 65, 135 and 160 MeV neutrons showed good agreement with predictions of Monte Carlo calculations (a factor of 5 and 10 increase at 50 and 10 MeV respectively)³⁶. One acknowledged shortcoming of this group's work was to not consider the directional variation in sensitivity of their cylindrical shaped remmeter.

A group at Lawrence Berkeley Laboratory combined the Hankins modifications and the Italian lead collar. They utilized the 88" Cyclotron and the Bevalac at LBL to create neutron beams of energies of 40, 400 and 1050 MeV energies. They found the response of their detector compared to the A-B detector to be 1.8, 6.6 and 9.8, respectively, which were in good agreement obtained with Monte Carlo calculations³⁷.

The detectors that were used for environmental monitoring at the ALS were of this latter design. They also underwent a developmental process, primarily in the electronics design. This work was undertaken by Ted de Castro at LBL who coordinated the design's commercialization with Health Physics Instruments of Goleta, CA. The design cycles were typically of a 1 year duration. A major breakthrough came when the detectors were enabled to run at low voltages and low currents. This allowed for the use of a single coax to each detector (instead of separate ones for the voltage supply to the instrument and the measurement signal) and less impedance. It also allowed for much lighter cable and cable cost. The prototype amplifiers were incorporated into PC boards for the March 1993 set of detectors (this March 1993 set of detectors were the ones located in the environmental shed and whose values were used for this study). Over the course of development, both diurnal and seasonal trends were observed in the data from these prototype instruments. It was

determined that relative humidity effects (in the early morning and during the rainy season) were causing electrical arcing. Initially, this arcing would destroy the insulation and cause the detector to completely malfunction. With later designs, however, a self-healing process would occur which resulted in distorted data over the time during which this occurred. The final generation of detectors were commercially produced and featured an environmentally-sealed electronics package which was tested at the manufacturer in 100% humidity for 24 hours without disfunction. This final generation of detectors were the ones used for the in-close(mezzanine and cupola) measurements at the ALS. It should be noted that this last generation of neutron detectors (Model 6060 Pulse Link Extended Range Neutron Area Monitor) came with 30% Boron-doped synthetic rubber jackets (the standard being 5%). The effect of the increased boron concentration has not been investigated as of this writing; however, the calibration results for the two remmeters used for this work indicate a lower sensitivity than the previous remmeter.

Remmeters have found wide use in neutron monitoring because of their simplicity of use and large range of detection. Known shortcomings include the overresponse to midrange neutrons and incident angle response sensitivity (avoid pointing the top of the remmeter towards the source). The problems of false pulses generated by intense burst X-rays and count loss during instrument dead time need to be addressed. In general, proportional counters are 1000 times less sensitive to photons than neutrons and the lower discrimination setpoint eliminates them. Still, intense burst X-rays appear at the upper energy channels. One author investigated this phenomena and discussed solutions to this problem by either anti-coincidence counting or pulse height discrimination³⁸. The latter methods was chosen for this work and is described in the procedure section of this paper. The second problem of count loss during dead time becomes significant with increasing neutron dose rate (with the former problem diminishing provided an upper discrimination point has been set).

The same authors provide a correction formula:

$$N = \int_0^{\infty} \frac{n(t)}{1 - \tau n(t)} dt$$

where $n(t)$ is the count rate and τ is the dead time of the instrument.

This action was not required for this work due to our low count rate. A final concern in using remmeters is that they overrespond for highly collimated sources. This was not a concern for this experiment because the radiation field is comprised of a diffuse source of particles. In general, it is reasonable to anticipate errors in remmeter readings to be at least on the order of a factor of two³⁹. The photon detection system, by contrast, is relatively uncomplicated and straightforward. This is true both for the instrumentation, as well as in the consensus of accepting 1 as the quality factor for conversion to dose equivalence (although there is a faction of health physicists that argues for a scale of 1 to 3 for the QF). By accepting a QF of one there is no need to measure the photon energy spectrum for radiation protection measurements. A standard Geiger counter was used for both the shed detectors and the in-close detectors. The latter were of larger dimensions and sealed against environmental conditions.

Both the remmeter and the Geiger counters put out a pulsed signal. For this project the data were stored and then retrieved from a DL-1 Nuclear Instrumentation Module(NIM) based data logger. The DL-1 has up to four channels for recording pulsed data. The counting times are variable from 1 second to 99 hours. When the preset counting time interval is ended, the instrument stores the counts in memory and resumes another interval with no time lost in between. Using four channels set for ten minute intervals, six weeks of data can be stored. After this period, new data are written over old. Communication with the DL-1 is via RS-232 front or rear I/O connectors and may be done remotely. Access requires a programmable password. The DL-1 has an internal clock and battery, thus no data are lost in the event of power failure. Retrieved data are decoded with a conversion program. A few glitches remain in the operation including a periodic insertion of a date-time group stamp(DTG) which causes a displacement of the data in columns (an error which was manually corrected). The precise timing of initial wake-ups (switchin the data loggers on after resynchronizing their internal clocks) often will not correspond to the second setting; however, the integrity of the time interval is **almost always** maintained. Also, the instrumentation seems to be sensitive to large numbers of interrupts, which can randomly change the interval start time.

PROCEDURE

The objectives of this study require the synchronized measurement of radiation at the monitoring shed, the cupola and at evenly spaced intervals around the mezzanine. This procedure section describes the instrument calibration, detector positioning and movement, the control room data mapping (to quantify storage ring operating modes for synchronization of all data), and the complex spreadsheet and statistical programs used for the analyses.

Instrument Calibration

The final generation of detectors to be used on the mezzanine and cupola (the shed detectors were not changed for this work) arrived in June and were each put through a warm-up period of 24 hours prior to calibration. A special instrument electronics box was designed by HPI that interfaced with the neutron remmeters to allow voltage changes for the calibration procedure. All voltage settings were entered in Hexadecimal code.

The neutron remmeter required the determination of both operating high voltage and discriminator voltage setpoints. The remmeters were exposed to a calibrated source at a measured, predetermined distance of 1 m. The source was ^{244}Pu with an average neutron energy of 4.5 MeV. The source was first calibrated on 11/13/63 and updated by computer. To determine the high voltage setting, voltages were incrementally increased and the pulsed count rates, measured on a separate scaling device, were plotted against them. A computer code was devised by to allow the curve to be generated automatically with a standardized acclimation period after each voltage increment. A typical voltage curve is shown in diag 11. The actual curves for these detectors were generated on a computer and a hard copy was not available. The operating high voltage setting was selected as a point along the top of the

knee. There is a trade-off in maximizing the voltage for sensitivity (the higher the better) versus increasing the instrument susceptibility to disruptive environmental conditions (the lower the better). High voltage setting of 1440 and 1463 Volts for the two remmeters were chosen. These are listed in the top half of Table 1.

Next the discriminator voltage (the threshold voltage for the detector's electronic scalar to register a count) had to be set. Another series of points was plotted for count rates as the discriminator set point was incrementally increased, also by the computer program. The discriminator setpoint was chosen as a point soon after the bend of the knee on the relatively level part of the curve. A typical discriminator curve is shown in diagram 12. With the discriminator, a balance is achieved between sensitivity (higher voltage) and avoidance of electronic noise (lower voltage).

In addition to utilizing the curve plotting method above, a multichannel analyzer and oscilloscope (Tracor North TN-1705 Multichannel Analyzer and Tektronix 475A Oscilloscope) were provided by Mr Edson Wong to evaluate the lower and upper discrimination set points. By this method, the discriminator was set by viewing the multichannel analyzer and selecting a cutoff- voltage at the tail of the photon peak. An upper discrimination level was not set. There was a slight discrepancy between the value of the discriminator set point determined by this methods and the curve plotting method above. The multichannel analyzer was deemed more accurate and used for the final, calibrated setpoints. Setpoints were made in hexadecimal code, and due to a voltage offset phenomena for the instrumentation, could not be accurately converted to a voltage value. A ballpark conversion voltage would be 0.2 V. All of the final setpoints for the remmeters are shown in the top half of table 1. Once set, these two voltage setpoints did not change. A 3 R/hour gamma source was exposed to the detectors and no counts were recorded, verifying the excellent discrimination of the BF₃ proportional counter.

The standard output of remmeters is counts in real time. Time intervals were controlled by the dataloggers. To convert counts to mrem, conversion factors, determined from the known energy spectrum and flux rate of the calibrating source. are necessary. These are listed in table 1.

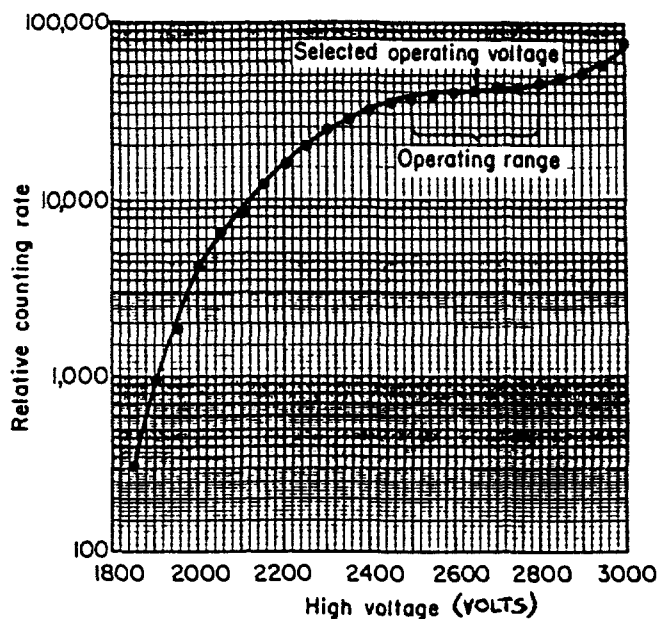


Diagram 11. Typical high voltage curve for a remmeter with a BF_3 counter.

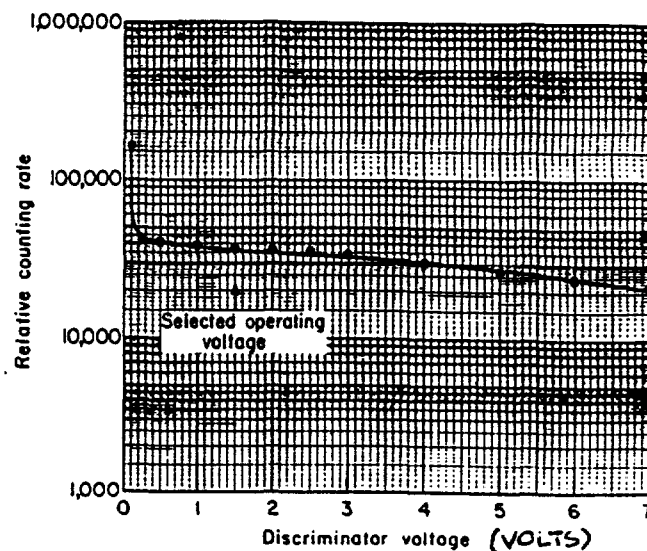


Diagram 12. Typical discriminator voltage curve for a remmeter with a BF_3 counter.

Particle	Location	Detector	High Voltage setpoint (V)	Discriminator setpoint (mV)	number of counts per 1000 sec	number of counts per hour	source strength (mRem/hr)	conversion factor (μ Rem/count)
Neutron	in-close	remmeter	1440	E*	211370	760932	84.5	0.1110
	in-close	remmeter	1463	E*	198725	715410	84.5	0.1181
	shed	remmeter						nominal 0.150

* E is in hexadecimal code, not directly convertible to a voltage value. It is equivalent to the number 15 in decimal code and represents a discrimination point that would be around 0.2 Volts of a 2 Volt span. Since there is a unknown Voltage offset on the instrumentation, it cannot be precisely known.

Particle	Location	Detector	Voltage set point	number of counts per minute for 1mrem/ hour	number of counts per minute for 0.1 mrem/hr	conversion factor (mrem/count)
Photon	in-close	G-M Tube	Factory Set	7854	1000	0.0000021148
	in-close	G-M Tube	Factory Set	7959	1004	0.0000020873
	shed	G-M Tube	Factory Set			0.000067

Table 1. Calibration of Neutron and Photon Detectors. This table shows the calibration data for the neutron remmeters and photon G-M tubes. The discriminator setpoints for the in-close remmeters were determined using a multichannel analyzer. The shed remmeter conversion factor was not available and was taken as the nominal value listed in the table. The shed remmeter had a 5% doped boron liner as opposed to 30% for the in-close. The G-M tubes were calibrated at the LBL calibrating facility. The shed detector was a smaller G-M tube, which explains the large difference from in the conversion factors.

Intense burst X-rays, such as may result from beam dump events are likely to be counted as neutrons by the remmeter, as discussed earlier in the section on radiation measurement. A correction formula was unnecessary due to the low count rate.

The photon detectors were large Geiger-Mueller tubes. Like the remmeters, time intervals were controlled by data loggers, the standard output was counts and conversion factors to mrem were necessary. Unlike the remmeters, their high voltage set points were determined and set at 450 V at the factory. They were then calibrated with a JL Shepherd & Associates Model 81 Calibrator using a ^{137}Cs 30 mCi source with a 15° bea (this device itself was last calibrated on 11/22/91). The calibration procedure consisted of exposing the detectors to the source at two different distances and taking several count readings for each position. The counts were averaged. The doses were known for these distances, so the count:dose ratio was established. Conversion factors are listed in Table 1.

Placement and Movement of Detectors

The shed and cupola detectors were stationary, whereas the mezzanine detectors were mobile. The position of each are shown in diagram 13 below. The shed is an 8 x 10 foot galvanized metal structure located approximately 8 meters below the level of the storage ring. Of this fifteen feet, the lower ten is comprised of earth. Any direct line of sight from the storage ring would have to pass through this earth; thus the assumption that all radiation measured at the shed is due to "skyshine".

Inside the shed are four detectors, designated channels 1 through 4. Channels 1 and 3 have identical, lead-lined remmeters. Channel 2 has a G-M counter and Channel 4 has an unlined remmeter. None of these detectors were sealed to the environment; however, it did not rain during the entire summer in Berkeley. Previous generations of detectors had not experienced electronic problems during seasons of low relative humidity.

The cupola had a set of new (final generation) detectors. The cupola was estimated to be 50 meters above the floor of the building. The steel girders of the accelerator roof

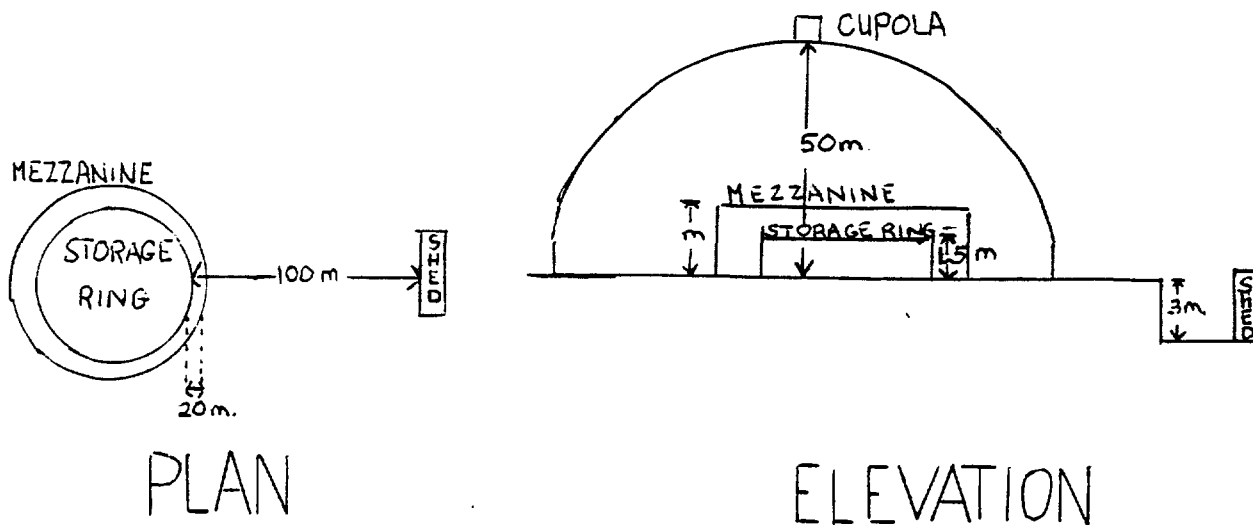


Diagram 13. Plan and Elevation Drawings to show the relative distances between detector locations.

dome converged below the cupola in a central hub. The hub was a two-tiered structure, about 12 feet in diameter with four coinciding, symmetrical two foot holes cut through the steel in both tiers. A steel mesh was placed over two opposite holes in the top tier and the detectors were centered on the holes. The remmeter was placed with the nosecone facing the accelerator floor. The G-M tube was laid on its side along the hole's diameter, exposing a maximum surface area towards the accelerator floor. The ideal location for these detectors would have been over the holes in the first tier, but this was not available for this work. The chosen location was subjected to shielding and scattering by the steel underpinnings and lower platform. Electric power was supplied by a cable running from a fan power box on the roof. A portable NIMBIN, the datalogger and 12 V power supply modules were used. The data were downloaded with a laptop computer using Procomm software.

The mezzanine had a set of detectors which were mounted on a plywood brace (for seismic safety concerns) designed to minimize scattering and shielding. The detectors were approximately 10 meters above the height of the storage ring and 20 meters radially out from it. The accompanying NIMBIN, datalogger modules and an uninterrupted power supply (UPS) were placed on a narrow cart that could be pushed to each mezzanine location. The UPS was included because extension cords for covering hundreds of feet were not available and to protect against power supply interruptions (this occurred once during the study).

Diagram 14 shows the mezzanine positions. Twenty four columns are numbered along the inner circumference of the mezzanine. Sectors, in turn, are indicated by circled numbers on the outer periphery of the figure. Each sector is centered on an odd-numbered column and includes the portion of the mezzanine located between the preceding and following even-numbered columns. It is important to understand this layout now. Later it will be necessary to combine data from several different column locations and ascribe them to a theoretical detector covering two adjacent sectors of the mezzanine.

The detectors were centered between each set of columns and the position was labelled by the lower-numbered of the two columns. Thus the detector readings coming from between columns 1 and 2 were labelled position 1. With only two exceptions, the detector were moved between 12:00 and 12:10 AM and PM (or 00:00 to 00:10 and 24:00 to 24:10, respectively). The exceptions occurred because the detectors were never moved during a storage ring fill or dump period. Generally, a detector was left in one location for 12 hours (noon to midnight) unless at least one fill had not occurred, in which case another twelve hours was included.

It is assumed that for any given mezzanine detector location, radiation originating from three sectors (two preceding its location and from the sector in which it is located) is measured. Although there are three additional, adjacent sectors (which precede these) that also generate forward - directed radiation relative to the detector's position, they are not thought to contribute to the measured radiation field. This is because a large, central, permanent magnet (remaining from the Cyclotron) is assumed to absorb the radiation from the first quarter of the ring across from the detector.

Due to a 2 foot steel track (for the crane movement), approximately the lower 2/3 of both detectors was blocked from direct line of site at every mezzanine location except one, where the detector brace was placed on top of the platform where the risers to the roof began. This platform was located above the steel track and thus there was no obstruction to the detectors (although the forward scattering angle would be slightly increased). The implication for the remaining measurements is that they underrepresent the actual radiation present at the mezzanine. However, since this "shielding" is constant, there should not be any consequence for predictive models of shed radiation..

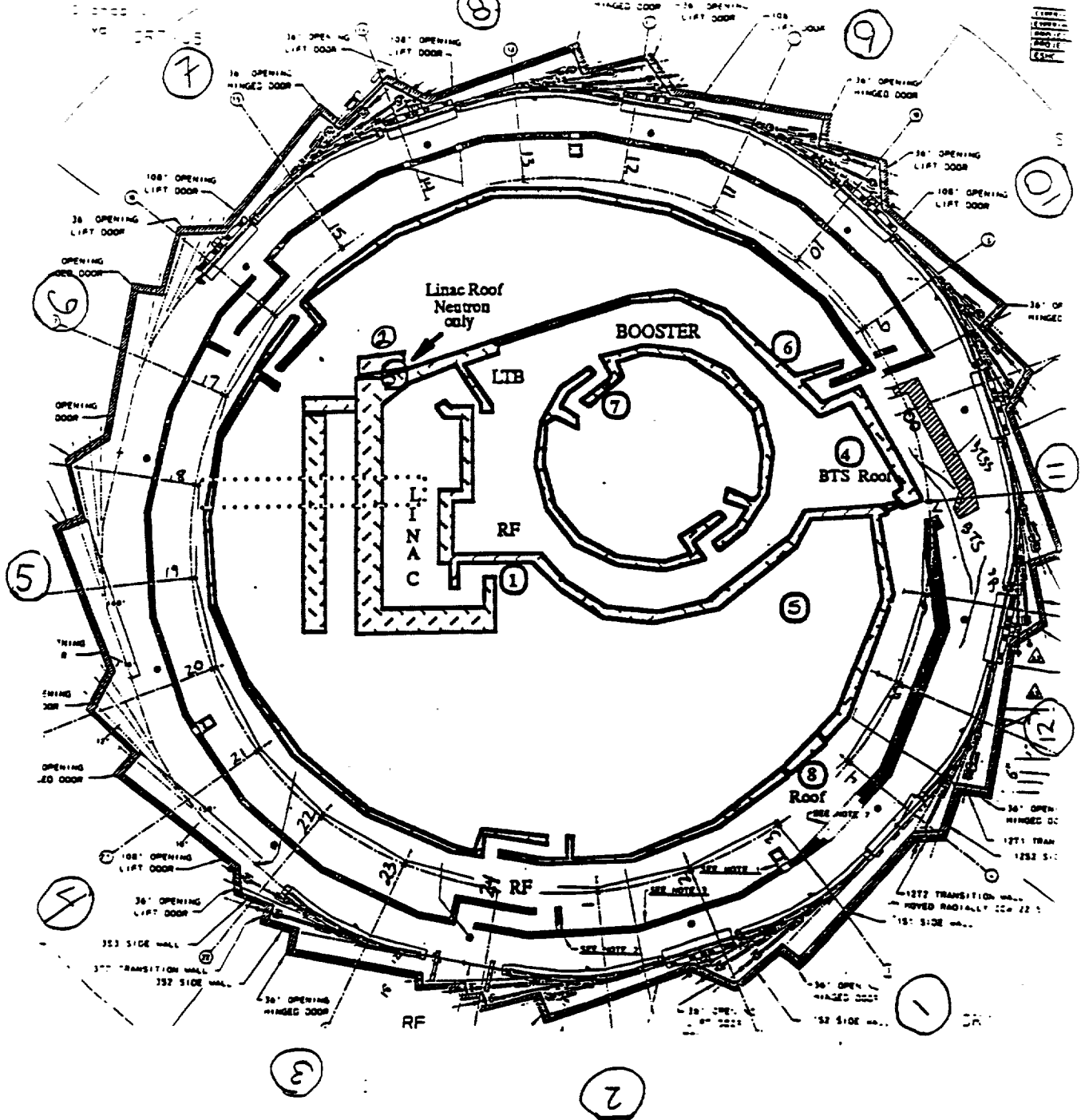


Figure 8. Layout of the mezzanine with theoretical detector locations marked by an X and labeled with an "m". Their inclusive mezzanine portions are shown with thickened bold lines. Sectors are shown with outer, circled numbers. Column numbers are labelled on the radial spokes that represent their positions. Detector measurements obtained from all positions located within the inclusive mezzanine area are ascribed to the corresponding theoretical detector.

Control Room Data Mapping

Two programs were utilized to record accelerator operation as a function of time. One program was in existence and operating at the time. The other was scripted for this study. Both programs were written by Dr. Hiroshi Nishimura. The first was a storage ring beam current datalogger which recorded and archived the storage ring DCCT (direct current current transformer) with a readout in mA. This program was scheduled to record the DCCT value every minute. The second program was designed to determine when the electron gun to the Linac (linear accelerator) was on, whether the accelerated electrons were directed to the beam test facility (BTF) or the booster ring, whether the booster ring successfully ramped the electron packets to 1.5 GeV, and finally whether the Beam to Storage Ring (BTS) steering /septum magnets were energized to allow storage ring filling (if not, the electrons went to the beam dump). This latter program was required for this study because LBL physicists were free to experiment with the Linac and booster independently from their primary function of filling the storage ring. The Linac was known to be on for the entire workweek, although without a source of electrons to accelerate, it was discounted as a source of radiation as were the Radio Frequency accelerator cavities in the storage ring.

Synchronization of All Dataloggers

The WWV international time signal put out from Hawaii and Greenwich was monitored in Mr. De Castro's laboratory. The monitor had a signal processing device that indicated when the signal (and corresponding time display) was in "high specification" status. This high spec status indicator was activated when the receiver's electronics determined that the frequency of signals were arriving at sufficiently precise frequency intervals and thus any deviation from the exact time was minimal. Upon achieving this "high spec" status, the time was transposed to the dataloggers. Daylight saving time was not used for the shed and a

correction was later made to harmonize the data. This same "high spec" time was programmed into the cupola and mezzanine datalogger, using a digital watch to transfer the time. Thus, the synchronization amongst the detectors was off by, at most, two seconds. The shed datalogger's recording interval had been previously set at ten minutes. The cupola and mezzanine were set for one minute intervals to better bracket beam operating events.

These recorded times are accurate to within one second. The dataloggers in the control room were synchronized by setting the central file server time. This was checked on a weekly basis with the high spec time. There was some uncertainty associated with this latter synchronization, although at no time was an error of greater than five seconds evident.

Data Processing: Spreadsheet and Regression Work

The goals of this study are to compare measured radiation levels at the different detector locations in real time, determine any correlations between specific operations of the accelerator and the synchronized detectors, and then to generate predictive models of radiation seen at the site boundary in terms of accelerator operating parameters and the (anticipated) larger quantities of radiation detected at the mezzanine detectors.

At the conclusion of the experimental data gathering period, several sets of raw data existed. These were continuous ten minute interval shed detector data, continuous one minute cupola and mezzanine detector data and continuous one minute accelerator operation data from the control room. Both the detector data and the control room data had to be processed with a spreadsheet program prior to its being of a useable form to proceed with this study. These steps will be described subsequently in the following paragraphs. Quattro Pro v. 5.0™ for Windows™ was the spreadsheet program used for all data manipulation and simple linear regressions. Multiple variable regressions were performed with SYSTAT™. The nature of these regressions will also be described.

Prior to any analysis, all of the raw data from the detectors were converted to ASCII alphanumeric and "cleaned-up". The "cleaning-up" of the data was necessary because of

a glitch in the datalogger software. Periodic DTG (date-time group) stamps were inserted into the lines of converted data thus disrupting the time continuity of the data. These had to be manually removed and the data columns shifted up or down one row as appropriate to make continuous data blocks available for averaging.

To compare background radiation levels at the different detector locations, the detector intervals were combined into corresponding one hour blocks, covering periods when the accelerator was not operating (weekends). The results of this comparison showed that background radiation measurements varied with time and detector location. Thus each detector reading for each accelerator operating functions had to be individually corrected for background. A set of procedural rules for accomplishing this is described later in this section.

It was necessary to delineate the accelerator operation both in terms of time and quantitative operating parameters. Initially, this was only done for the storage ring. The data to delineate and quantify the storage ring operation was located in the DCCT program running on the file server in the control room. This program recorded one minute storage beam current in milliamperes.

The DCCT data were imported into a spreadsheet template that calculated, in addition to the time and current columns, a ΔmA (change in storage ring current from the previous minute) column. Based on the value of the current and the change in current (ΔmA), the storage ring operation could be classified as Fill, Decay (steady beam loss - close to exponential decay), Dump (rapid beam loss in < 1 minute), or Off. These time intervals could then be arranged chronologically to account for the complete day's operating status. Since the DCCT values were only recorded on the minute, the precise second of changing from one mode to another was not recorded. For the purposes of this experiment, that is not so important, as long as the intervals for the detectors coincide with the intervals for the control room to within a few seconds (which they do or they are not used for the analysis).

Another spreadsheet program was designed to determine the H ν Gun and Booster Ring On periods. This was required since both of these components could be operated and thus produced radiation independently of the storage ring operation. This spreadsheet program, which tracks the $h\nu$ gun, linac and booster ring activity, is more complex than the

storage ring program in that it is monitoring more than one component of the accelerator (from the electron gun through the booster). However, it is simpler in that only a qualitative characterization (on-off and where the electrons are directed) was required. Further, all three accelerator components are on during storage ring Fill cycles.

The electron gun status was determined by an increase in *hν* Gun voltage (from the off value of approximately 0.0 volts). The booster ring current can not be evaluated with a DCCT program like the storage ring because it is pulsed at 1 Hz intervals. However, it is possible to compare the height of the beginning of the pulse to the height of the tail and determine whether the electrons are being successfully ramped to 1.5 GeV. The remainder of the qualitative picture is completed by determining which steering magnets are on from their voltage readings (if they are Off, the ramped electrons are directed to the beam dump). For September 15, the booster ring was not operated independently of the storage ring and the *hν* Gun were operated for two minutes before and after the Fills of the storage ring.

The daily summaries from these two programs were combined and encoded into a master spreadsheet of accelerator operation. The *hν* Gun and Booster Ring were coded as either on (0) or off (1). The storage ring operating modes were encoded as (1)Fill, (2)Decay, (3)Dump, and (4)Off. Each functional period was coded for starting amperage (START), rate of operation (RATE), and duration time (TIME). Off periods only had a duration time and were only used for background calculations. The RATE was calculated by subtracting the final beam amperage from the initial and dividing by the TIME. This introduced an error for the Decay RATE parameter because it is not a linear decay process. As the decay process proceeds, the shape of the storage ring beam current plot transforms from an exponential decay function to a more linear one. To simplify an already complicated procedure, the linear value was used.

Having thus obtained a daily chronological map of the status of all radiation generating functions of the accelerator, it now remained to manually sum detector measurement values for each period. All accelerator operations were resolved on a one minute time scale. Since the recorded detector measurement values were logged on the minute, on occasion, a judgement had to be made concerning which one minute intervals to

sum the counts for. For the Decay and Off periods, this was not a problem. Decay periods always began immediately after a Fill and Off periods always immediately after a Dump. For the Fill cycles, the beginning and end were indicated by an abrupt change in the rate of counts and the interspaced intervals were summed. Dump cycles are known to occur on a time scale of seconds and therefore are represented by one time interval. On the few occasions where the spreadsheet indicated that it happened over a two minute period (right on the border between two time intervals), the neutron and photon counts were summed, two appropriate background counts subtracted and this difference recorded as a one minute value.

After compiling these tables, it now remained to correct the values for background. For each operational cycles, the background values were calculated with the following rules:

- ▶ Only completely Off (no electron gun or booster could be on) values were used.
- ▶ If only 1 Off value were available for that day, either before or after the cycle:
 - it was taken as the background period, and divided by the time to produce a background rate
- ▶ If more than one Off value for that day when the cycle occurred:
 - beam cycles sandwiched between Off values; used an average of the two for background
 - beam cycles before the first or after the last Off value; used those respective, single values
- ▶ If no Off values were available for that day:
 - the first Off values preceding and following that day were averaged for the background.

This procedure worked without a problem for the mezzanine and cupola locations.

The shed data presented a problem because it was recorded on ten minute intervals. A lot of the storage ring operation cycles overlapped these ten minute intervals. Off periods were strictly chosen that excluded all other accelerator components (Gun and Booster) On periods. Fill times were taken by bounding the actual fill time to the nearest ten minutes. Dumps were taken as one ten minute interval (except once, when it overlapped two ten minute intervals). Decay intervals were taken that had no overlap with other functions. A

minute intervals). Decay intervals were taken that had no overlap with other functions. A fair number of beam events were excluded because of these strict rules; however, the independence of beam events was a critical assumption for the multiple regression models subsequently used.

Both linear and multiple regressions were used for the analyses in this study. Simple linear regressions were utilized for conducting comparisons between two variables, whether for the same particles at different detector locations or different particles at the same location. These were for background (natural) radiation levels, and individual storage ring operating modes (Fill, Decay, Dump). The latter set was used for investigating skyshine phenomena and determining mezzanine "hot spots" (locations on the mezzanine that receive greater quantities of radiation) during specific storage ring operating modes.

Having completed these preliminary regressions, it now remained to determine if the radiation measured at the shed could be predicted with a multiple regression model utilizing in-close (cupola and mezzanine) detector measurements. It was decided to treat each of the accelerator functions independently, thus generating three separate regression models (Fill, Decay, Dump) rather than one, all-encompassing multivariate regression. Three series of multiple regressions were performed. The first series of regressions were to determine which mezzanine detector positions to use in the regression. For each accelerator functional period, the Mezzanine position (column numbers 1 to 24) was treated as a categorical variable and encoded into the data file. This was done by using 23 independent mezzanine position variables and using a 0 or 1 to indicate the location of the detector for that measurement. The multiple regression was run for corrected shed detector measurements on the left hand side of the equation and the storage ring operating parameters and mezzanine positions on the right. Each detector channel was run separately. The initial results showed that an insufficient number of mezzanine position data points existed to generate the multiple regressions. To remedy this the mezzanine column positions were combined into sectors (two columns to a sector) and the regressions repeated. This proved successful for generating mezzanine sector and cupola regression coefficients.

The next, second series of regressions were run with the appropriate detectors (as

measured at these positions). Again, upon initially using the combined sector-position measurement values, the regression program indicated that there were an insufficient number of data points. Accordingly, another consolidation of mezzanine detector locations was required. This process is detailed in the discussion section, where the results from the first regression are listed and clarify the consolidation scheme. The end result of the consolidation was four theoretical detectors to which were ascribed actual measurements from the nearest, adjacent sectors adjacent to these theoretical detector locations. This consolidation was successful in producing one location that had enough data points to be useful as a continuous variable. With the inclusion of this mezzanine measurement variable and cupola detector measurements, good-fitting multiple regression models were generated for each storage ring operating mode.

The multiple regression process was repeated with the theoretical detector measurement values uncorrected for background radiation. The benefit of a generating successful regression models with this data would a tremendous savings of time from not having to correct the data for background.

These theoretical detector data sets were also used to construct predictive models for occupational dose equivalents likely to be received on the mezzanine.

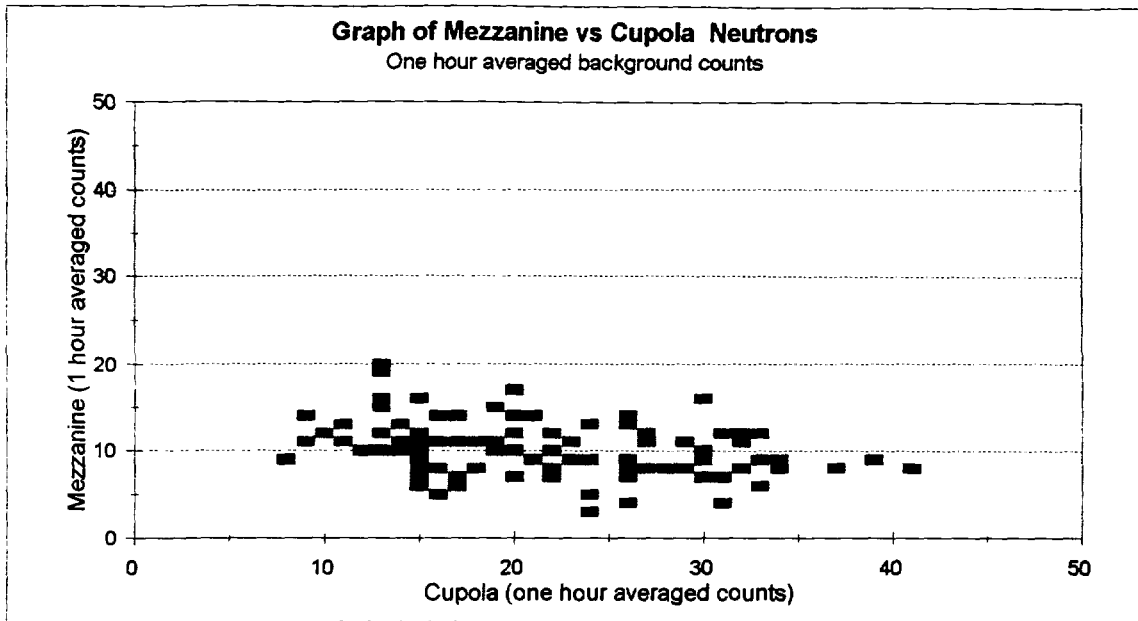
Finally, comparisons were made between the results of the predictive regression models obtained in this work to both the analytical method and Morse Code Modelling predictive methods discussed in the Background section.

RESULTS AND DISCUSSION

Corrections for Background (Natural) Radiation

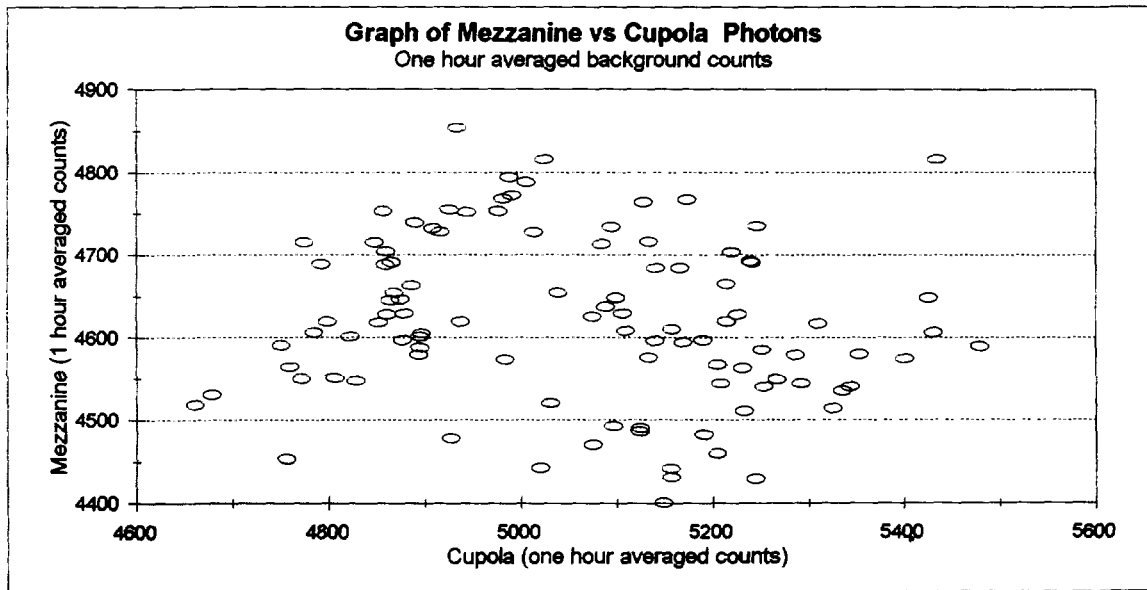
A comparison of background radiation (due to cosmic radiation) at the three detector locations was conducted. Data for all three sets of detectors collected on the weekends (accelerator completely shut down) were averaged over one hour periods. Figure 1 compares these hourly averages on the mezzanine to the cupola for neutrons and photons, respectively. Linear regression coefficients and R squared values are shown under each graph. From these graphs and coefficients it is seen that no correlation exists between the background radiation in the cupola and on the mezzanine. Similarly, Figure 2 shows no correlation between the cupola detectors and the shed detectors. There is, however, an order to the intensity of background radiation simultaneously measured at the three locations, namely Cupola > Shed > Mezzanine. The explanation is that the mezzanine is well shielded by the accelerator roof and walls. The cupola is approximately 300 feet higher in altitude than the shed which is approximately one half of the low energy neutron mean free path in air. The shed is also in the shadow of large cooling towers. This variation in background complicates the next phase of the work because detector values corresponding to each accelerator function had to be individually corrected for background.

Table 3 lists approximately one fifth of the data values that were corrected for background radiation and used in this report. In it, each row represents one of the storage ring operating modes. Fill, Decay and Dump cycles were corrected for background using the appropriate Off period(s) count rate, which are indicated by the shaded rows, according to the rules listed in the data processing section. Though not shown in this spreadsheet, the actual days were superimposed upon these sequential operational periods to comply with these background correction rules.



NEUTRONS - Mezzanine vs. Cupola Regression Output hourly averages - off

Constant	13.6783424	No. of Observations	55	X Coefficient(s)	-0.1177
Std Err of Y Est	3.06227617	Degrees of Freedom	53	Std Err of Coef.	0.0594
R Squared	0.06882697				



PHOTONS - Mezzanine vs. Cupola Regression Output hourly averages - off

Constant	4345.0941	No. of Observations	55	X Coefficient(s)	0.0676
Std Err of Y Est	76.1573498	Degrees of Freedom	53	Std Err of Coef.	0.0656
R Squared	0.01965427				

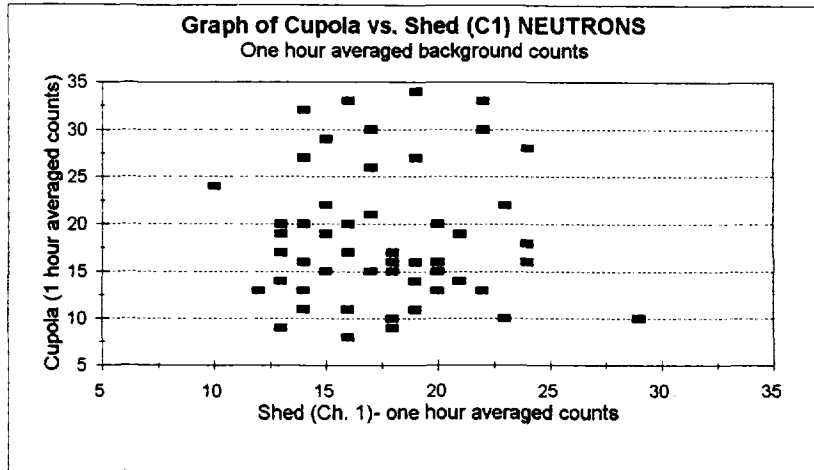
Figure 1. Comparison of hourly background radiation values - Cupola vs. Mezzanine

REGRESSIONS

Cupola vs Shed (C-1) Neutrons
OFF one hour average counts

Regression Output:

Constant	17.9296991
Std Err of Y Est	3.81710209
R Squared	0.00098009
No. of Observations	55
Degrees of Freedom	53
X Coefficient(s)	-0.0168969
Std Err of Coef.	0.07410065



Cupola vs Shed (C-3) Neutrons
OFF one hour average counts

Regression Output:

Constant	15.3886696
Std Err of Y Est	3.4293124
R Squared	0.01133601
No. of Observations	55
Degrees of Freedom	53
X Coefficient(s)	0.05189662
Std Err of Coef.	0.06657256

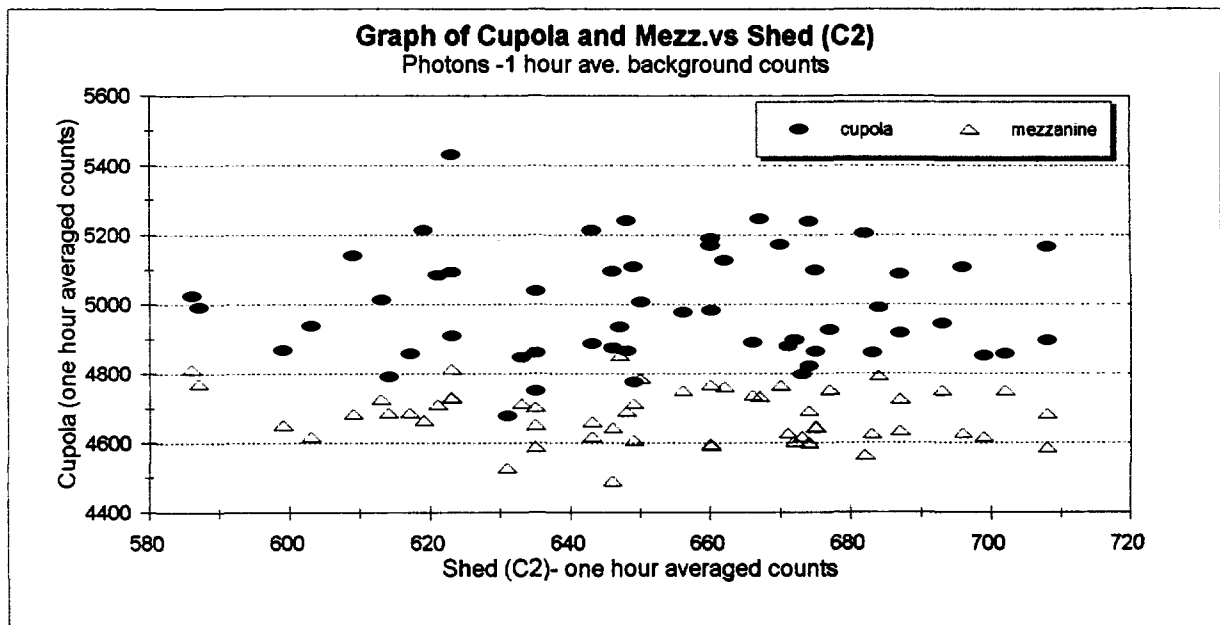
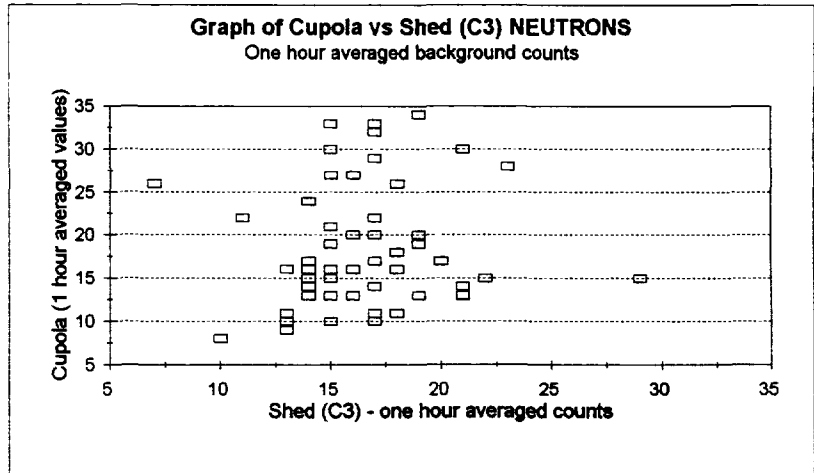


Figure 2. Comparison of hourly, background radiation measurements - Cupola vs. Shed
Two top graphs and corresponding regressions are for the shed neutrons.
Lower graph is for background photons for all three detector locations.

BACKGROUND CORRECTION SPREADSHEET

C1-neutrons			C3-neutrons			C2 -photons			CUPOLA				MEZZANINE				ACCELERATOR STATI			OPERATIONAL PARAMETERS			
raw	time	corrected	raw	time	corrected	raw	time	corrected	neutrons		photons		neutrons		photons		hV	Booster	Storage	Starting	Rate(R)	Time(T)	R x T
counts	(min.)	counts	counts	(min.)	counts	counts	(min.)	counts	raw	corr.	raw	corr.	raw	corr.	raw	corr.	Gun	Ring	Ring	Amperage		Duration	
																	0-Off	1-On		mA	mA/min	min	mA
123	390	-37.65	96	390	-46.21	4128	390	215.65	103	83.7	37349	-998.4	82	4.6	34823	209.7	0	0	Decay	230	-0.1326	445	-59
5	10	1.00	6	10	2.50	106	10	5.00	4	4.0	100	13.8	5	4.8	457	379.2	0	0	Dump	188	-188.2	1	-188
6	20	0.40	7	20	0.4	252	20	10.1	1	0.0	1962	86.2	4	0.2	1789	77.8	0	0	Off	0		23	0
									1	0.9	176	3.7	1	0.7	171	15.4	1	0	Off	0		2	0
12	20	3.80	7	20	0.00	228	20	24.70	85	84.2	2603	965.7	174	170.7	3618	2140.1	1	1	Fill	0	21.07	19	400
									1	0.9	192	19.7	1	0.7	158	2.4	1	0	Decay	400	-0.22	2	-0.44
66	220	-22.30	58	220	-19.26	2406	220	186.51	54	44.3	19204	-12.8	55	16.2	17410	64.5	0	0	Decay	400	-0.22	223	-49.1
114	430	-15.24	137	430	19.06	4630	430	291.67	85	11.2	37415	-12.2	60	-3.7	38348	4682.2	0	0	Decay	350	-0.22	437	-96.1
									0	-0.7	329	-13.6	0	-0.6	302	-6.2	1	0	Decay	265	-0.22	4	-0.88
									2	-0.7	1429	58.7	3	0.7	1305	72.4	1	2	Decay	265	-0.22	16	-3.52
									31	6.2	13249	659.1	27	5.6	11897	572.4	0	0	Decay	260	-0.22	147	-32.3
									0	-0.5	297	40.1	0	-0.4	257	25.9	1	0	Decay	225	-0.22	3	-0.66
7	20	0.85	12	20	5.53	228	20	22.10	88	85.1	2219	763.0	55	52.5	2498	1188.3	1	1	Fill	225	10.47	17	178
36	100	5.70	30	100	2.38	1098	100	83.60	29	13.0	8527	390.7	15	1.2	7512	193.4	0	0	Decay	400	-0.31	95	-29.5
178	680	42.00	206	680	70.00	7405	680	537.00	161	-39.0	59444	1564.0	149	69.0	60622	8742.0	0	0	Decay	375	-0.21	680	-143
3	10	1.00	4	10	2.00	103	10	2.00	7	6.7	100	14.9	4	3.9	99	22.7	0	0	Dump	225	-226	1	-226
2	10	0.20	2	10	0.2	161	10	10.1	5	0.3	1447	65.1	2	0.1	1297	75.1	0	0	Off	0		17	0
									1	0.4	211	40.8	3	2.5	155	4.9	1	0	Off	0		2	0
									4	3.4	211	40.8	3	2.5	218	67.9	1	2	Off	0		2	0
8	10	9.00	4	10	3.00	109	10	12.00	75	70.6	2038	761.2	83	79.6	3588	2462.0	1	1	Fill	0	16.59	15	249
									15	14.7	158	70.3					1	2	Dump	250	-250	1	-250
8	10	17.60	6	10	12.80	109	10	1.60	139	130.3	4541	1733.1	206	195.3	7543	5180.3	1	1	Fill	0	12.49	32	400
									38	-3.9	14139	626.1	45	-6.3	19533	8162.7	0	0	Decay	400	-0.24	154	-37
183	600	24.70	171	600	38.16	6644	600	100.28	124	-25.7	47384	14232.8	0	0			0	0	Decay	260	-0.24	449	-108
0	10	-2.50	5	10	3.00	94	10	-14.50	23	22.7	290	216.2	0	0			0	0	Dump	250	-250	1	-250
									2	0.3	143	73.8	0	0			0	0	Off	0		6	0
									0	-0.7	152	4.3	1	0			1	0	Off	0		2	0
									6	5.7	231	157.2	1	1			1	1	Fill	0	20.28	1	20.3
15	30	4.40	17	30	8.07	302	30	-33.73	107	101.5	2912	923.8	135	129.5	3365	1599.5	1	1	Fill	25	16.08	22	354
4	20	-3.00	5	20	1.50	112	20	-180.00	7	-0.5	2506	-205.3	5	-2.5	2371	-36.5			Decay	400	-0.054	30	-1.62
7	10	4.00	4	10	2.00	109	10	-7.00	12	11.8	139	48.6	3	2.8	98	17.8			Dump	384	-384	1	-384
									2	0.3	723	90.4	2	0.3	642	80.3			Off	0		8	0
1	10	-3.80	5	10	5.70	107	10	-17.10	94	85.3	2523	861.7	130	119.7	3112	1542.1	1	1	Fill	0	21.11	19	401
106	410	-17.54	127	410	46.43	4353	410	-415.78	110	-83.9	35017	-1969.1	163	-66.1	33977	-973.4			Decay	400	-0.37	423	-157

Table 3. This table shows approximately one fifth of the total number of sequential storage ring operating cycles used in this study. Each row represents one beam cycle. The detector measurement values in raw counts for the cycle is listed for each detector location. The referenced Off periods are shaded. The appropriate Off period radiation rate is multiplied by the time duration of the measurement period (shed detector time periods may differ from cupola and mezzanine time periods, due to the different time measurement intervals used) and subtracted from the raw counts. 24 hour periods were superimposed on this table to determine which Off reference period to use.

To illustrate, the first five rows from the top are discussed. The five operating cycles represented by these rows all occurred on August 24th. The first row represents a decay period of 390 minutes. For Channel 1 (shed) neutrons, the nearest background radiation rate was 0.4 neutrons/min as seen from row 3 under the corrected counts column. The time (390) is multiplied by the background rate and this product is subtracted from the total counts to yield the total, corrected counts for this decay period to yield (negative) -37.65 neutrons. The resulting, negative yield of neutrons in row 1 for this decay cycle is not logical. This problem results from the low radiation produced by the storage ring for this decay cycle with respect to the unmeasurable and instantaneous variation in natural radiation reaching the detector at the same time. When the rate of net radiation production is considered (divide by the total time of the decay period) the significance of this result to the mean production rate is diminished. However, the negative result for this decay cycle and others were to have impact on the final model confidence interval including a negative value.

The additional neutron and photon table entries for the Cupola and Mezzanine are derived in a similar fashion. However, separate columns for Time are not listed for each of them because their measurements all cover the time periods indicated in the Time Duration column (the second column in from the right end of the table).

Row 2 is a Dump event that occurs over a second or two. Since the time scale of the shed is on a ten minute basis, ten minutes is multiplied by the same (chronologically nearest) Off background rate and this product is subtracted from the total counts to yield one net neutron due to the dump. Row 3 is the referenced Off period. Row 4 is a storage ring Off period, but was not used because the booster spreadsheet program found that the $h\nu$ gun was operational during this period. Row 5 is a Fill cycle and the net neutron and photon production is calculated in the same way as for the Decay period.

In subsequent rows of the table, no entries appear under different columns. This is because data was not recorded for these detectors. If appropriate Off background correction values were not available (as often was the case for the shed, which was restricted to measurement intervals of 10 minutes), the next closest off values were used in accordance with the rules listed in the procedure section. This correction process was completed for all of the useful data and included over 225 separate accelerator operations.

Comparison of Corrected Detector Measurements for Specific Accelerator Functions

After correcting all of the detector measurement values for background radiation, the data were configured into three spreadsheets corresponding to each of the three storage ring operation modes, which are comprised of Fill, Decay, and Dump cycles. The purpose for this was to compare radiation measurements for the same cycles at the three detector locations, compare neutron versus photon production for each of the three detector locations and look at radiation production as a function of the RATE parameter, one of three storage ring operational parameters. The Fill cycles generated the most radiation at all of the detector locations and yielded the fewest negative net count rates. Thus the Fill data set is the best for intercomparisons between detector locations and offers the most insight into radiation skyshine phenomena.

The Fill data is shown in Table 4 and is described in detail. Similar data were compiled for the Decay and Dump cycles. Each row represents an independent Fill cycle. The detector locations are listed at the top left half of the table, and each detector has two columns assigned to it: one for total counts and one for count rates (total counts divided by TIME). All of the count entries are corrected for background as previously discussed. The Accelerator Stati columns list the status of the electron Gun to Linac, Booster ring and Storage ring. Since Table 4 comprises Fill cycles, all of these accelerator components are on and indicated by 1 digits. Later, for the Decay cycles, the electron gun and booster ring are treated as categorical variables to determine if they have an effect on measured radiation. The Fill (and Decay and Dump) cycles are characterized by three storage ring operational parameters: storage ring beam amperage at the start of the operation (START), the time duration of the operation in minutes (TIME), and the of the rate of amperage change during operation (RATE). The mezzanine detector locations were encoded into the spreadsheet by the digit 1 indicated under the column number (1 to 24) that represents the lower of the two column numbers, between which the detectors were placed.

Graphs and simple linear regressions were performed on the Fill data to compare the three detector locations, two at a time. These results are shown in Figure 3. The top two

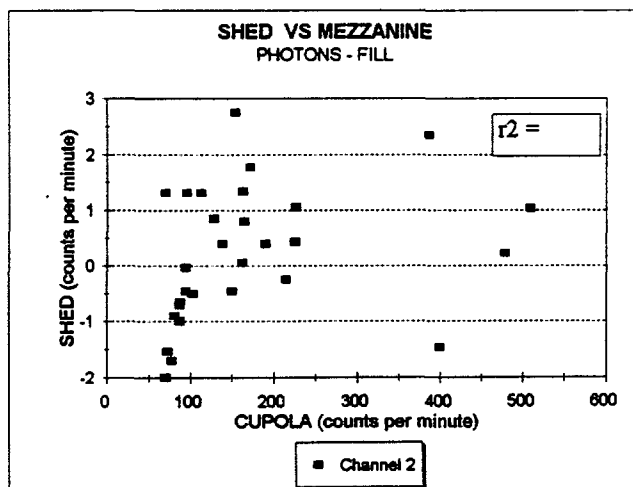
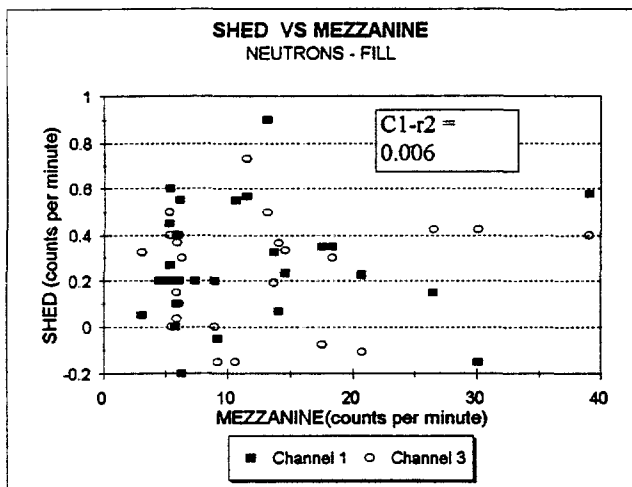
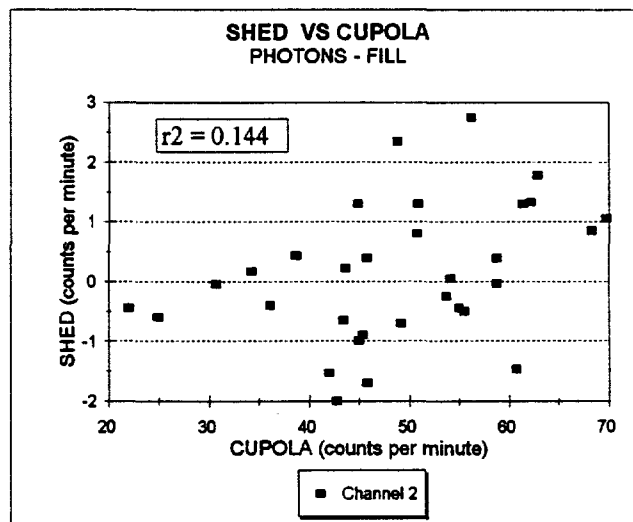
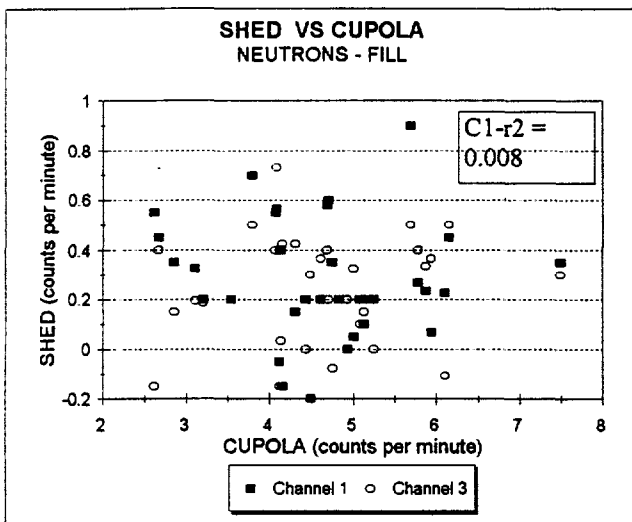
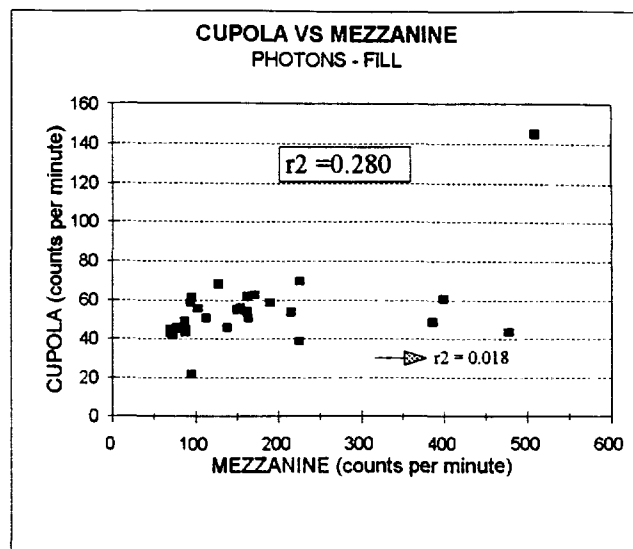
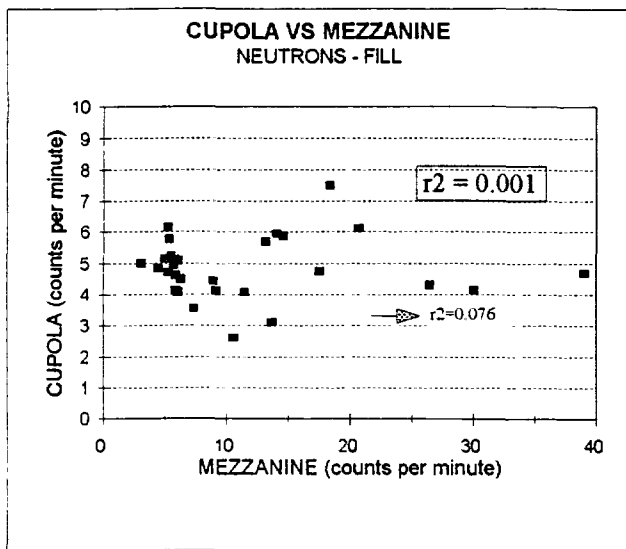


Figure 3. Graphs comparing two detector locations for storage ring Fill cycles. All detector measurement rates have been corrected for background radiation. All axes are in counts per minute. The regression correlation coefficient for each graph is printed in the box in the body of the graph. For the top two graphs, the data points to the right of the shaded arrows were eliminated (as outliers) and the regressions repeated. The new results are printed directly to the right of the arrows. Not much improvement resulted for these.

graphs and their included correlation coefficients (r^2) compare the cupola to the mezzanine. The boxed r^2 values consider all of the data points and indicate poor correlations for both types of radiations. By treating the data points to the right of the shaded arrows as outliers, the neutron r^2 value improves to 0.076 while the photon r^2 values worsens to 0.018. Even with the removal of these "outliers" the correlations are still poor. By reversing the variables in the linear regression, the regression coefficients for the mezzanine versus cupola for photons and neutrons (minus outliers) are 3.2 and 1.8, respectively. The distance from the source (collision points in the storage ring) to the cupola is approximately twice that to the mezzanine. Based on distance alone and the inverse square law, a factor of 4 would be expected in the difference. The photon coefficient is closer to 4 than the neutron coefficient. The implication is that there is a greater forward peak for the photons than the neutrons, since photons of all energies are forward biased, whereas only high energy neutrons are. This is consistent with the electromagnetic and nuclear cascade theories. Two considerations weaken the strength of this conclusion from this data. First, the correlation coefficients for the regressions are low. Second, the differing extent of detector blockage in the cupola versus the mezzanine, which can not be evaluated, factor into this finding. The remedy to this latter problem is to reposition the detectors and gather more data.

The middle graphs compare the shed to the cupola for the same Fill cycles. Both photon and neutron correlation coefficients decreased from the Cupola-Mezzanine comparisons. The Channel 3 shed neutron detector yielded a correlation coefficient with the cupola twice that of Channel 1. By inverting the photon regression coefficient, a value of 3.8 was obtained. Again this closely approximates the ratio of 4 which is expected according to the inverse square law, previously demonstrated at LBL for up to 500 meters from the source (Bevatron).

Comparisons with averaged mezzanine values and the shed were not expected to yield good correlations and did not. Later when multiple regression were conducted, specific sectors showed better correlation.

Using the same Table for Fill cycles, neutron and photon measurements at the same detector locations were compared. The correlation coefficients for the cupola and the shed ranged from 0.07 to 0.11. The correlation coefficient for the mezzanine neutrons versus photons was a high 0.77. The forward bias for both neutrons and high energy neutrons may account for this finding.

Next, three series of graphs (corresponding to Fill, Decay, and Dump cycles) were constructed plotting corrected detector count rates versus RATE. The purpose was to see the effect of beam operation rates on radiation production and to determine if any outlying data points should be eliminated.

For the Fill graph series (Figure 4), a trend with fill rate (smaller fill rates are more inefficient with greater loss of energized electrons) are indicated for the cupola neutrons and possibly for cupola photons. The neutron detector graph for channel 3 also hinted at linearity, whereas channel 1 did not. For cupola photons, one outlier was eliminated as indicated.

Similar trends are seen in the Dump graph series (Figure 5), although channel 3 no longer shows much linearity. One outlier for mezzanine photons was deleted from the data..

The Decay graph series (Figure 6) did not demonstrate any dependence on rate, but this judgement was hindered by the accuracy of assessing the decay rate. The decay rate was calculated as a linear function, but is closer to an exponential function (see diagram 17). There appears to be a dependence on whether the electron Gun or Booster are on. This will be investigated during the multiple regressions to come later.

None of the mezzanine data plotted for any of the storage ring operating modes demonstrated any linearity. This was to be expected in part because the mezzanine " value" represented values from 24 positions around the mezzanine.

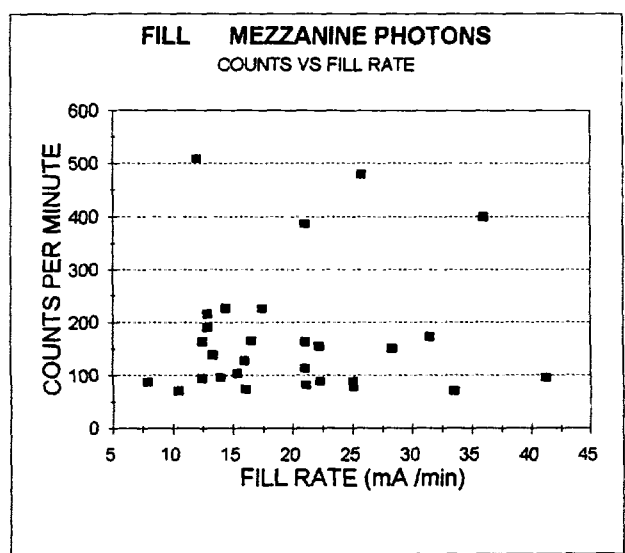
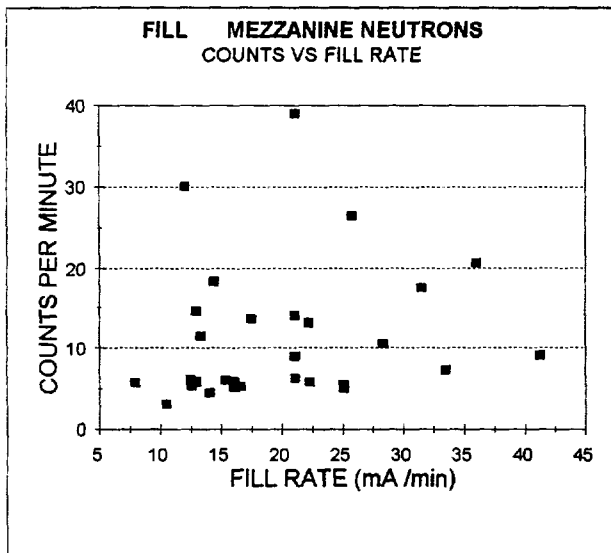
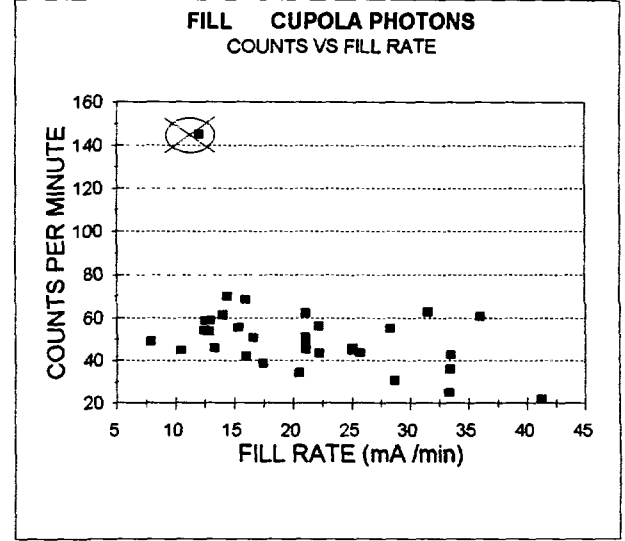
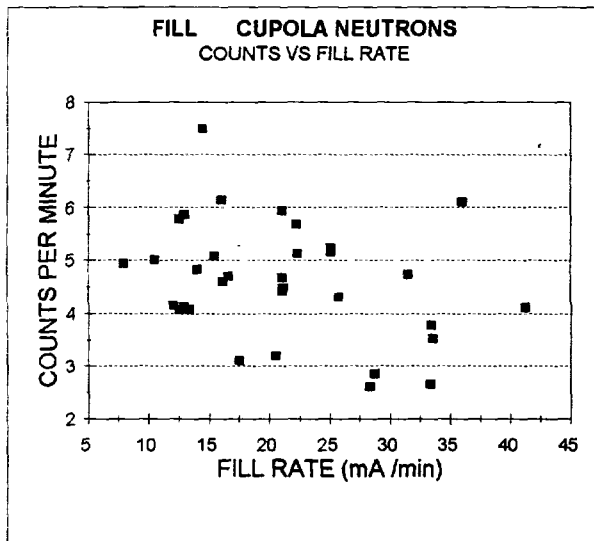
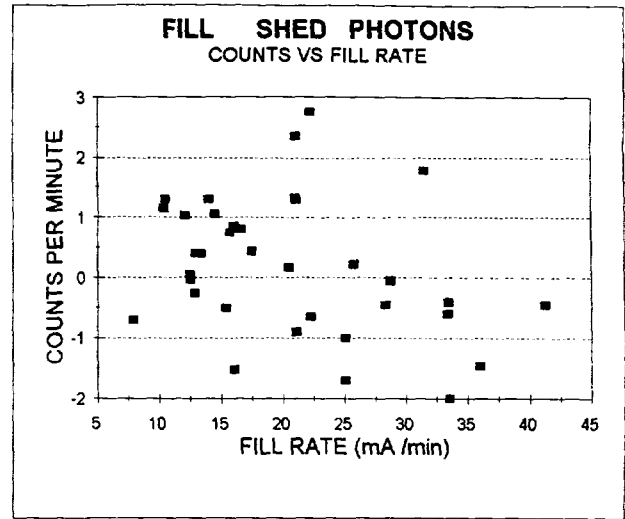
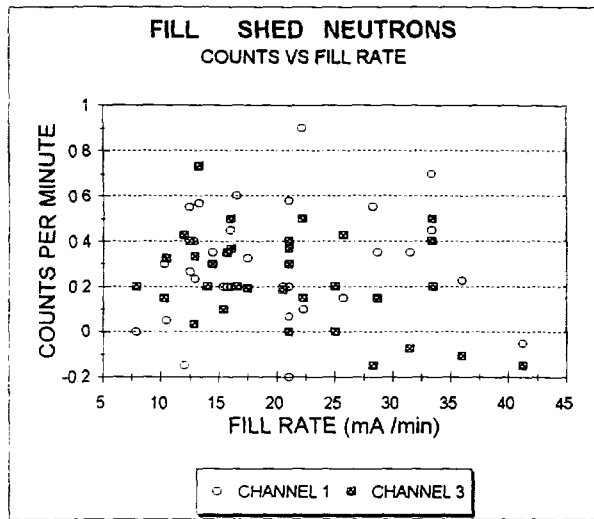


FIGURE 4. Plots of detector count rates at the three different location for the FILL operating mode. All count rates are corrected for background radiation. One outlier for cupola photons was deleted from data set prior to regression analysis.

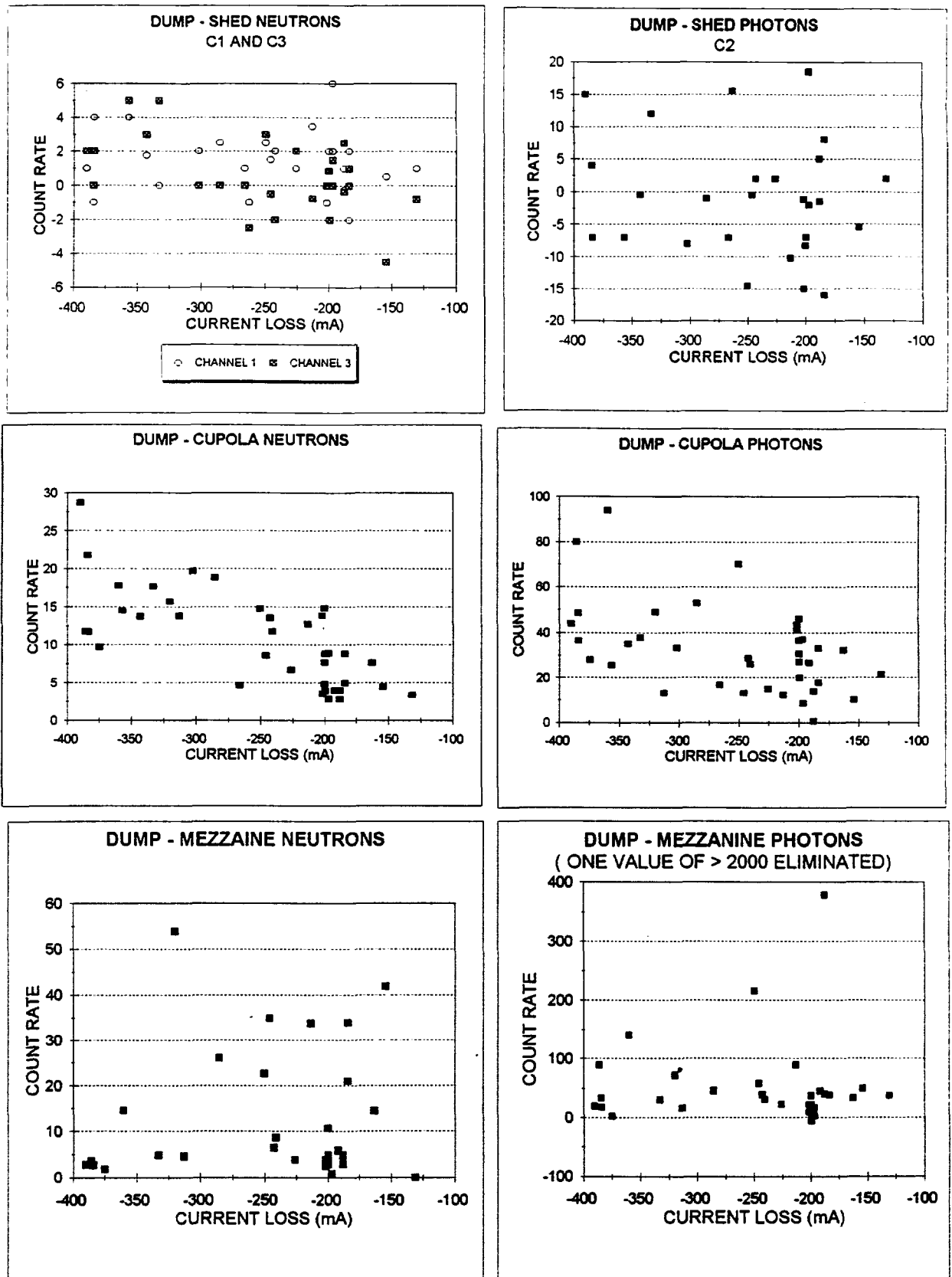


FIGURE 5. Plots of detector count rates at the three different location for the DUMP operating mode. All count rates are corrected for background radiation. One outlier for mezzanine photons was deleted from data set prior to regression analysis.

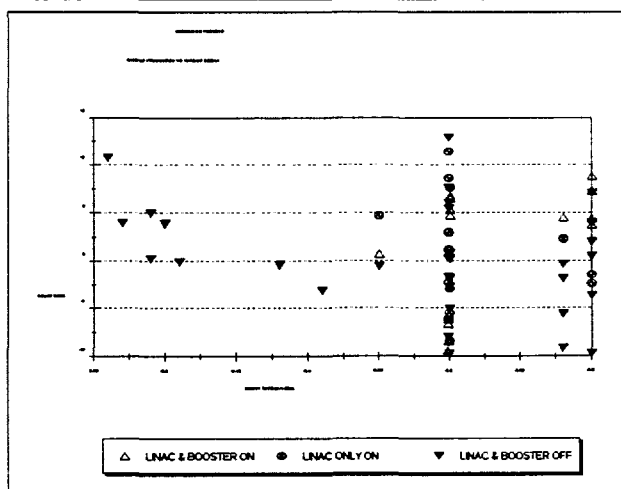
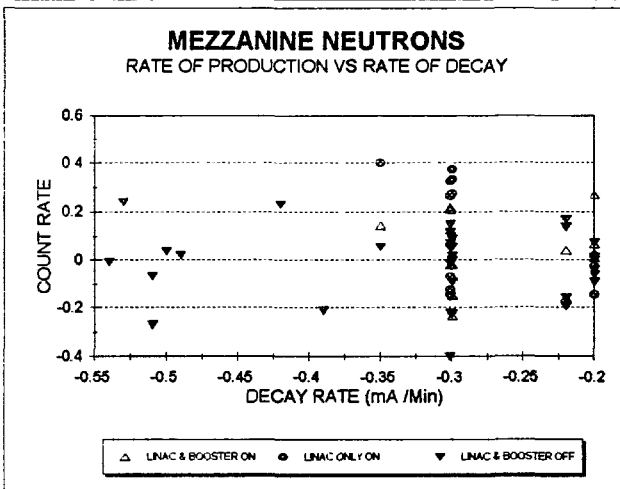
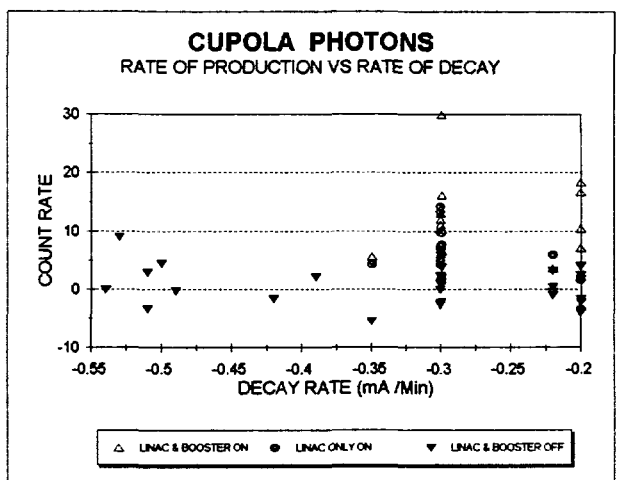
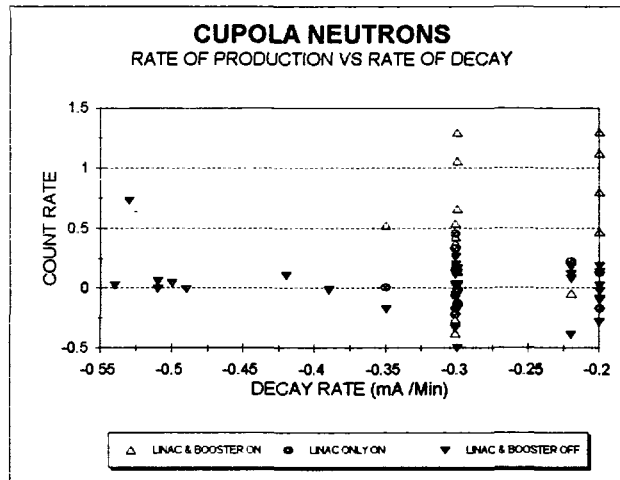
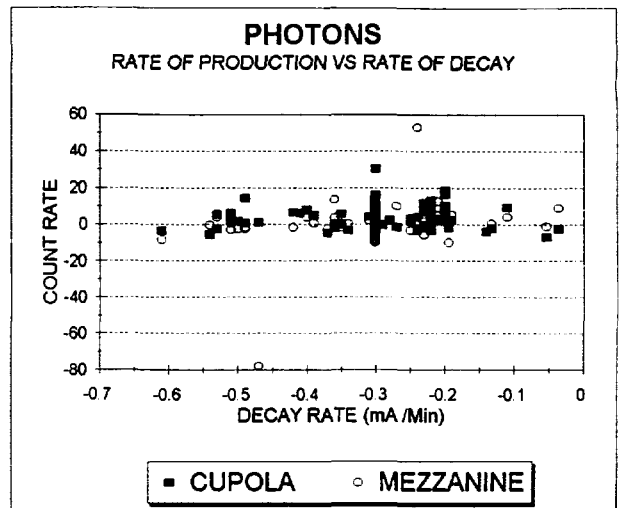
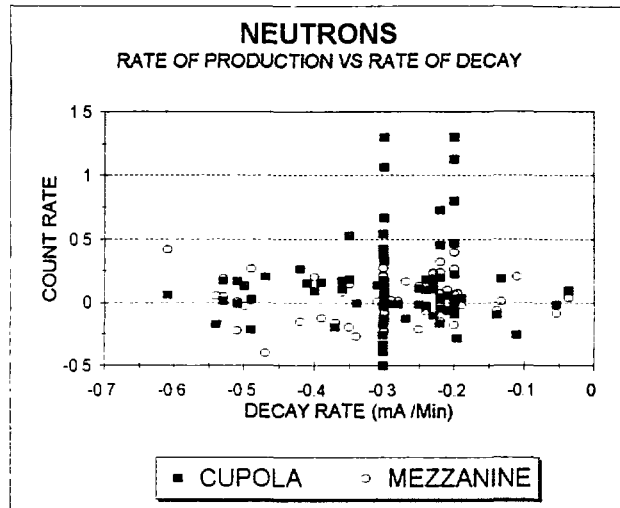


FIGURE 6. Plots of detector count rates at the three different location for the DECAY operating mode. All count rates are corrected for background. Rates were not calculated with sufficient accuracy to evaluate the booster and electron gun impacts on radiation detection.

Determination of Mezzanine "Hot Spots"

A series of graphs were generated to visualize mezzanine "hot spots" during the three storage ring operating functions. These are shown in Figure 7. Column positions labelled on the X-axis represent the lower-numbered column of the two columns between which the detectors were centered. All of the Y axes are corrected count rates per minute of the corresponding detector. The column numbers corresponding to hot spots are also indicated in the body of the graphs.

For the Fill cycles, positions 14 and 20 are relative hotspots for both neutrons and photons. Position 1 is also a likely hotspot for both.

For the Dump cycles, positions 1 and 20 again appear to be hotspots for neutron production. A neutron detection hotspot is indicated at position 16 and at position 9, although only one value was available for graphing for the latter. Positions 4 and 9 appeared to be hotspots, though again, only one value was available for graphing.

For the decay function, only position 9 is indicative of a hot spot for photons.

The explanation for mezzanine "hotspots" could be their distance from the radiofrequency accelerator cavities or from the BTS entrance point into the storage ring. This work was conducted shortly after a fairly strong earthquake (4.8 on the Richter Scale). According to operators, subsequent to the earthquake, storage ring filling required somewhat different magnet settings. It is possible that these "hot spots" will change location or even be rendered insignificant with time and future magnet adjustments.

With these results, two purposes are served. First, the mezzanine locations where the highest yearly exposures are likely to be received are identified and may be referred to the Radiation Safety Office of the ALS. Second, these hotspots should be considered for detector locations for which measurements can be input as independent variables into the regression models for predicting yearly environmental DE.

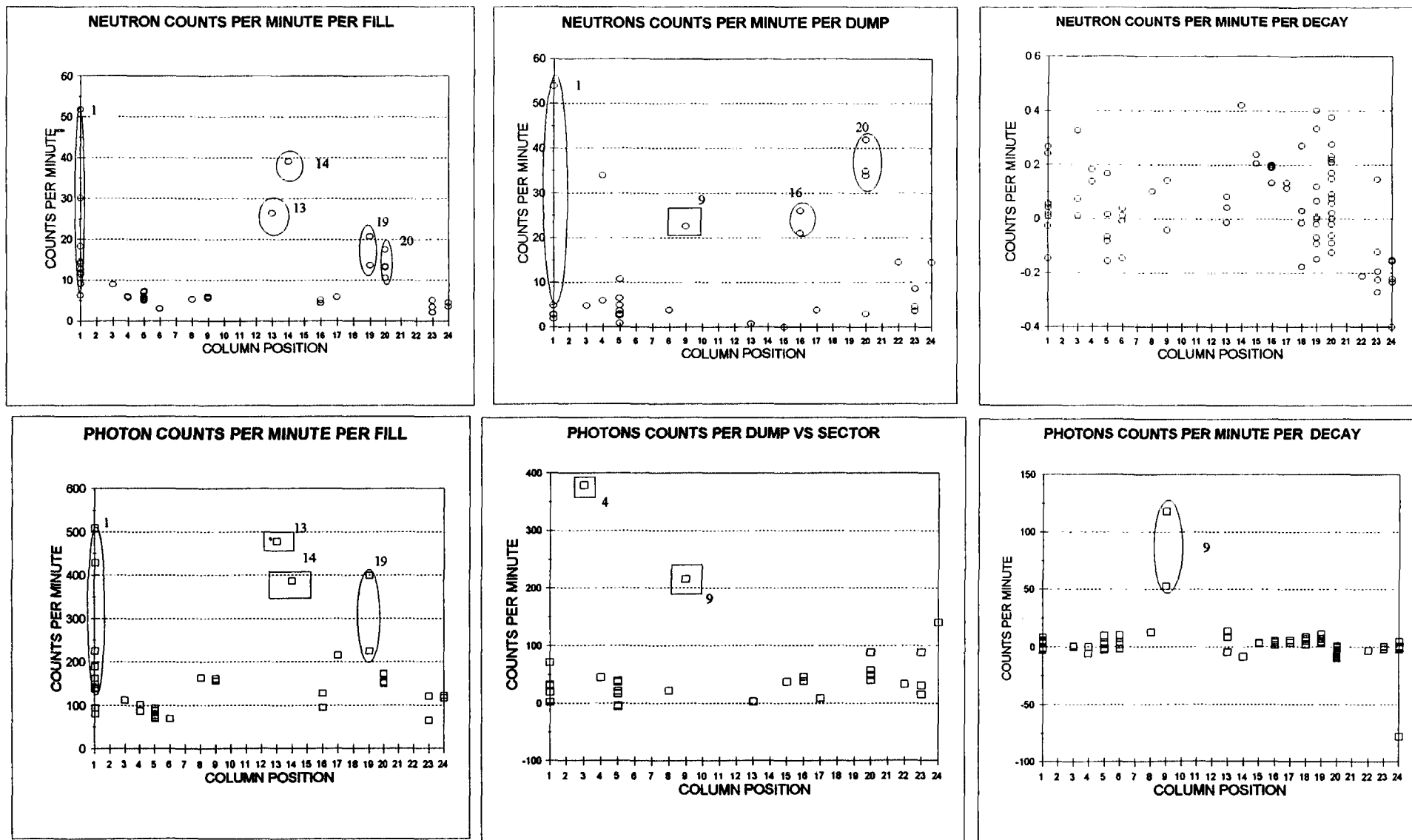


Figure 7. Plots of minute count rates for mezzanine detector locations for FILL, DUMP, and DECAY CYCLES. All count rates are corrected for background. For Fill and Decay graphs no consideration was given to the rates of filling or decaying. Values circled in ellipses are evident "hotspots". Values enclosed were located in squares are potential "hot spots" and need more evaluation. Column position values signify that the neutron and photon detectors between that pole and the next higher one up. Later, these locations are consolidated to allow the mezzanine detector values to be regressed.

First Set of Multiple Regression to Determine which Variables to Use in Predictive Models of Radiation Measured at the Environmental Shed

After correcting the data for background and eliminating one outlier from the data set, the first phase of generating predictive models of shed-measured radiation production from the operation of the accelerator could begin. The objective of this first stage is to determine which variables are required in the regression model. As stated previously, it was decided to treat each independent storage ring operation mode (Fill, Decay, and Dump) and radiation type (neutrons and photons) separately. Thus it is anticipated that six regression equations will be necessary to completely describe the radiation measured at the shed.

Ideally, radiation measurement in the shed could be predicted using only the quantified storage ring operation parameters (continuous variables) of START, TIME and RATE for each storage ring operation mode. Preliminary regression models were constructed with corrected shed radiation measurements as the dependent variable (left-hand side of the equation) and the storage ring operating parameters on the right. These regression models had unacceptably low regression coefficients and high p values. It became apparent that cupola and/or mezzanine detector measurements needed to be included as variables in the regression equations.

To determine which mezzanine positions should be included in a regression model the mezzanine positions were treated as categorical (dummy variables - represented by a 0 or 1) and were substituted in an experimental fashion on the right hand side of the regression equation. The goal of this trial and error process was to achieve the highest overall regression coefficient for the regression model and lowest overall p value at the same time. Individual variables on the right hand side of the regression equation with high p values were avoided.

The first attempt to use the original column numbers to encode mezzanine positions failed for a lack of data for individual column locations. This was remedied by combining the 24 columns into 12 sectors as described in the data processing section. Sector 9 was the reference sector for using the sector position dummy variables. The complete set of corrected, consolidated data for the Fill, Dump and Decay cycles are listed in Tables 5 and 6. Column headings are described in the caption of Table 5.

SHED DETECTORS			CUPOLA DETECTORS		MEZZANINE DETECTORS		ACCELERATOR STATI			OPERATING PARAMETERS			MEZZANINE SECTOR POSITIONS											
Channel 1 neutrons	Channel 3 neutrons	Channel 2 photons	Cupola neutrons	Cupola photons	Mezzanine neutrons	Mezzanine photons	hν Gun	Booster Ring	Storage Ring	START	RATE	TIME	s1	s12	s11	s10	s9	s8	s7	s6	s5	s4	s3	s2
			91.2	1208.0	85.4	2810.4	1	1	1	175	7.00	24	0	0	0	0	0	0	0	0	0	0	0	1
			137.4	2006.0	173.8	4682.8	1	1	1	1	10.53	38	0	0	0	0	0	0	0	0	0	0	0	1
			52.6	721.0	38.2	1111.7	1	1	1	0	23.53	17	0	0	0	0	0	0	0	0	0	0	0	1
			103.4	1578.0	141.8	3402.8	1	1	1	0	14.30	28	0	0	0	0	0	0	0	0	0	0	1	0
			44.8	591.9	59.8	1034.7	1	1	1	0	18.21	11	0	1	0	0	0	0	0	0	0	0	0	0
			111.4	1531.0	97.8	3408.8	1	1	1	0	14.32	28	0	0	0	0	0	0	0	0	0	0	1	0
			162.1	1609.7	367.1	4090.4	1	1	1	0	13.79	29	0	0	0	0	0	0	0	0	0	0	0	1
					5.7	157.2	1	1	1	0	20.28	1	0	0	0	1	0	0	0	0	0	0	0	0
			103.4	1169.3	250.2	3131.5	1	1	1	0	19.08	21	0	0	0	0	0	0	0	0	0	0	0	1
			43.6	414.0	83.7	1212.8	1	1	1	0	35.70	7	0	0	0	0	0	0	0	0	0	1	0	0
			12.7	306.3	155.2	1289.0	1	1	1	0		3	0	0	0	0	0	0	0	0	0	0	0	1
			83.8	917.8			1	1	1	0	26.72	15	1	0	0	0	0	0	0	0	0	0	0	0
-3.80	5.70	-17.10	85.3	861.7	119.7	1542.1	1	1	1	0	21.11	19	0	1	0	0	0	0	0	0	0	0	0	0
-1.50	4.25	10.25	41.5	1452.1	300.9	5085.3	1	1	1	275	12.04	10	0	0	0	0	0	1	0	0	0	0	0	0
-0.20	-0.60	-1.80	16.5	88.0	36.8	379.7	1	1	1	0	41.25	4	0	0	0	0	0	0	0	0	0	1	0	0
0.00	1.20	-4.20	29.6	295.0	34.6	523.0	1	1	1	150	7.90	8	0	1	0	0	0	0	0	0	0	0	0	0
0.85	5.53	22.10	85.1	763.0	52.5	1188.3	1	1	1	225	10.47	17	0	0	1	0	0	0	0	0	0	0	0	0
0.90	1.35	-5.85	46.2	390.9	52.8	795.7	1	1	1	0	22.29	9	0	1	0	0	0	0	0	0	0	0	0	0
1.00	0.93	0.86	16.0	171.3			1	1	1	150	20.52	5	0	0	0	0	0	0	0	0	1	0	0	0
1.20	1.20	-12.00	21.3	256.5	44.3	421.5	1	1	1	0	33.51	6	0	1	0	0	0	0	0	0	0	0	0	0
1.27	6.97	25.33	113.0	1180.4	287.5	3091.9	1	1	1	0	21.05	19	0	0	0	0	0	0	0	0	0	0	0	1
1.40	3.15		35.9	337.2	49.4	661.1	1	1	1	0	28.57	7	0	1	0	0	0	0	0	0	0	0	0	0
1.60	1.60	-8.00	42.0	368.7	40.3	701.0	1	1	1	0	25.08	8	0	1	0	0	0	0	0	0	0	0	0	0
1.60	-0.00	-13.60	41.3	359.9	43.9	622.1	1	1	1	0	25.08	8	0	1	0	0	0	0	0	0	0	0	0	0
1.65	4.68	2.48	47.4	480.2	291.7	5281.1	1	1	1	0	25.77	11	0	0	0	0	0	1	0	0	0	0	0	0
1.65	-0.45	-1.35	7.8	165.0	31.8	451.5	1	1	1	165	28.33	3	0	0	0	0	0	0	0	0	0	1	0	0
2.10	1.05	8.05					1	1	1	325	10.34	7	0	0	0	0	0	0	1	0	0	0	0	0
2.25	-1.07	-14.64	18.3	182.2	62.1	1198.8	1	1	1	140	36.00	3	0	0	0	0	0	0	0	0	1	0	0	0
2.80	-0.60	14.20	38.0	502.5	140.5	1373.5	1	1	1	0	31.50	8	0	0	0	0	0	0	0	0	0	1	0	0
3.25	1.93	4.36	18.7	232.4	82.3	1353.5	1	1	1	132	17.50	6	0	0	0	0	0	0	0	0	1	0	0	0
3.80	0.00	24.70	84.2	965.7	170.7	2140.1	1	1	1	0	21.07	19	1	0	0	0	0	0	0	0	0	0	0	0
4.20	7.35	15.75					1	1	1	0	15.73	21	0	0	0	0	0	0	1	0	0	0	0	0
4.20	4.20	27.30	101.5	1288.0	94.0	2006.0	1	1	1	0	14.02	21	0	0	0	0	0	0	0	1	0	0	0	0
4.40	8.07	-33.73	101.5	923.8	129.5	1599.5	1	1	1	25	16.08	22	0	1	0	0	0	0	0	0	0	0	0	0
4.90	2.10	-0.70	40.0	429.8			1	1	1	0	28.71	14	0	0	0	0	0	0	0	0	0	1	0	0
5.20	2.60	-13.00	132.3	1444.3	158.3	2885.3	1	1	1	0	15.39	26	0	1	0	0	0	0	0	0	0	0	0	0
5.25	4.50	15.75	112.5	1046.5	275.5	3390.0	1	1	1	175	14.45	15	0	0	0	0	0	0	0	0	0	0	0	1
5.40	4.80	-7.20	32.0	298.8			1	1	1	0	33.38	12	0	0	0	0	0	0	0	0	0	1	0	0
7.23	10.33	12.40	182.2	1822.0	452.9	5800.3	1	1	1	0	12.94	31	0	0	0	0	0	0	0	0	0	0	0	1
7.47	11.20	-0.93	162.0	1645.7	149.3	2638.0	1	1	1	0	12.51	28	0	1	0	0	0	0	0	0	0	0	0	0
8.40	6.00	-4.80	45.5	433.4			1	1	1	0	33.41	12	0	0	0	0	0	0	0	0	0	1	0	0
9.00	3.00	12.00	70.8	781.2	79.8	2462.0	1	1	1	0	16.59	15	0	0	0	1	0	0	0	0	0	0	0	0
11.00	7.60	44.85	89.1	927.4	742.0	7350.2	1	1	1	0	21.05	19	0	0	0	0	0	0	1	0	0	0	0	0
11.25	12.50	21.25	153.8	1706.0	131.0	3192.0	1	1	1	0	16.01	25	0	0	0	0	0	0	0	1	0	0	0	0
12.40	1.03	-7.75	128.1	1665.1	182.7	8668.9	1	1	1	0	12.90	31	0	0	0	0	0	0	0	1	0	0	0	0
16.20	9.00	49.50	102.5	1012.3	238.8	2779.5	1	1	1	0	22.21	18	0	0	0	0	0	0	0	0	0	1	0	0
17.00	22.00	12.00	122.5	1375.0	345.0	4155.5	1	1	1	0	13.33	30	0	0	0	0	0	0	0	0	0	0	0	1
17.60	12.80	1.60	130.3	1733.1	195.3	5180.3	1	1	1	0	12.49	32	0	0	0	1	0	0	0	0	0	0	0	0

Channel 1 neutrons	Channel 3 neutrons	Channel 2 photons	Cupola neutrons	Cupola photons	Mezzanine neutrons	Mezzanine photons	hν Gun	Booster Ring	Storage Ring	START	RATE	TIME	s1	s12	s11	s10	s9	s8	s7	s6	s5	s4	s3	s2
-5.00	1.00	-123.00			22.7	216.2	0	0	3	250	-250.00	1	0	0	0	1	0	0	0	0	0	0	0	0
-2.00	1.00	-18.00	4.9	17.7	33.9	2038.7			3	350	-184.00	1	0	1	0	0	0	0	0	0	0	0	0	0
-2.00	-2.00	-7.00	8.8	46.2	2.9	-5.7			3	199	-198.40	1	0	1	0	0	0	0	0	0	0	0	0	0
-1.00	-2.50	15.50							3	280	-262.80	1	0	0	0	0	0	0	1	0	0	0	0	0
-1.00	-0.00	4.00	21.8	36.4	2.8	33.5	0	0	3	385	-384.50	1	0	0	0	0	0	0	0	0	0	0	0	1
-1.00	-0.00	-15.00	3.5	41.4	2.5	21.9			3	202	-201.60	1	0	1	0	0	0	0	0	0	0	0	0	0
-0.25	-0.35	-1.45	2.8	0.7	3.0	40.5	0	0	3	188	-188.00	1	0	0	0	0	0	0	0	0	0	1	0	0
0.00	5.00	12.00	17.7	38.0	4.9	30.8	1	0	3	333	-333.00	1	0	0	0	0	0	0	0	0	0	0	0	1
0.00	-0.00	-7.00	4.8	36.6	4.9	-3.1			3	200	-199.80	1	0	1	0	0	0	0	0	0	0	0	0	0
0.00	0.00	-1.17	13.8	43.6	3.9	9.4			3	200	-201.70	1	0	0	0	0	0	0	0	1	0	0	0	0
0.50	-4.50	-5.50	4.4	10.1	41.9	49.6	0	0	3	154	-154.40	1	0	0	0	0	0	0	0	0	0	1	0	0
1.00	2.50	5.00	4.0	13.8	4.8	379.2	0	0	3	188	-188.20	1	1	0	0	0	0	0	0	0	0	0	0	0
1.00	2.00	2.00	6.7	14.9	3.9	22.7	0	0	3	225	-228.00	1	0	0	0	1	0	0	0	0	0	0	0	0
1.00	-0.00	-7.00	4.6	16.7			0	0	3	288	-288.40	1	0	0	0	0	0	0	0	0	0	1	0	0
1.00	2.00	15.00	28.7	44.0	2.9	19.8	0	0	3	390	-390.00	1	0	0	0	0	0	0	0	0	0	0	0	1
1.00	-0.80	2.00	3.3	21.5	0.0	37.7			3	131	-65.75	2	0	0	0	0	0	0	1	0	0	0	0	0
1.50	-0.50	-0.50	8.6	13.0	34.9	58.2	0	0	3	246	-246.00	1	0	0	0	0	0	0	0	0	0	1	0	0
1.75	3.00	-0.50	13.8	35.1			0	0	3	343														

The results of these preliminary regressions are shown in Table 7. The left hand side of the equation (dependent variable) is one of the three shed detector measurements. For each storage ring operation mode, the mezzanine sector position (categorical variables) for each channel detector are listed as well as each variable's regression coefficient and individual p value. For each regression, only the sectors that increased the overall regression coefficient while not drastically increasing the overall p value are. Generally, sectors with with individual p values (which is the probability that fit of the variable is due to random chance) of > 0.2 were not desirable; however, by liberally deleting variables with higher p values, the overall model's correlation coefficient (r^2) was rendered lower. Further, this is a preliminary regression to consider which mezzanine sector position variables to transform into continuous variables (comprised of the actual mezzanine detector measurements) for the final, predictive regression model. Therefore the individual p values were not used for discarding a variable if it contributed significantly to the overall r^2 value.

Significant storage ring operation parameters (continuous variables) are listed next. It should be noted that for Dumps, START and RATE are identical (except for the sign) since all dump cycles occur over one minute and go from the START value to zero. The RATE variables may need to be discarded in the next set of regression due to their high p values. For this preliminary regression, they are kept in to maintain the optimal, overall r^2 value. Finally, the overall regression equation coefficients are listed. The overall p values are all below 0.02, which is excellent at this stage. The r^2 values are low and will be improved upon in the next set of regressions. The improvement will come by including both cupola and mezzanine detector measurements as continuous variables, which is discussed in the next section.

Conspicuously missing are Decay cycle regressions for all three shed channels and a Dump cycle regression for photons (channel 2). This is because radiation produced during decay cycles was indiscernible above background. Further, photon background radiation is an order of magnitude higher than neutrons. Therefore the net photon counts for the Dump cycle were inadequate to produced a good regression model.

Dependent Variable (SHED DETECTORS)	Storage Ring Operating Mode	Categorical Variables			Continuous Variables		Overall Regression Model Coefficients	
		mezzanine sector	regression coefficient	p value	storage ring operating paramete	p value	overall r2 coefficient	overall p value
(Channel 1) Neutrons	FILL	10	4.9	0.14	TIME	0.00	0.679	0.00
		11	-5.0	0.25	RATE	0.94		
		12	-2.5	0.34				
		4	2.7	0.40				
	DUMP	2	-3.9	0.02	START(RATE)	0.33	0.31	
		12	-1.9	0.09				
		1	-1.1	0.48				
		4	-0.6	0.55				
(Channel 3) Neutrons	FILL	2	5.8	0.03	TIME	0.00	0.662	0.00
		8	5.1	0.15	RATE	0.97		
		7	3.7	0.22				
		4	3.6	0.24				
		5	3.7	0.29				
		12	2.7	0.28				
	DUMP	12	-1.9	0.06	START(RATE)	0.00	0.52	0.02
		4	-1.6	0.10				
		1	0.8	0.55				
		2	-0.3	0.86				
(Channel 2) Photons	FILL	12	-24.5	0.03	RATE	0.30	0.53	0.04
		5	-14.7	0.32				
		1	13.5	0.44				

Table 7. Results of First Regression series treating consolidated mezzanine detector positions as categorical variables (sectors) and storage ring operating parameters as continuous variables. Note START and RATE continuous variables are the same except for the sign for Dump Cycles. These results were used to determine which sectors to use when changing the independent variables from mezzanine positions to actual measurements.

Consolidation of Mezzanine Positions to Allow Conversion to Continuous Variables

Having determined which mezzanine sector positions contributed the greatest to fitting regression models to shed detector measurements, the procedure was now repeated with two necessary modifications. First, the cupola neutron and photon detector measurements were added to the continuous variable pool. Secondly, instead of entering mezzanine positions as categorical variables as before, the measured mezzanine detector counts were ascribed to the appropriate mezzanine positions and added as additional continuous variables to the regression pool. For example, for the shed channel 1 (neutron) Fill regression model (see Table 7), the mezzanine neutron measurements made when the detector was located in sector 10 (comprised of data taken from the original column 8 and column 9) were handled as a new continuous variable. However, upon running the regression software with this "new" variable, an error message of insufficient data sets was output. Thus, although it had been demonstrated that the detector values obtained from this sector were important in generating a predictive regression model for the shed, it was apparent that an adequate number of data points did not exist.

A further consolidation of the mezzanine positional data was necessary. This meant increasing the number of data points attributable to significant mezzanine positions. The only way to accomplish this was to redivide the mezzanine into appropriate sextants (comprised of two sectors each) and create theoretical detectors to which the adjacent, inclusive sector measurements were attributed. In performing this data consolidation, several considerations were made. First, as many of the sectors indicated in table 7 as possible should be included. Second, these theoretical detectors measurements, comprised of data from adjacent, real detectors, needed to be located in the center of the combined sectors that they were theoretically measuring. Three additional considerations were important, should theoretical detector positions be utilized to locate actual detectors in the future (say should this work be repeated with unimpaired lines of sight to the detectors). The detectors should coincide as closely as possible with Mezzanine "hot spots" determined previously in this work. The limit of four detectors per datalogger module means timing synchronization becomes more difficult

as more units are added and need to be synchronized. Finally, an economy of scale needed to be incorporated, both for the high costs associated with the equipment and time involved in constructing data files for regression work.

The final consolidation resulted in four theoretical detectors with labels m2, m20, m14 and m5. Their locations and inclusive sectors and hotspots are shown in Figure 8 and Table 8, respectively. The large Xs mark the location of the four theoretical detector locations and the heavy bold lines show which segments of the mezzanine each theoretical detector measures.

As an example, consider theoretical detector m14. In Table 7 and for shed-channel 3 - Fill cycle regression variables, both sectors 7 and 8 are important for the regression model. The sectors are indicated by the circled, outer numbers in Figure 8. Since they are adjacent, the measurements made in each of them are combined and ascribed to an theoretical detector, which would be mounted on column 14 and labeled "m14". This consolidation strategy successfully provides enough data points for entering the detector measurements covering the mezzanine area from mezzanine position 12½ through 15½. It is not a flawless arrangement, but is the best available under the circumstances.

adjacent, contributing sectors indicated in table 9	2	4, 5	7, 8	12
mezzanine "hotspots" column locations located in the above sectors (parenthesis indicate that the hotspot is just outside of above sectors)	(1)	19,20	13,14, (16)	12
column number where theoretical detector is mounted	1	20	14	5
theoretical monitor label for regression work	m1	m20	m14	m5
inclusive mezzanine area that theoretical detectors cover (column positions upper and lower bounds)	24½ - 1½	18½ - 21½	12½ - 15½	4½ - 5½

Table 8. This table indicates the mezzanine position consolidation scheme to enable a final regression to be performed with continuous variables (detector measurements) instead of mezzanine positions (dummy or categorical variables). Significant sectors were extracted from Table 7. Mezzanine hot spots were determined from Figure 7. The theoretical detector would be mounted on the central column that bisects the sectors listed in the corresponding column above. Detector measurements obtained from all positions located within the inclusive mezzanine area are ascribed to the corresponding theoretical detector.

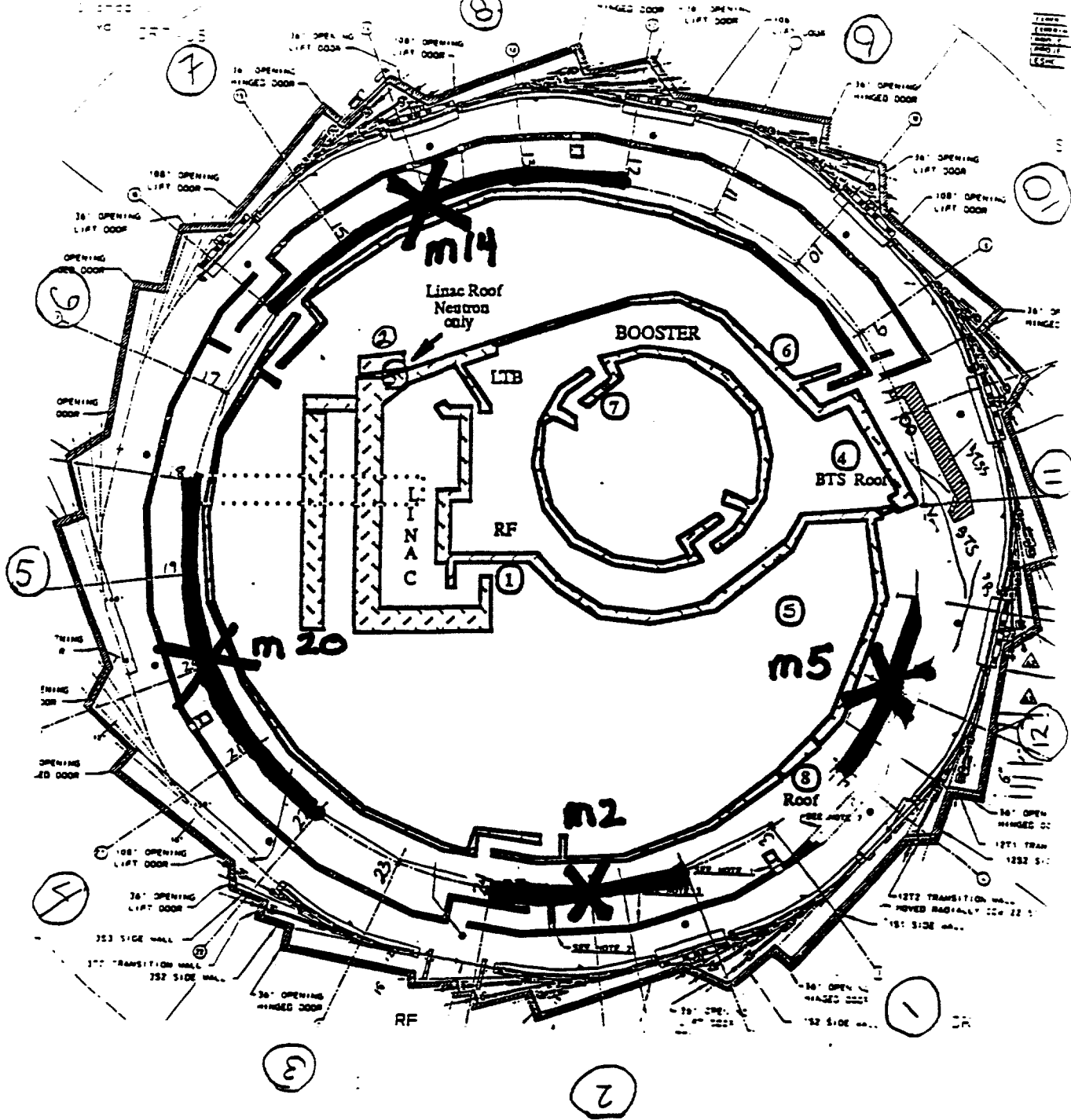


Diagram 14. Layout of the ALS with column (poles) and sectors marked. Columns(1-24) are labelled along the lines extended out from them and in small circles at the ends of the lines. Sectors are labelled at the figure periphery of the diagram in large circles. The detectors were located in the middle of two columns, with each off these positions labelled with the lower column number. The Linac, Booster and Storage Ring shielding are superimposed, though not to scale. Radiation alarm positions are also indicated in the center of the diagram by small circled numbers.

The Second Set of Multiple Regressions to Generate Predictive Models of Radiation Measured at the Environmental Shed

The pool of right hand side variables for the multiple regression was now increased by adding neutron and photon measurements at the cupola and the four theoretical detector measurements on the mezzanine. The final, corrected data used for the Fill and Dump cycles are shown in Table 9. Each row represents one independent operating cycle. The number of complete rows was limited by the m5 detector measurements. Decay cycle data are shown in Table 10. More data points are available because mezzanine detector measurements were not included (the number of measurements for individual mezzanine detectors were insufficient to conduct successful regressions). This group of data rows is limited by Gun and Booster data. The shed measurement values in Table 10 are listed as one minute rates and thus appear much lower than the shed values for Fill or Dump cycles.

With these complete data sets tabulated, it remained to generate regression models that could predict the radiation measured at the shed detectors. For this work linear regression models were first used and later confirmed. All of the considered independent variable have a logical basis for being included. START, TIME and RATE quantify how much energy is available to convert to stray radiation. Cupola and the mezzanine detectors measure the actual energized particles on their paths to being scattered to the shed detectors.

The results of the regressions are shown in Table 11, which is divided into four sections. The left section lists the significant variables and their coefficients for each storage ring operating mode that were included in the best (combination of highest regression coefficient and lowest p values) regression equation. The next, second (shaded) section contains diagnostic test results for each of the regression models. The third section is a worksheet that uses the best regression model to predict the mean and 95% confidence interval of radiation produced for a single operation mode. The fourth (also shaded) section is also a worksheet to calculate yearly means and confidence intervals for: a) yearly radiation for each operating mode for each channel b) the combination of the two shed neutron channels, and c) the sum of all three operating modes using the two neutron channel averages. The table details are first reviewed and the conclusions are discussed.

DECAY

SHED DETECTORS			CUPOLA DETECTORS		ACCELERATOR STATI			OPERATING PARAMETERS		
Ch. 1 Neutron Count Rate	Ch. 3 Neutron Count Rate	Ch. 2 Photon Count Rate	Cupola Neutron Count Rate	Cupola Photon Count Rate	hv Gun	Booster Ring	Storage Ring	START (min)	RATE (mA/min)	TIME (min)
0.18	-0.04	0.89	0.03	2.10	0	0	2	400	-0.3	89
0.18	-0.04	0.89	0.03	2.10	0	0	2	400	-0.3	89
0.13	0.01	0.78	0.11	1.21	0	0	2	350	-0.3	134
0.13	0.01	0.78	0.11	1.21	0	0	2	350	-0.3	134
0.10	0.03	0.50	0.02	1.87	0	0	2	240	-0.2	448
-0.10	0.30	0.73	0.02	-2.66	0	0	2	400	-0.53	32
-0.10	0.30	0.73	0.02	-2.66	0	0	2	400	-0.53	32
-0.08	-0.10	0.48	0.19	-2.24	0	0	2	230	-0.1326	445
0.07	-0.06	0.23	0.03	2.40	0	0	2	222	-0.19	266
0.21	0.17	-0.36	-0.03	6.22	0	0	2	400	-0.538	166
-0.09	-0.34	0.45	-0.28	-1.64	0	0	2	220	-0.195	359
-0.09	-0.34	0.45	-0.28	-1.64	0	0	2	220	-0.195	359
-0.10	-0.09	0.84	0.20	-0.06	0	0	2	400	-0.22	223
0.06	0.10	0.79	-0.06	2.30	0	0	2	375	-0.21	680
0.13	-0.10	0.53	0.02	2.34	0	0	2	250	-0.27	183
0.25	0.14	-0.45	-0.14	-3.15	0	0	2	402	-0.531	85
0.00	0.10	-0.40	-0.17	-5.51	0	0	2	400	-0.54	21
0.00	0.10	-0.40	-0.17	-5.51	0	0	2	400	-0.54	21
-0.05	-0.37	-0.10	0.11	-1.66	0	0	2	250	-0.23	268
-0.04	-0.38	-0.72	-0.33	-2.39	0	0	2	380	-0.301	274
-0.04	-0.38	-0.72	-0.33	-2.39	0	0	2	380	-0.301	274
-0.02	0.25	-0.07	0.73	8.95	0	0	2	200	-0.22	54
-0.02	0.25	-0.07	0.73	8.95	0	0	2	200	-0.22	54
-0.04	-0.25	0.53	-0.01	-0.27	0	0	2	250	-0.29	134
-0.04	-0.25	0.53	-0.01	-0.27	0	0	2	250	-0.29	134
-0.05	-0.37	-0.10	0.11	-1.66	0	0	2	250	-0.23	268
0.06	0.03	0.88	0.14	4.11	0	0	2	400	-0.31	95
-0.03	0.04	0.67	0.03	-0.03	0	0	2	350	-0.22	437
0.15	0.10	-0.67	0.14	3.20	0	0	2	400	-0.301	62
0.10	0.03	0.50	0.02	1.87	0	0	2	240	-0.2	448
0.11	-0.01	0.96	0.06	2.99	0	0	2	280	-0.21	652
0.11	-0.01	0.96	0.06	2.99	0	0	2	280	-0.21	652
0.20	0.18	-0.26	0.04	-5.31	0	0	2	401	-0.41	329
0.08	0.30	0.75	0.15	0.16	0	0	2	374	-0.52	36
0.07	0.10	0.37	0.13	1.56	1	0	2	400	-0.5	47
0.07	0.10	0.37	0.13	1.56	1	0	2	400	-0.5	47
0.10	0.07	1.02	-0.01	1.94	1	0	2	400	-0.51	133
0.10	0.07	1.02	-0.01	1.94	1	0	2	400	-0.51	133
0.13	-0.13	0.80	1.13	18.38	1	1	2	238	-0.2	20
0.13	-0.13	0.80	1.13	18.38	1	1	2	238	-0.2	20

Table 10. Data compiled for second series of multiple regressions - Decay cycles. First five columns are detector measurement values in counts. Each row represents one operational cycle. All cupola measurements were corrected for cosmic background radiation. Gun and Booster are indicated as 0 (Off) or 1 (On).

FILL	SHED DETECTORS			CUPOLA DETECTORS		MEZZANINE NEUTRON DETECTORS				MEZZANINE PHOTON DETECTORS				OPERATING PARAMETERS		
	Ch. 1 Neutron	Ch. 3 Neutron	Ch. 2 Photon	Cupola Neutron	Cupola Photon	m20 Neutron	m2 Neutron	m14 Neutron	m5 Neutron	m20 Photon	m2 Photon	m14 Photon	m5 Photon	STAR (min)	RATE (mA/min)	TIME (min)
	1.27	6.97	25.33	113.0	1180.4		267.5						3091.9	0	21.0526	19
	7.23	10.33	12.40	182.2	1822.0		452.9						5900.3	0	12.94	31
	5.25	4.50	15.75	112.5	1046.5		275.5						3390.0	175	14.45	15
				12.7	306.3		155.2						1289.0	0		3
				103.4	1169.3		250.2						3131.5	0	19.08	21
				162.1	1609.7		367.1						4090.4	0	13.7931	29
	17.00	22.00	12.00	122.5	1375.0		345.0						4155.5	0	13.3333	30
	11.00	7.60	44.65	89.1	927.4			742.0						0	21.05	19
	1.65	4.68	2.48	47.4	480.2			291.7					7350.2	0	25.77	11
	4.20	7.35	15.75										5261.1	0	15.73	21
	2.10	1.05	8.05											325	10.34	7
	1.65	-0.45	-1.35	7.8	165.0	31.8				451.5				165	28.33	3
	0.68	-0.32	4.39	18.3	182.2	62.1				1198.8				140	36	3
				43.6	414.0	93.7				1212.8				0	35.7	7
	16.20	9.00	49.50	102.5	1012.3	236.8				2779.5				0	22.21	18
	1.95	1.16	2.61	18.7	232.4	82.3				1353.5				132	17.5	6
	-0.20	-0.60	-1.80	16.5	88.0	36.8				379.7				0	41.25	4
	2.80	-0.60	14.20	38.0	502.5	140.5				1373.5				0	31.5	8
				44.8	591.9				59.8				1034.7	0	18.21	11
	3.60	5.70	-17.10	85.3	861.7				119.7				1842.1	0	21.11	18
	0.00	1.20	-4.20	29.5	295.0				54.5				525.6	150	7.9	8
	0.90	1.35	-0.95	46.2	390.9				52.6				785.7	0	22.79	9
	1.20	1.20	-12.00	21.3	256.5				44.3				491.5	0	33.51	6
	1.40	3.15		35.9	337.2				49.4				661.1	0	28.67	7
	1.60	1.60	-8.00	42.0	360.7				40.3				701.0	0	25.00	5
	1.60	-0.00	-13.60	41.3	359.9				43.9				622.1	0	25.06	6
	4.40	6.07	-33.73	101.5	923.8				123.5				1889.5	25	16.10	22
	5.20	2.60	-13.00	132.3	1444.3				185.3				2685.3	0	15.34	26
	7.47	11.20	-0.93	152.0	1646.7				149.3				2659.0	0	12.61	28

DUMP	Ch. 1	Ch. 3	Ch. 2	Cupola	Cupola	m20	m2	m14	m5	m20	m2	m14	m5	STAR	RATE	TIME
	Neutron	Neutron	Photon	Neutron	Photon	Neutron	Neutron	Neutron	Neutron	Photon	Photon	Photon	Photon	(min)	(mA/min)	(min)
	1.00	2.00	15.00	28.7	44.0		2.9				19.8			390	-390	1
				9.7	28.0		1.9				2.8			375	-375	1
				15.7	49.0		53.9				71.8			320	-320	1
	0.00	5.00	12.00	17.7	38.0		4.9				30.8			333	-333	1
	-1.00	-0.00	4.00	21.8	36.4		2.8				33.5			385	-384.5	1
	1.50	-0.50	-0.50	8.6	13.0	34.9				58.2				246	-246	1
	-0.25	-0.35	-1.45	2.8	0.7	3.0				40.5				188	-188	1
	3.50	-0.75	-10.25	12.8	12.2	33.8				89.3				213	-213.2	1
	0.50	-4.50	-5.50	4.4	10.1	41.9				49.6				154	-154.4	1
	-1.00	-2.50	15.50											260	-262.8	1
	6.00	1.50	18.50	2.9	37.1			0.8				3.8		200	-197	1
				7.7	27.1				10.7				37.3	200	-200	1
				3.9	26.7				5.9				45.7	192	-191.9	1
				3.9	20.0				3.7				21.4	200	-199.5	1
	-2.00	1.00	-16.00	4.9	17.7				33.9				2036.7	360	-184	1
	-1.00	-0.00	-15.00	5.5	41.4				2.5				21.8	202	-201.8	1
	4.00	2.00	-7.00	11.5	48.6				2.8				17.6	384	-384	1
	-2.00	-2.00	-7.00	5.5	46.2				2.5				5.7	199	-199.4	1
	0.00	-0.00	-7.00	4.5	36.5				4.9				3.1	200	-199.6	1
	2.00	-0.00	-2.00	5.5	8.7				5.9				16.2	197	-197.0	1
	2.00	-2.00	2.00	13.5	25.6				6.5				39.4	243	-242.7	1

Table 9. Data compiled for second series of multiple regressions - Fill and Dump cycles. First thirteen columns are detector measurement values in counts. Each row represents 1 operational cycle. All cupola and mezzanine detector measurements were corrected for background radiation. Shaded blocks are actual data used in regression models.

Variable (dependent)	Operating Mode	Individual Continuous Variables			Overall Model		Regression Model Diagnostics				Mean for Continuous Variable	Product of Mean x Coefficient	Average Particles per Event	95% Confidence Interval	Average Number of Events/hr	Yearly Environmental Dose Equivalent counts			Final DE Value Used for Annual Estimate		
		variable	coefficient	p value	r2	p value	P PLOT	STUDENT	ACF	COOKS						Mean	95% CI	Mean	95% CI		
Channel 1	Fill	TIME	0.508	0.02	0.679	0.000	g	g	g	g	13.91	7.07	3.99	5.615 2.357	2	5978.8	0.396	0.061	0.360	1.276	
		RATE	-0.039	0.42			22.40	-0.87	2xsd=	-0.555											
		cn	-0.031	0.42			71.1667	-2.21	1.63												
	Dump	START	0.023	0.02	0.834	0.049	g	g	f	g	253.57	5.83	0.46	1.315 -0.402	2	885.0	0.046	0.102	0.014	0.544	
		cp	-0.108	0.04			32.53	-3.51	2xsd=	-0.516											
		m5n	-0.240	0.01			7.76	-1.86	0.86												
	Decay	cn	-0.162	0.08	0.396	0.000	g	f	g	f	0.09	-0.02	0.05	0.081 0.028	440	17609.2	1.191	1.775	0.582	0.630	
		cp	0.016	0.01			1.49	0.02	2xsd=	0.554											
		RATE	-0.141	0.00			-0.32	0.05	0.03												
Channel 3 Neutrons	Fill	cn	0.263	0.01	0.963	0.001	f	g	g	g	69.72	18.34	3.22	4.059 2.388	2	4835.1	0.222	0.404	0.238		
		TIME	-0.168	0.14			13.90	-2.31	2xsd=												
		m5n	0.040	0.32			82.21	3.29	0.84												
		m5p	-0.013	0.01			1218.90	-15.85													
		RATE	-0.012	0.74			20.75	-0.25													
	Dump	START	0.025	0.08	0.898	0.194	g	g	g	g	237.50	5.94	-0.17	0.448 -0.796	2	-260.7	-0.017	0.045	-0.030		
		cp	-0.064	0.18			35.01	-2.24	2xsd=												
		cn	-0.395	0.11			8.56	-3.38	0.62												
		m5n	-0.144	0.55			3.40	-0.49													
	Decay	START	-0.001	0.00	0.421	0.000	g	fg	fg	g	327.74	-0.33	-0.00	0.048 -0.051	440	-404.5	-0.027	1.063	0.907	1.827	
		RATE	-0.957	0.00			-0.33	0.31	2xsd=	0.086											
		cn	0.439	0.00			0.07	0.03	0.05												
Booster	-0.579	0.00	0.03	-0.01																	
Channel 2 Photons	Fill	cp	0.058	0.01	0.864	0.005	f	f	g	g	668.87	38.79	-12.01	-7.918 -16.102	2	-18015.0	-1.207	-0.7954	-1.6153		
		time	-0.686	0.28			14.78	-10.14	2xsd=												
		m5n	-0.519	0.02			78.04	-40.50	4.09												
	Dump	cn	0.483	0.29	0.881	0.067	g	g	g	g	8.56	4.13	-5.39	-2.330 -8.451	2	-8086.3	-0.542	-0.2542	-0.1494		
		cp	-0.344	0.03			35.00	-12.04	2xsd=												
		m5n	0.740	0.49			3.40	2.51	3.0604												
	Decay	RATE	1.515	0.14	0.441	0.001	g	g	fg	g	-0.33	-0.49	0.24	0.405 0.081	440	60295.6	5.380	6.9816	1.7960	3.631	7.836
		cp	0.032	0.23			1.06	0.03	2xsd=	-0.874											
		Booster	-0.515	0.41			0.03	-0.01	0.16												
Gun		0.479	0.13	0.13			0.06														
START		0.002	0.03	327.70			0.68														

Table 11. Results from second set of multiple linear regressions for the shed detectors for neutrons (channels 1 & 3) and photons (channel 2) for all storage ring operating modes. Independent variables include beam operating parameters and detector measurement values from the cupola and one "theoretical" detector (m5) mezzanine location (described in the text). m5 is in the directional line of the shed. All detector measurement values were corrected for background. The table is divided into four parts. The first (left, unshaded) lists the appropriate variables and regression model fit parameters (p values and r²). The next section (shaded) gives regression diagnostic test results (see text) for each regression. The third section (unshaded) uses data to calculate the mean radiations produced per event the 95% confidence intervals for these means. The fourth and final (shaded) section generates yearly mean dose equivalents for each radiation type and channel and then sums these quantities. Confidence intervals are calculated for all of the mean values.

The left section concerns the included regression model variables and model parameters that measure the "fit" of the model to the data. For each detector channel in the shed and for each operating mode, the significant variables that contribute to the regression model are listed along with their individual regression coefficients and p values. The continuous variables are abbreviated as follows: cn & cp - cupola neutron and photon counts, respectively; m5n & m5p - theoretical mezzanine detector (on column 5) neutron and photon counts, respectively; and the storage beam operating parameters of START, TIME and RATE. Even with the detector data extensive consolidation scheme, only "m5" had enough data points to use for the shed regression analyses. Fortunately, the orientation of this theoretical detector was in the general direction of the shed. Since it was previously shown that more radiation is produced at the mezzanine (particularly for hotspots) than in the cupola, it is logical that the "m5" detector measurements should play a significant role in all shed regressions. Mezzanine "hot spots" not directed towards the shed ("measured" by theoretical detectors m14 and m20) would not be expected to contribute to the shed regression models significantly. As mentioned, the hv Gun and Booster stati (which were the only remaining categorical variables) were included for the decay regression models. The next two columns follow with overall regression correlation coefficient (r^2) and p value. For this last stage of the model development, r^2 values of >0.90 and p values of <0.05 were desirable.

In the second, shaded section of the table are the regression diagnostic test results for each regression model. Since there was only one dependent variable on the left hand side of these equations, four types of regression diagnostic tests could and were performed on the individual equations. For each regression, the test results were listed across the top row. The result was either very good (v.g), good (g), fair (f), or poor (p). The tests conducted were:

- 1) probability plot (PLOT) of the residuals - a good result is a straight line
- 2) student (STUDENT) plot - a good result is evenly distributed points above and below zero
- 3) ACF plot - this showed how many values were outside of parenthetical limits
- 4) Cooks (COOK) plot - very good values are close to zero, good under ten, above that fair

The third section of the table is designed to predict the mean and 95% confidence interval of radiation produced for a given operation. To accomplish this, mean values for each included continuous variable were calculated from Tables 9 & 10 and listed in the "mean

for continuous variable" column. These mean values were then multiplied by their respective regression coefficient and summed in the "average particles per event" column. To calculate the 95% confidence interval(CI), statistical assumptions of linearity for the model; normal distributions for dependent variable and error terms; independence and homoscedasticity of the dependent variables. The CI was calculated with a formula of $\mu \pm 1.96 \sqrt{\sigma^2}$, where $\sigma^2 = (X'X)^{-1} \cdot \mu^2$ (mean square error of residuals).

To arrive at yearly DE estimates and confidence intervals, the fourth, shaded part of the Table was used. To get the yearly mean value, the number of events per 8 hour shift in the next column was multiplied by the "average particles per event". This product was then multiplied by number of shifts per year column (750 for environmental exposures). For the final dose equivalent, instrument conversion factors described under the Instrument Calibration section were used to convert counts to mrem.

Since the two neutron channels had virtually identical detectors, it was appropriate to average the two channels for each of the three operating modes. This was done and the 95% CI calculated by adding or subtracting to the mean, 1.96 times the square root of the combined variances. For the Fill Mode this formulae was

$$\pm 1.96 \sqrt{(1/4[\sigma^2_{\text{FILL channel 1}} + \sigma^2_{\text{FILL channel 3}}])}$$

Finally, the three, yearly DE for all three operating modes were summed and this time a 90% CI calculated by adding or subtracting to the mean, 1.65 times the square root of the combined variances according to the formula

$$\pm 1.65 \sqrt{(\sigma^2_{\text{FILL}} + \sigma^2_{\text{DUMP}} + \sigma^2_{\text{DECAY}})}$$

For neutron measurement regressions we evaluated channels 1 and 3. As mentioned these channels were combined to get the yearly DE. For channel 1, the Fill cycle regression equation had an overall correlation coefficient (r^2) of 0.679. This was much lower than channel 3 regression coefficient. It was encouraging to obtain a final DE value that was within 25% agreement. The channel 3 regression had a very good fit ($r^2 = 0.963$) and p value ($p=0.001$). The contributing independent variables were: cn, m5n, m5p, RATE and TIME. The detector measurement variables are listed in order of their significance to the regression model (based on the values of their regression coefficients). The individual p values indicated that the m5 neutron count ($p=0.09$), TIME ($p=0.14$), and RATE ($p=0.15$) may have had been

random contributors to the regression based on their p values (with $p = 0.05$ as significant). The final yearly dose equivalent (averaged over both channels) was 0.36 ± 0.92 mrem/year.

For the Dump mode, channel 3 again had a better fitting regression model than channel 1. For channel 3, the overall regression correlation coefficient was 0.898, however, it also had an unacceptably high overall p value of 0.194. For channel 1, the contributing independent variables were: START, cp, and m5n. The detector measurement variables are listed in order of their significance to the regression model (based on the values of their regression coefficients). The individual p values indicated that all of these variables contributed in a non-random way to the regression based on their p values and the acceptance of $p = 0.05$ as significant. The final yearly dose equivalent (averaged over both channels) was 0.014 ± 0.53 mrem/year.

For the Decay mode and with m5 detector values included in the variable pool, both channels 1 and 3 would not run with the regression software. Subsequently, they were eliminated and the regressions were repeated with the data from Table 10. The apparent price of eliminating the mezzanine detector values from the regression was a severe decrease in the value of the correlation coefficient of the models. Nevertheless, this was the only option available so these models were considered. After substituting the regression variable mean values, the Channel 3 regression model yielded a negative particle production rate. For channel 3, the overall regression correlation coefficient was 0.421 with an overall p value of 0.00. For Channel 1, the contributing independent variables were: cp, RATE, and cn. Based on the values of their regression coefficients, cp had a greater influence on the regression than cn. The individual p values indicated that the cupola neutron count ($p=0.09$) may have been a random contributor to the regression based on its p value and the acceptance of $p = 0.05$ as a significance level. The overall regression correlation coefficient was 0.396 and the p value was 0.00. The final yearly dose equivalent (averaged over both channels) was 0.582 ± 0.028 mrem/year. This was the only mode that did not include 0 in the 95% CI.

For photon measurements in the shed only one channel (2) was available. The Fill regression had a good fit ($r^2 = 0.846$) and an excellent overall p value ($p=0.005$). The contributing independent variables were: cp, TIME, and m5n. Based on the values of their regression coefficients, cp had a greater influence on the regression than m5n. The individual

p values indicated that none of the independent variables were chance contributors to the regression based on the acceptance at $p = 0.05$ as a significance level. Upon substituting the mean values for the variables, a negative "average particles per event" value was obtained. The final yearly dose equivalent was $-1.20 \pm .41$ mrem/year. The confidence interval did not include zero or any positive values. This was an illogical outcome. Unfortunately, unlike the neutron detection provisions, there wasn't a redundant channel to try.

The Dump regression for channel 2 had good overall fit parameters ($r^2 = 0.881$ and $p = 0.067$). The contributing independent variables were: cn, cp, and m5n. The detector measurement variables are listed in order of their significance to the regression model (based on the values of their regression coefficients). The individual p values indicated that the cupola neutron count ($p=0.09$) and mezzanine photon count ($p=0.49$) may have been random contributors to the regression based on the acceptance of $p = 0.05$ as a significance level. Like the preceding Fill regression model, upon substituting the mean values for the variables, a negative "average particles per event" value was obtained. The final yearly dose equivalent was $-.54 \pm 0.31$ mrem/year. Again, the confidence interval did not include zero or any positive values, the result was illogical and no redundancy of detector channels existed.

For Channel 2 during Decay cycles, a poor fitting model ($r^2 = 0.44$) with a good overall p value ($p=0.001$) was obtained. The contributing independent variables were: RATE, Gun, cp, START and Booster. The individual p values indicated that only the Start variable was a non-random contributor to the regression based on its p value ($p=0.03$) and the acceptance of $p = 0.05$ as a significance level. The final yearly dose equivalent was 5.38 ± 3.58 mrem/year. The 95% confidence interval did not include zero.

The success of the shed detector regression models provided impetus to repeat the shed regressions, but using detector measurements that were uncorrected for background at the m5 and cupola locations. The advantage of using such uncorrected data would be a tremendous saving of time in not having to manually correct the data. The tabulated data is shown in Table 12. The regression results are shown in Table 13. These tables are structurally identical to their corresponding tables with corrected cupola and mezzanine detector values (Tables 9 & 10, and 11 respectively).

Rather than review Table 13 in detail, a following summary follows. Overall, similar regression fit parameters and final yearly environmental dose equivalents were obtained.

	SHED DETECTORS			CUPOLA DETECTORS		MEZZANINE DETECTORS		OPERATING PARAMETERS		
FILL	Ch. 1 Neutron	Ch. 3 Neutron	Ch. 2 Photon	Cupola Neutron	Cupola Photon	m5 Neutron	m5 Photon	STAR (min)	RATE (mA/min)	TIME (min)
	1.40	3.15		37	903	50	1184	0	28.57	7
	4.40	8.07	-33.73	107	2912	135	3365	25	16.08	22
	-3.80	5.70	-17.10	94	2523	130	3112	0	21.11	19
	1.60	-0.00	-13.60	43	1067	45	1271	0	25.08	8
	5.20	2.60	-13.00	134	3585	160	4852	0	15.39	26
	1.20	1.20	-12.00	24	752	47	902	0	33.51	6
	1.60	1.60	-8.00	43	1031	43	1290	0	25.08	8
	0.90	1.35	-5.85	47	1150	54	1496	0	22.29	9
	0.00	1.20	-4.20	30	789	35	1023	150	7.9	6
	7.47	11.20	-0.93	1	4035	154	4731	0	12.51	28
DUMP	Ch. 1 Neutron	Ch. 3 Neutron	Ch. 2 Photon	Cupola Neutron	Cupola Photon	m5 Neutron	m5 Photon	STAR (min)	RATE (mA/min)	TIME (min)
	2.00	-2.00	2.00	14	116	7	122	243	-243	1
	-2.00	-2.00	-7.00	9	127	3	69	199	-199	1
	2.00	-0.00	-2.00	9	93	1	94	197	-197	1
	-1.00	-0.00	-15.00	4	124	3	102	202	-202	1
	0.00	-0.00	-7.00	5	125	5	78	200	-200	1
	-2.00	1.00	-16.00	5	100	34	2120	350	-350	1
	4.00	2.00	-7.00	12	139	3	98	384	-384	1
DECAY	Ch. 1 Neutron Count Rate	Ch. 3 Neutron Count Rate	Ch. 2 Photon Count Rate	Cupola Neutron Count Rate	Cupola Photon Count Rate	Gun	Booster	STAR (min)	RATE (mA/min)	TIME (min)
	0.13	0.01	0.78	0.34	80.48	0	0	350	-0.3	134
	0.20	0.18	-0.26	0.41	82.99	0	0	401	-0.41	329
	0.11	-0.01	0.96	0.28	82.26	0	0	280	-0.21	652
	0.18	-0.04	0.89	0.28	82.30	0	0	400	-0.3	89
	0.10	0.03	0.50	0.25	81.14	0	0	240	-0.2	448
	0.07	-0.06	0.23	0.23	80.73	0	0	222	-0.19	266
	0.21	0.17	-0.36	0.31	81.97	0	0	400	-0.538	166
	0.13	-0.10	0.53	0.21	80.68	0	0	250	-0.27	183
	0.25	0.14	-0.45	0.36	83.22	0	0	402	-0.531	85
	0.06	0.10	0.79	0.24	87.42	0	0	375	-0.21	680
	0.10	0.07	1.02	0.31	86.97	1	0	400	-0.51	133
	-0.05	-0.37	-0.10	0.30	81.62	0	0	250	-0.23	268
	-0.04	-0.38	-0.72	0.29	80.49	0	0	380	-0.301	274
	-0.04	-0.25	0.53	0.24	80.54	0	0	250	-0.29	134
	-0.03	0.04	0.67	0.19	85.62	0	0	350	-0.22	437
	-0.08	-0.10	0.48	0.23	83.93	0	0	230	-0.1326	445
	-0.09	-0.34	0.45	0.34	81.24	0	0	220	-0.195	359
	-0.10	-0.09	0.84	0.24	86.12	0	0	400	-0.22	223
	-0.10	0.30	0.73	0.25	78.91	0	0	400	-0.53	32
	0.07	0.10	0.37	0.45	86.60	1	0	400	-0.5	47
0.06	0.03	0.88	0.31	89.76	0	0	400	-0.31	95	
0.15	0.10	-0.67	0.39	82.55	0	0	400	-0.301	62	
0.08	0.30	0.75	0.36	80.11	0	0	374	-0.52	36	
-0.02	0.25	-0.07	0.96	90.52	0	0	200	-0.22	54	
0.00	0.10	-0.40	0.14	79.52	0	0	400	-0.54	21	
0.13	-0.13	0.80	1.35	97.65	1	1	238	-0.2	20	

Table 12. Data compiled for second series of multiple regressions for Fill, Dump and Decay cycles. All cupola and mezzanine detector are not corrected for background radiation. Each row represents 1 operational cycle. Booster and hv Gun are indicated as On (1) or Off (0).

Variable (dependent)	Operating Mode	Individual Continuous Variables			Overall Model		Regression Model Diagnostics				Mean for Continuous Variable	Product of Mean x Coefficient	Average Particles per Event	95% Confidence Interval	Average Number of Events/hr		Yearly Environmental Dose Equivalent courts		Final DE Value Used for Annual Estimate		
		variable	coefficient	p value	r ²	p value	F	T	ACF	COOK					Mean	95% CI	Mean	95% CI	Mean	95% CI	
Channel 1 Neutrons	FILL	cp	0.008	0.06	0.555	0.111	f	p	f	p	1874.70	15.00	2.11	3.861 0.360	2	3166	0.311	0.39	0.316	1.323	
		RATE	0.049	0.49			20.75	1.02	2xsd=	0.360											
		m5n	-0.163	0.13			85.30	-13.90	1.75												
	DUMP	start	0.033	0.01	0.870	0.030	d	d	f	f	253.60	8.37	0.13	0.904 -0.651	2	190	0.013	0.09	0.005	0.428	
		cp	-0.057	0.02			117.70	-6.71	2xsd=	-0.651											
		m5p	-0.004	0.01			383.30	-1.53	0.78												
	DECAY	cn	0.131	0.19	0.373	0.030	g	f	g	p	0.36	0.05	0.05	0.091 0.012	440	16992	1.326	2.40	2.160	2.107	
		cp	-0.002	0.21			83.67	-0.17	2xsd=	0.012											
		RATE	-0.123	0.56			-0.32	0.04	0.04												
		START	0.0004	0.36			331.23	0.13													
	Channel 3 Neutrons	FILL	cn	-0.053	0.03	0.949	0.003	f	d	f	d	56.00	-2.97	4.21	5.206 3.209	2	6311	0.951	0.92		
			TIME	0.044	0.49			13.90	0.61	2xsd=											
RATE			-0.054	0.32	20.75			-1.12	1.00												
m5p			-0.004	0.10	2322.60			-9.29													
m5n			0.199	0.02	85.30			16.97													
DUMP		START	0.027	0.01	0.955	0.024	g	g	g	g	253.60	6.85	-0.02	0.310 -0.357	2	48	-0.002	0.03			
		cn	-0.308	0.01			8.29	-2.55	2xsd=	-0.357											
		cp	-0.029	0.02			117.70	-3.41	0.33												
		m5n	-0.113	0.02			8.00	-0.90													
DECAY		cn	0.506	0.04	0.418	0.033	p	g	f	p	0.36	0.18	0.14	0.206 0.084	440	47820	5.188	4.52	2.481	3.381	
		cp	-0.006	0.01			83.67	-0.50	2xsd=	0.084											
		RATE	-0.473	0.17			-0.32	0.15	0.06												
	Booster	-0.446	0.12	0.04			-0.02														
	START	0.001	0.32	331.23			0.33														
Channel 2 Photons	FILL	cp	-0.046	0.01	0.982	0.001	f	f	g	g	1982.67	-91.20	-13.75	-11.726 -15.766	2	20819	-1.361	-1.18			
		cn	-0.248	0.00			58.11	-14.41	2xsd=												
		RATE	-0.145	0.21			19.88	-2.88	2.02												
		TIME	0.114	0.37			14.78	1.68													
		m5p	0.038	0.01			2449.11	93.07													
	DUMP	cn	1.395	0.04	0.961	0.019	g	g	g	p	8.29	11.56	-7.52	-5.340 -9.697	2	-11278	-0.756	-0.94			
		cp	-0.106	0.09			117.71	-12.48	2xsd=	-9.697											
		m5p	-0.002	0.48			383.29	-0.77	2.18												
		START	-0.023	0.44			253.60	-5.83													
	DECAY	cn	-0.820	0.12	0.478	0.005	f	g	f	p	0.36	-0.29	0.38	0.581 0.187	440	128784	8.485	12.88	6.956	9.907	
		cp	0.013	0.01			83.67	1.09	2xsd=	0.187											
		RATE	1.558	0.05			-0.32	-0.50	0.20												
Gun		0.788	0.05	0.12			0.09														

Table 13. Results from second set of multiple linear regressions for the shed detectors for neutrons (channels 1 & 3) and photons (channel 2) for all storage ring operating modes. Independent variables include beam operating parameters and detector measurement values from the cupola and one "theoretical" detector (m5) mezzanine location (described in the text). m5 is in the directional line of the shed. All detector measurement values were NOT corrected for back-ground. The table is divided into four parts. The first (left, unshaded) lists the appropriate variables and regression model fit parameters (p values and r²). The next section (shaded) gives regression diagnostic test results (see text) for each regression. The third section (unshaded) uses data to calculate the mean radiations produced per event the 95% confidence intervals for these means. The fourth and final (shaded) section generates yearly mean dose equivalents for each radiation type and channel and then sums these quantities. Confidence intervals are calculated for all of the mean values.

Summary of Regression Results and Total Predicted Yearly DE for the Shed

A summary of all the incorporated shed regression independent variables (corrected data regressions taken from Table 11 and Uncorrected data regressions taken from Table 13) is shown in Table 14. For each regression model where more than one detector measurement is used as independent variables, the detectors are ranked from greatest to least significance based on the value of their regression coefficients. Also, the individual p values for each of the independent variables for each regression model are ranked in the adjacent column. A single x in this column indicates a p value in the range .06 - .10, double xx means a p value of > .10. As anticipated, the appropriate storage ring operating parameters appear in all of the regressions, with the exception of the Channel 1 Fill regression for the uncorrected data set (where it was indirectly incorporated through the Rate parameter).

It was anticipated that the mezzanine detector data would have contributed more to the predictive strength of the shed regression models than the cupola detector values. This was the only the case for the Channel 3- Fill- uncorrected data regression. The other Fill and Dump regressions ranked the cupola detector(s) higher. This may have been due to greater shielding of the mezzanine detectors. This question could be better answered if the study were repeated with unhindered detectors and simultaneous mezzanine measurements at all of the theoretical detector locations. There were also not enough mezzanine measurement values to determine this comparison for the Decay cycles. What was apparent was that the Booster and hv Gun were factors for predicting shed radiation for Decay periods.

The final summed yearly dose equivalent results from both sets of regressions are listed in Table 15. In it, mean values and confidence intervals are given for corrected and uncorrected data sets. First the neutron results are discussed, then the photon and combined.

Based on the confidence intervals, the neutron results for the corrected and uncorrected data showed good agreement for the Fill and Decay operating modes. The lower confidence interval for both modes and both types of data were negative numbers, thus not eliminating zero from the range. The data did allow the generation of Decay regression models when mezzanine detector data was excluded from the pool of independent variables.

SHED CHANNEL	CYCLE	CORRECTED DATA SET		UNCORRECTED DATA SET	
		LIST OF COEFFICIENTS (Detector Values ranked in decreasing order)	COEFFICIENTS RANKED BY DECREASING P VALUE	LIST OF COEFFICIENTS (Detector Values ranked in decreasing order)	COEFFICIENTS RANKED BY DECREASING P VALUE
CHANNEL 1	FILL	TIME	1	RATE	xx
		RATE	xx	cp	1
		cn	xx	m5n	2
	DUMP	START	2	START	1
		cp	3	m5p	2
		m5n	1	cp	3
	DECAY	cp	2	Booster	xx
		RATE	1	START	xx
		cn	x	cp	xx
				cn	xx
			RATE	xx	
CHANNEL 3	FILL	cn	2	TIME	x
		m5n	x	m5n	xx
		m5p	1	m5p	1
		RATE	xx	RATE	xx
		TIME	xx	cn	2
	DUMP	START	1	START	1
		cp	4	cp	3
		m5n	3	m5n	4
		cn	2	cn	2
	DECAY	cn	1	cn	1
		START	2	START	2
		Booster	3	cp	3
		RATE	4	Booster	4
			RATE		
CHANNEL 2	DECAY	RATE	1	RATE	2
		cp	x	Gun	3
		START	2	cp	1
		Gun	xx	cn	xx
		Booster	3		

Table 14. Summary of all incorporated shed regression independent variables (corrected data regressions taken from Table 11 and Uncorrected data regressions taken from Table 13). For each regression the detectors are ranked from greatest to least significance based on the value of their regression coefficients. Next to each coefficient is the p value ranking of that coefficient in that particular regression. A single x in this column indicates a p value in the range 0.06-0.10, double xx means a p value of > 0.10.

STORAGE RING OPERATION MODE	YEARLY DOSE EQUIVALENT from CORRECTED DATA (mrem)				YEARLY DOSE EQUIVALENT from UNCORRECTED DATA (mrem)			
	NEUTRONS		PHOTONS		NEUTRONS		PHOTONS	
	MEAN	95% CI	MEAN	95% CI	MEAN	95% CI	MEAN	95% CI
FILL	0.36	(0.56) - 1.28	(-1.21)	(-0.90) - (-1.90)	0.32	(0.69) - 1.32	(-1.30)	(-1.10) - (-1.50)
DUMP	0.01	(0.52) - 0.54	(-1.74)	(-0.22) - (-0.85)	0.01	(0.42) - 0.43	(-0.76)	(-0.34) - (-0.97)
DECAY	0.58	0.55 - 0.61	5.38	1.80 - 8.96	2.16	2.12 - 2.20	8.50	4.13 - 12.86
TOTAL	0.96	0.09 - 1.88	3.63	(0.57) - 7.84	2.48	1.58 - 3.34	6.36	3.91 - 8.81

TOTAL FOR BOTH TYPES OF RADIATION	MEAN	90% CI	MEAN	90% CI
	4.29	0.04 - 8.63	8.84	6.23 - 11.45

Table 15. Summary of yearly dose equivalents predicted from the two sets of regression models (corrected and uncorrected data sets). All numbers are in units of mrem. Numbers in parenthesis are negative values. Shaded areas are illogical results i.e. net negative dose equivalent values, while statistically valid, are not possibly in reality. These occurred for photon DE, where detection of radiation is more difficult due to higher relative background gamma radiation values.

regressions. Poor fits were obtained for both corrected and uncorrected data regression models (r^2 ranges from 0.373 to 0.421 from tables 11 and 13). Further, the resultant means between the two data sets had an error of almost 300%, much greater than for the previous operating modes. This is understandable, given the much longer time intervals for the Decay cycles and the lack of correction for background radiation. One encouraging finding was the confidence intervals for both Decay regression models were tight and did not include zero.

The mean DE value and the 95% confidence intervals summed for all three operating modes were 0.96 (0.09 - 1.88) mrem/year and 2.48 (1.58-3.34) mrem/year for the corrected and uncorrected data regression models, respectively. The overall good agreement from the two methods is encouragement for future use of the uncorrected measurement data, at least for the Fill and Dump modes, which would result in a large savings of time and effort.

For the shed photon, models could not be generated that could predict a positive net radiation dose at shed for the Fill and Dump cycles. Both mean values and confidence intervals for corrected and uncorrected data regressions were all negative (as the table shading highlights). Unlike the neutron detection, there was not a redundant photon detector in the shed. However, it is unlikely that another detector would have made a difference. The problem is that the background cosmic gamma radiation is over an order of magnitude larger than the background neutron radiation. Photon exceedances above background due to the accelerator operation are thus nearly impossible to detect.

Successful regression models were obtained for the Decay mode; however, mezzanine values had to again be excluded due to a shortage of data points. The means and 95% CI are listed in table 15 for both the corrected [(5.38 (1.80 - 8.96) mrem/yr] and uncorrected data [8.50 (4.13 - 12.86) mrem/yr] sets. The mean values are within a respectable 58% error margin. However, upon summing over the three operating modes, only the uncorrected results in a 95% CI that doesn't include zero. Interestingly, for both neutron and photon summations, the uncorrected data yielded both higher means and more confidence that the dose equivalent wasn't undetectable.

Finally, the yearly DE for both types of radiation were summed. The corrected data models yielded 4.29 (0.04-8.63) mrem/yr and uncorrected 8.89 (6.23 - 11.45) mrem/yr. These two were not averaged. 90% confidence intervals were used to avoid the inclusion of zero for the corrected set, which was the final yearly DE reported for this work.

Regression Model for Yearly Dose Equivalents Received on the Mezzanine

In addition to the regression models for predicting yearly environmental dose equivalent at the shed, a similar method was used to predict yearly occupational exposures on the mezzanine. The current architectural plan for the mezzanine is to use the space for offices. It would be useful to estimate the likely occupational exposures at these locations. Also, the regression model predictions can be compared to the two existing prediction methods (analytic method and Morse Code modeling).

For each mezzanine regression model, the dependent variable was to be the measured radiation value at specified mezzanine detector locations, preferably at the demonstrated "hot spots". The corrected values of these measurements were to be used. Again, a shortage of measurements for actual detectors lead to using the theoretical detector positions described earlier. The theoretical detectors that included mezzanine hotspots were m1 [1], m20 [19,20] and m14 [13,14,almost16] (original column positions bracketed for hotspots - refer back to Table 8 and Figure 8 to see the locations involved). The dependent variables were comprised of the storage ring operating parameters START, TIME and RATE, measured cupola neutrons and photons and the categorical variables for hv Gun and Booster ring stati.

The results of the regressions are shown in table 15. This table has a similar layout to table 12 with two exceptions. First, only the Fill cycles produced reasonable models. Thus, the idea of predicting a yearly DE with confidence intervals was not to be realized. Second, a difference exists in the last two columns where a high and low value is given for the yearly dose equivalent in mrem. This is because of the unfortunate mistake of not recording the mezzanine and cupola detectors numbers. However, this error proved minor (ranging from 1 to 7%), as can be seen in the differences between the high and low estimate columns. This is because the calibration factors were within 7% for the neutron detectors and 0.1% for the photon detectors. Further, the significance of these errors was small compared to the fact that for the shed neutron detector only a nominal conversion factor was available (these shed detectors were the last generation of prototypes). Nevertheless, to be conservative both high and low yearly dose equivalents were calculated for the mezzanine locations and cupola , using the larger and smaller calibration factors, respectively.

Radiation Type	Operating Mode	Variable (dependent)	Individual Continuous Variables		Overall Model		Regression Model Diagnostics				Mean for Continuous Variable	Product of Mean x Coefficient	Average Particles per Event	Average Number of Events/8 hr	Yearly Environmental Dose Equivalent			
			variable	coefficient	p value	r2	p value	PLOT	STUDENT	ACF					COOKS	counts	High Estimate mrem	Low Estimate mrem
Neutrons	FILL	m2n	time	75.69	0.23	0.990	0.151	g	f	g	f	21.14	1600.15	162.51	2	81253.06	9.596	9.019
			rate	93.14	0.29							15.30	1425.00					
			start	5.26	0.26							50.00	262.75					
			C	-3125.39	0.23								-3125.39					
	m20n	time	13.27	0.00	0.940	0.000	g	f	f	g	7.00	92.90	97.70	2	48848.50	5.769	5.422	
		C	4.80	0.72								4.80						
		m14n		not enough data														
	DUMP		all detectors resulted in poor models									USE MEAN VALUE	28.40	2	14200.00	1.677	1.576	
	DECAY		all detectors resulted in poor models									USE MEAN VALUE	0.04	440	4400.00	0.520	0.488	
	Photons	FILL	m2p	time	124.53	0.01	0.807	0.01	g	g	f	g	21.14	2632.61	3578.01	2	1789006.24	3.783
C				945.41	0.19								945.41					
m20p				time	139.36	0.00							0.846	0.00				
C		274.40	0.28		274.40													
m14 p		not enough data																
DUMP		all detectors resulted in poor models									USE MEAN VALUE	59.40	2	29700.00	0.063	0.062		
DECAY		all detectors resulted in poor models									USE MEAN VALUE	2.18	440	240020.00	0.508	0.501		

Table 1. Results from multiple regression for the MEZZANINE. Both types of radiations and all three storage ring operation modes are shown. The only independent variables used were beam operating parameters. All detectors values (dependent variables) were corrected for background. Mezzanine detectors m2, m20 and m14 were theoretical detector locations described in the text. Individual independent variable coefficients and p values are listed. The overall regression model fit, p values and regression diagnostic results (see text) are given. The mean value for each variable was determined from tables 9-11 and entered in the appropriate column. This mean value was then multiplied by the regression coefficient to give the "particles per event" value. The number of events per 8 hour shift was multiplied by this column and then multiplied by (5 x 50) to get yearly particles produced. Finally, the yearly particle counts column was multiplied by the large and small conversion factors (explained in text) to yield annual occupation dose equivalent.

For the mezzanine Fill cycles, a good fit was obtained for both "m20" photons (m20p) and neutrons (m20n). TIME was the only independent variable for both, but it had a very good p value of 0.00. The RATE parameter was expected to be a predictor variable, but it reduced the overall correlation coefficient of the regression model. More data points might have changed this. The regression diagnostics were satisfactory. The mean values were calculated from the data in Table 9 and the final high and low dose equivalents were computed for neutrons and photons as 9.596 / 9.019 and 3.783 / 3.734 mrem/yr, respectively.

For the m2 detectors, the correlation coefficient was also good, though slightly less in value than the "m20" value. To increase the r^2 value for the m2n regression from 0.7 to 0.9, the START variable had to be included. This was not desirable because the mean START value did not seem like a logical or useful number. The m2n neutron regression overall p value was 0.136, higher than the target value of 0.05. Overall, this is not a good model for "m2" neutron production for filling. The "m2" photon regression was a good fit. The final high and low dose equivalents were computed for neutrons and photons as 5.769 / 5.422 and 1.322 / 1.304 mrem/yr, respectively.

For all of the theoretical detectors, neither the Dump, nor the Decay cycles had good fitting regression lines for either photons or neutrons. Accordingly, to generate 8 hour particle yields, the mean minute rate of radiation production was inserted into the "average particles per event" column and multiplied through to obtain yearly dose equivalent values.

The conservative dose equivalents for detectors m2 and m20 are in Table 16 below.

STORAGE RING OPERATION MODE	m2-Theoretical Detector Occupational DE (mrem)		m20-Theoretical Detector Occupational DE (mrem)	
	NEUTRONS	PHOTONS	NEUTRONS	PHOTONS
FILL	9.6	3.78	5.77	1.32
DUMP	1.68	0.06	1.68	0.06
DECAY	0.52	0.5	0.52	0.50
TOTAL	11.8	4.34	7.97	1.88
TOTAL FOR BOTH TYPES OF RADIATION	16.12		9.85	

Table 16. Summary of yearly occupational dose equivalents predicted two theoretical detector locations on the mezzanine. Mezzanine "Hot spots" corresponding to column numbers 9, 13 and 14 are not represented.

Comparison of Predictive Regression Model Results from this Work to the Previous Analytic and Morse Code Modeling Results

In table 17, the results from this work (aptly labeled the empirical/statistical method) are assembled with the predictions from the Morse Code Model, the Analytic Method, and the original on-off time averaging schemes (both the standard and worst case scenarios- see app. I). For this work, the environmental dose equivalent values from table 15 are entered.

LOCATION & TYPE	YEARLY DOSE EQUIVALENTS (mrem/year)				
	Empirical/ Statistical Model	Morse Code Modeling	Analytic Method	On-Off Averaging	
				standard	worst case
mezzanine -occupational	(m20) 9.85 (m2) 16.14	2.81(ave)	330		
shed -environmental	4.29 (0.04-8.63)	0.68	11	0.45	4.50

Table 17. Comparison of yearly dose equivalents generated by this work (empirical / statistical method), Morse Code Modeling and the Analytic Method used in Shielding Design for the ALS.

Based on the mean values arrived at by this work, it is seen that the Morse Code modeling under predicts the shed value and the analytic method (used for shielding calculations) overpredicts it (especially for the occupational DE). The Morse Code and Analytic methods both underestimated the actual concrete thicknesses in their results. They both used conservative values for storage ring current (800 mA) and both of these methods use an energy balance approach that does not adequately treat either variable filling efficiencies or the random dump events. The main difference in these latter two methods lies in how the radiation producing showers are mathematically handled and in skyshine transport equations. Further, locations and distances to the detectors are not specified in the Analytic

Method. All things considered and given the large sources of uncertainty mentioned in various sections throughout this paper, there is remarkably good agreement amongst the shed results.

The means from the on-off worst case averaging method, which was the predecessor of this work, did show remarkable, though fortuitous, agreement with the result from this work. Unfortunately, confidence intervals were not calculated for the former to compare them with the ones determined in this work.

The unexpected finding of this work is the larger contribution to the yearly DE by the photons produced during accelerator operation. Numerous factors make this finding suspect including, the lack of a redundant photon detector in the shed, the lack of adequate mezzanine measurement values to input into the regression, and the likely background correction errors introduced by the high relative photon background radiation. Indeed, the most improvement for this work would be made through adaptations to address these problems discussed under the recommendations section. For the Table 17 values, all three modeling methods used the same operational schedule (3 shifts/day and two fills/ shift). In reality, this only holds for Wednesdays through Fridays. The accelerator is generally not on until late Monday afternoons. From that time to the routine operation on Tuesday midnight physics experiments are conducted which are characterized by a much greater frequency of Fills, Dumps and Off periods; although they seldom achieve beam currents of 100 mA. The two shift shortage can easily be handled by multiplying the final results by 13/15. Characterizing the physics experimentation periods would require a much larger data gathering and analysis effort. The only justification for such a massive effort would be the elimination of the shed detectors altogether, and this issue has a regulatory answer of negative.

For the occupational DE received on the mezzanine, similar relationships hold between the three methods, except the analytic method severely overpredicts the yearly DE. This fact combined with the difference with the Morse Code method for the shed results suggests the difference in the two methods is in the radiation shower calculations and not in the skyshine scattering equations. The theoretical values reported for this work are inclusive of mezzanine "hot spots" whereas, those from the Morse Code are average mezzanine values. In addition, the Morse Code modeling underestimates the DE because of incorrect shielding parameters and neglecting photons and high energy neutrons.

RECOMMENDATIONS

This empirical/statistical approach to estimating the yearly dose equivalent was successful in that it presented the most accurate and statistically confident estimates for environmental dose equivalents at the ALS to date. Possibly and or more importance, it was demonstrated that logical, well-fitted regression models can be constructed that are of utility for conducting this task. Below, I have summarized the steps required to improve upon this technique. However, prior to engaging in this work, the question of whether it is worth the effort needs to be answered. If a reasonably accurate, automatically-generated, prediction of radiation dose levels is acceptable in lieu of actual site measurement under regulatory guidelines, then I believe the need for these remote detectors and the unpleasant task of continual correcting for background radiation can be eliminated. Arguing against this, it is unlikely that the action level of 10 mrem/yr at the site boundary is being exceeded. The upper confidence level of our findings was 8.6 mrem/year. Nevertheless, there is considerable uncertainty in these results due to the poor neutron decay regression model and all of the photon regressions.

The greatest problem with all of the regressions was a shortage of data, particularly from key mezzanine positions. Repeating the study could minimize this and other problems encountered and increase the overall confidence in the findings. If this work were to be further pursued, the goal should be to develop a single, multivariate regression model, that is, one overall regression equation as opposed to the three separate regressions generated in this work. Following are recommendations to improve the process of generating such a multivariate regression model. They are not in any particular order.

- ▶ *Verify with more data that the theoretical detector locations on the mezzanine are indeed the optimal locations to monitor "hot spots" and mount sets of detectors on the actual sites.*

- This is to compensate for the shortage of data points in this work. These need not be permanent as ideally only two sets would be needed . Also, mounting above the crane track with the base of the instrument pointed towards the oncoming beam and projected out from the pole to avoid scattering.

- ▶ *Mount permanent detectors in the cupola , but below the steel hub. Provide remote communications to this site.*

- This is to avoid shielding of the detector and avoid the unpleasant climb to the cupola every week that this work required.

- ▶ *Replace the shed detectors in channels 1 and 3 with the new remmeters. Replace channel 2 with a larger G-M tube and add another G-M tube to channel 4.*

- This is to have the most environmentally resistant and sensitive detectors in the shed. The backup photon detector could serve as an additional set of data to avoid having to use a zero value(much in the same way the two neutron channels worked in this study).

- ▶ *Automatically synchronize all detectors AND the control room network server to the WWV standard time.*

- This will diminish uncertainty associated with timing errors.

- ▶ *Wait until the next generation of dataloggers (with more ROM) to be produced . Specifically immunity from interrupts and precisely initiated wake-ups and recording intervals need to be achieved.*
 - This will eliminate the true drudgery of this task of "cleaning up spreadsheet" and trying to match corresponding time intervals

- ▶ *Change the intervals in the shed to one minute for the study and change the control room data logging to 30 second intervals.*

- ▶ *Combine the control room spreadsheets into one or better still, write a program that bypasses the spreadsheet altogether. In the future, the program could input into the model directly and avoid the use of mean variable values.*

- ▶ *Include the experimental physics weekly periods in the model, to evaluate the effect of more frequent but less intense fills and dumps.*

With the modifications in place, I estimate one man-year to complete the work.

CONCLUSION

This work showed that predictive models for radiation generation can be constructed by making measurements using detectors at the (environmental) location of interest and then regressing the in-close detector measurements to those simultaneously made at the location. Using such models, a mean yearly environmental dose equivalent due to the ALS of 4.3 mrem / year (with a 90% CI of (0.04 - 8.63) mrem/ year) at the location of the monitoring shed. This overall value was calculated based on averaged values for averaged beam operating parameters and detectors located in the cupola of the dome and on the mezzanine (at a position in the same general direction of the environmental monitoring shed). All radiation detector measurement values were individually corrected for background radiation. This value fell in between the Morse Code Skyshine modeling value and radiation shielding calculations. Both of these latter methods had erroneous assumptions about operating parameters and shielding types and thicknesses. Nevertheless, given the many sources of uncertainty of these methods the agreement within on order of magnitude was reasonable. Further, there was remarkable agreement with the original On-Off Worst case scenario method developed as a predecessor to this work. It is suspected, however, that this was a chance result.

Three reasonable assumptions were made to complete this work. First, all radiation detected at the shed was due to either the ALS or the solar radiation (background). Other accelerators are present at LBL but they are much farther away and were not very active during this study. Second, that the physics experimentation that occurs during the first four workshifts of every week are not much different in radiation production than the standard shift. The conversion coefficients from neutron fluence to ambient dose equivalent used with the remmeters were those adopted in ICRP publication 51(1987). Third, shed measurements

were made independently of each other. While an element neutron scattering from one detector to another was possible, it was not likely.

A number of recommendations to repeat and improve this work were suggested and included better detector mounting locations, improvements to the dataloggers used to store the data, improved timing synchronization between detectors and the control room server and specific locations for setting up more detectors. Since an earthquake occurred shortly before the commencement of this study occurred, and it had some affect on prior, typical beam position magnet settings, it is possible that the model estimates could change. Prior to conducting another involved project of this type, estimated to require at least one man-year, the benefits of such a work need to be evaluated. If greater confidence is required in this final estimate, then more and better data would be appropriate. If modeled results can replace the detectors in use at the shed and the tedious job of weekly reviewing the data, then the work should be worth pursuing. If additional health physics research were the goal, it may be advisable to utilize neutron spectroscopy techniques rather than remmeters.

In the course of this work, "hotspots" were identified on the mezzanine area, although none of them indicated a yearly DE above 20 mrem. Based on this work, there should be no problem with locating offices in the mezzanine area.

Since remmeters were the neutron detectors of choice and the detectors were partially shielded by steel for both in-close locations, not much insight was gained on the energies of the particles reaching the detectors. However, the mezzanine:cupola ratio for neutrons and photons (corrected for background) was 2.4 and 1.4 respectively. The differences could not be explained by the inverse square law of radiation degradation alone. Since giant resonance neutrons are isotropic, the implication is that a considerable proportion of the stray radiation field is due to high energy neutrons scattered in the forward angle. Neutron spectroscopy would be required to investigate this matter further.

REFERENCES

1. Maddox, B.J., Shapiro, J., Shurcliff, W.A.; "Radiation Levels Adjacent to City Streets Close to the Cambridge Electron Accelerator"; in Proc. First Intl. Congr. Radiation Protection, Pergamon Press, Oxford, 1968
2. Dutrannois, J., Baarli J., "Radiation Hazard Near High-Energy Accelerators and Occupational Exposures"; in Proc. First Intl. Congr. Radiation Protection, Pergamon Press, Oxford, 1968
3. Jenkins, T.M., "Neutron and Photon Measurements through Concrete from a 15 GeV Electron Beam on a Target- [Comparison with Models and Calculations"; Nuclear Instruments and Methods 159, 1979, p. 265-288
4. Birattari, C.; Esposito, A.; Fasso, A.; Ferrari, A.; Festag, J.G.; Hofert, M.; Nielsen, M. Pelliconi, M.; Faffnsoe, Ch.; Schmidt, P.; Silari, M.; "Intercomparison of the Response of Dosimeters used in High Energy Stray Radiation Fields"; Radiation Protection Dosimetry, Vol. 51, No. 2 pp. 87-94(1994)
5. Ajemian, R.C., Collins, H.E.; "Analysis of Environmental Radiation Monitoring at Lawrence Berkeley Laboratory"; LBL Report in press
6. 1-2 GeV Synchrotron Radiation Source; Conceptual Design Report - July 1986, LBL Pub-5172
7. Young, J., et al; "Status Report on the Advanced Light Control System", LBL 34776
8. Thomas, R.H. and Stevenson, G.R.; "Radiological Safety Aspects of the Operation of Proton Accelerators; IAEA, Vienna, IAEA Technical Report Number 283 in Swanson, W.P. and Thomas, R.H., "Dosimetry for Radiological Protection at High Energy Particle Accelerators", LBL- Report 24119 Rev. April 1989
9. Swanson, W.P. and Thomas, R.H., "Dosimetry for Radiological Protection at High Energy Particle Accelerators", LBL- Report 24119 Rev. April 1989
10. Patterson, W., Thomas, R.H.; Accelerator Health Physics, Academic Press, Ny, NY, 1973
11. DeStaebler, H., Jenkins, T.M., and Nelson, W.R., (1968). Shielding and Radiation. In "The Stanford Two Mile Accelerator," (R.B. Neal, ed.) Ch. 26 (Benjamin, New York), pp. 1029-1067 in Swanson, W.P. and Thomas, R.H., "Dosimetry for Radiological Protection at High Energy Particle Accelerators", LBL- Report 24119 Rev. April 1989
12. Dinter, H. and Tesch, K., (1977). Dose and shielding parameters of electron-photon stray radiation from a high energy electron beam. Nucl. Instrum. Methods 143, 349-355 in Swanson, W.P. and Thomas, R.H., "Dosimetry for Radiological Protection at High Energy Particle Accelerators", LBL- Report 24119 Rev. April 1989
13. Swanson, W.P. (1979), Radiological Safety Aspects of the Operation of Electron Linear Accelerators., IAEA, Vienna

14. Tesch, K.; Neutron Dosimetry in the Energy Range between 10 and 100 MeV", Nuclear Instruments and Methods, 83(1970) 295-299
15. Swanson, W.P., "Calculation of Neutron Yields Released by Electrons Incident on Selected Materials", Health Physics, Vol. 35 (1978) pp. 353-367
16. Swanson, W.P., "Improved Calculation of Photoneutron Yields Released by Incident Electrons", Health Physics, Vol. 37 (1979) pp. 347-358
17. DeStabler, H.; "Transverse Radiation Shielding for the Stanford Two-Mile Accelerator", USAEC Report SLAC-9, Stanford Linear Accelerator Center, Nov. 1962
18. Jenkins, T.M.; "Neutron and Photon Measurements Through Concrete From a 15 GeV Electron Beam on a Target- Comparison with Models and Calculations"; Nuclear Instruments and Methods, 159(1979)pp. 265-288
19. Moyer, B.J., "Evaluation of Shielding Required for the Improved Bevatron" LBL Lab Report UCRL-9769, June 1961 in Accelerator Health Physics, H. Wade Patterson and Ralph H. Thomas, Academic Press, NY 1973
20. Routti, J.T., Thomas, R.H.; "Moyer Integrals for Estimating Shielding of High Energy Accelerators, Nuclear Instruments Methods, 76, 157(1969) in Accelerator Health Physics, H. Wade Patterson and Ralph H. Thomas, Academic Press, NY 1973
21. McCaslin, J.B.; "Radiation Safety and Shielding"; ALS-4/HPN-158
22. Lindenbaum, S.J.; Brookhaven National Laboratory Proton Synchrotron, in Proceedings Conference on Shielding of High-Energy Accelerators, New York, April 11-13, 1957 USAEC TID-7545 in Rindi, A. and Thomas, R.H.; "Skyshine- A Paper Tiger"; Particle Accelerators, 1975 Vol. 7, pp.23-39
23. Case, K.M., de Hoffman, F., Placzek G.; Introduction to the Theory of Neutron Diffusion, Vol. 1, Los Alamos, 1953 in Patterson, H.W.; Thomas, R.H.; Accelerator Health Physics, Academic Press, New York, 1973
24. Ladu, M., Pelliconi, P., and Verri, G.; "A Contribution to the Skyshine Study"; Nuclear Instruments and Methods, 62, 51(1968) in Rindi, A. and Thomas, R.H.; "Skyshine- A Paper Tiger"; Particle Accelerators, 1975 Vol. 7, pp.23-39
25. Dakin, H.S. (Lawrence Radiation Laboratory); private communication to R. H. Thomas in "Skyshine- A Paper Tiger"; Particle Accelerators, 1975 Vol. 7, pp.23-39
26. Thomas, R.H., "The Proton Synchrotron as a Source of Radiation", in Engineering Compendium on Radiation Shielding, (Springer-Verlag, Berlin, 1968), Vol. 1 in "Skyshine- A Paper Tiger"; Particle Accelerators, 1975 Vol. 7, pp.23-39

27. Stevenson, G.R., Thomas, R.H.; "A Simple Procedure for the Estimation of Neutron Skyshine from Proton Accelerators", Health Physics, Vol. 46, No. 1, 1984, pp. 115-122
28. Hack, R.C., Health Physics in PLA Progress Report for 1966 RHEL R/136 edited by C. Baty and J.M. Dickson, Chpt. 9, in "Skyshine- A Paper Tiger"; Particle Accelerators, 1975 Vol. 7, p.23-39
29. Moin-Vasiri, M.; "Monte Carlo Calculation of "Skyshine" Neutron Dose from ALS", LBL 29762, June 1990
30. McCaslin J.B., Thomas, R.H.; " Practical Neutron Dosimetry at High Energies", Paper Read at the European Seminar on Radiation Protection Quantities for External Exposure at Physikalisch-Technische Bundesanstalt, Braunschweig, FRG
31. Tesch, K.; "Neutron Dosimetry in the Energy Range Between 10 and 100 MeV", Nuclear Instruments and Methods, 83(1970), pp.295-299
32. Andersson, I.O.; Braun, J.; " A Neutron Rem Counter", Nukleonik, Band 6, Heft 5 pp.237-241
33. Hankins, Dale, E.; " A modified A-B Remmeter with Improved Directional Dependence and Thermal Neutron Sensitivity"; Health Physics, 1978 Vol.34, pp.249-254
34. Brittari, C., Ferrari, A., Nuccetelli, C. Pelliccioni, M., and Silari, M.; "An Extended Range Neutron Rem Counter", Nuclear Instruments and Methods in Physics Research, A297(1990)250-257
35. Brittari, C., Esposito, A., Ferrari, A., Pelliccioni, M., and Silari, M.; "Calibration of the Neutron Rem Counter LINUS in the Energy Range from Thermal to 19 MEV"; Nuclear Instruments and Methods in Physics Research, A324, (1993), pp. 232-238
36. Brittari, C., Esposito, A., Ferrari, A., Pelliccioni, M., and Silari, M.; "Measurements and Characterization of High Energy Neutron Fields"; Nuclear Instruments and Methods in Physics Research, A338(1994)534-543
37. Sun, R.K., Krebs G.F., Smith A.R.; Hsu H.H.; "A Neutron Dose Detector with REM Response to 1 GeV"; LBL report LBL-32347, July 1992
38. Oda, K., Mukai, H., Koyama, H., Yamamoto, T. and Kawansihi, M. & Nakamura, T.; "Measurement of Neutron Dose Equivalent in Pulsed and Mixed Radiation Field Around an Electron Linear Accelerator";
39. Nachtigall, D., "Determination and Accuracy of Results of Rem-Counter Measurements" in Conference on Radiation Dose Measurements, Their Purpose, Interpretation, and Required Accuracy in Radiological Protection, European Nuclear Energy Agency, Stockholm, 1967, p391-415

Appendix i - On-Off method for Calculating ALS Site Dose Equivalent

Summary of Monthly Reports On Site Boundary Radiation Dose Reports

by Robert Ajemian

I. Dose Equivalent Calculation

Ten minute data intervals were provided from EHS for the four channels in the shed. Channels one and three had identical, lead lined remmeters, channel 2 had a G-M counter and channel 4 had an unlined remmeter. These ten minute intervals were summed to give 24 hour averages. All values were in mrem. Plots of these are seen in figure 1.

The monthly dose equivalent was calculated in a spreadsheet, such as the one shown in figure 2. The procedure was as follows. The 24 hour daily averages were listed in the four columns to the left. In the Acc-on column it was indicated whether the accelerator was operating that day or not. Based on that the data was segregated into on columns or background columns and these columns were averaged and standard deviations were calculated. The background average was subtracted from the on average to give the net daily dose (NDD). The NDD was multiplied by the number of days on to give the net monthly dose (NMD). Standard errors were calculated for both of these. Yearly cumulative values (YR-CUM) were the cumulative monthly sums from this process. A yearly projected amount (Yr-P) was calculated by multiplying the YR-CUM up to that month by 12/number of that month.

Two "sensitivity" analyses were performed. The first was to eliminate all negative values of net monthly doses in generating the yearly cumulative dose equivalent. The second was to calculate a "worst case" scenario. For this, rather than using average on and background values to get the net monthly dose, the highest on value and the lowest off value were used. This was done every month and the yearly cumulative was also calculated.

II. Results

The mean monthly values +/- 2 standard errors are shown in figure 3 for channels 1&3 (neutrons) and channel 2 (photons). Although most of the mean values are above zero, almost all of the confidence intervals include zero. Thus, it can not be stated that the net result is due to anything other than chance. A plot for monthly dose equivalent is shown in figure 4 using channel 1)neutrons and channel 2 (photons). Yearly projected amounts are listed in the table:

	standard method		sensitivity- no negatives		sensitivity- worst case scenario	
	6 month	year-pr	6 month	year-pr	6 month	year-pr
neutrons	0.15	0.30	0.155	0.31	0.95	1.9
photons	0.055	0.11	0.07	0.14	1.30	2.6
total	0.205	0.41	0.225	0.45	2.25	4.5

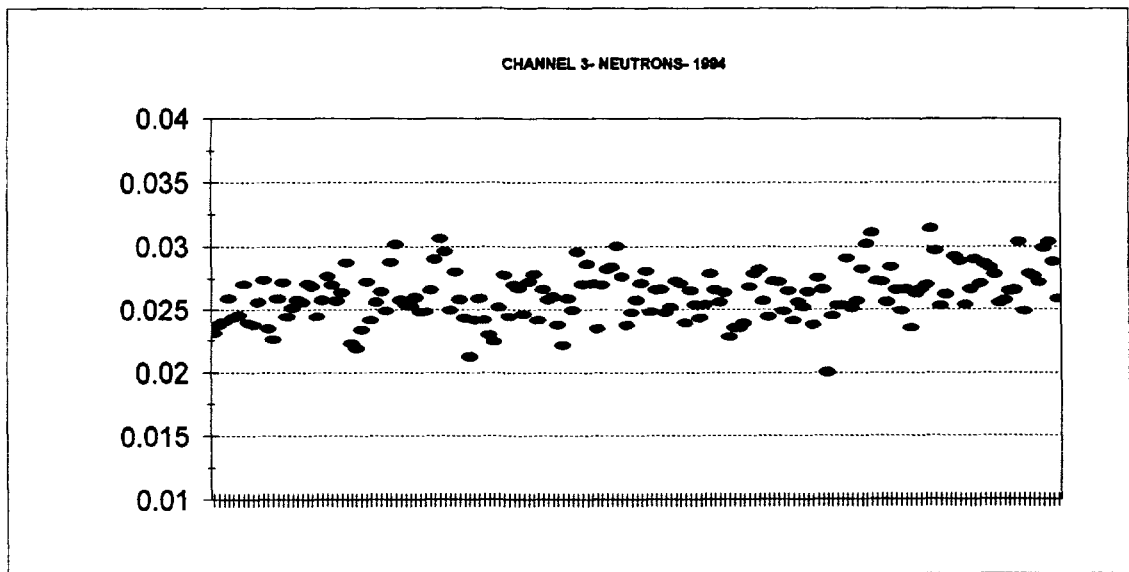
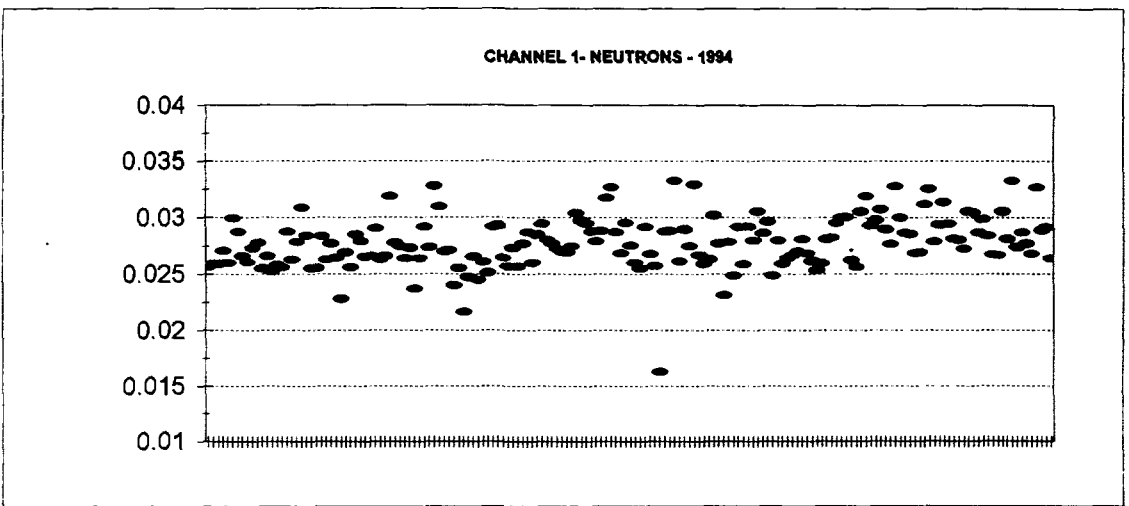
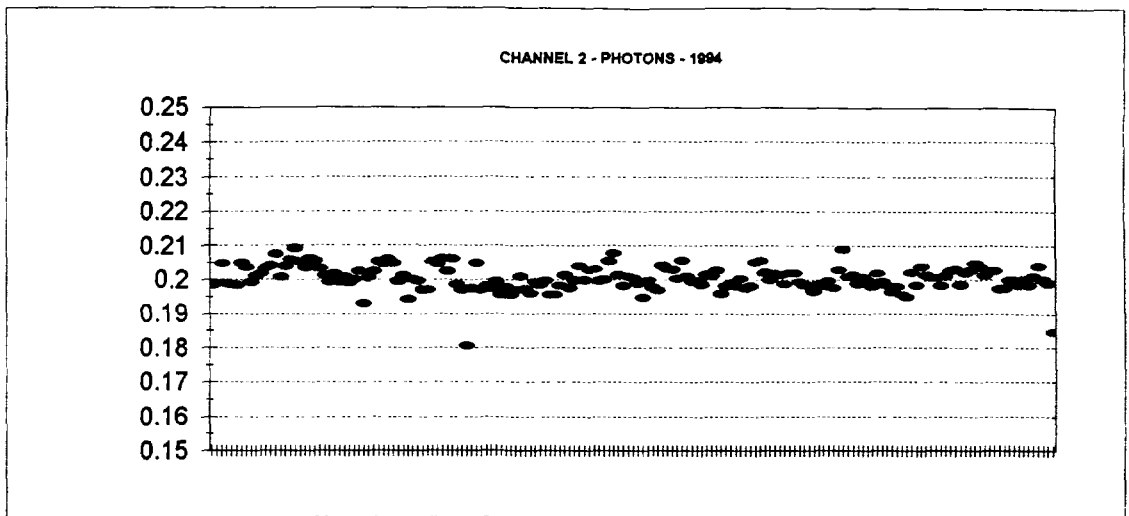


Figure 3. Plots of net daily dose equivalents over the first six months of 1994.

FEBRUARY 1994 2 PHOTONS NEUTRONS CHANNEL 1 NEUTRONS CHANNEL 3

CH 1(n.)	CH 2 (ph.)	Ch 3 (n.)	Ch 4 (n.)	Date	Acc-On	P-on-rw	P-bkg-rw	N1-on-rw	N1-bkg-rw	N3-on-rw	N3-bkg-rw
0.0279	0.1930	0.0272	0.0177	01-Feb-94	X	0.1930		0.0279		0.0272	
0.0265	0.2005	0.0242	0.0172	02-Feb-94	X	0.2005		0.0265		0.0242	
0.0266	0.2024	0.0256	0.0189	03-Feb-94	X	0.2024		0.0266		0.0256	
0.0291	0.2052	0.0264	0.0189	04-Feb-94	X	0.2052		0.0291		0.0264	
0.0263	0.2046	0.0249	0.0157	05-Feb-94							0.0249
0.0266	0.2059	0.0288	0.0184	06-Feb-94			0.2046 0.2059		0.0263 0.0266		0.0288
0.0319	0.2048	0.0302	0.0308	07-Feb-94	X	0.2048		0.0319		0.0302	
0.0278	0.1995	0.0258	0.0181	08-Feb-94	X	0.1995		0.0278		0.0258	
0.0275	0.2012	0.0254	0.0145	09-Feb-94	X	0.2012		0.0275		0.0254	
0.0264	0.1943	0.0253	0.0248	10-Feb-94	X	0.1943		0.0264		0.0253	
0.0273	0.2001	0.0260	0.0260	11-Feb-94	X	0.2001		0.0273		0.0260	
0.0237	0.1997	0.0248	0.0133	12-Feb-94			0.1997		0.0237		0.0248
0.0264	0.1970	0.0248	0.0168	13-Feb-94			0.1970		0.0264		0.0248
0.0292	0.1969	0.0266	0.0181	14-Feb-94	X	0.1969		0.0292		0.0266	
0.0274	0.2053	0.0290	0.0200	15-Feb-94	X	0.2053		0.0274		0.0290	
0.0328	0.2047	0.0306	0.0225	16-Feb-94	X	0.2047		0.0328		0.0306	
0.0309	0.2062	0.0296	0.0175	17-Feb-94	X	0.2062		0.0309		0.0296	
0.0270	0.2025	0.0250	0.0162	18-Feb-94	X	0.2025		0.0270		0.0250	
0.0271	0.2061	0.0280	0.0254	19-Feb-94			0.2061		0.0271		0.0280
0.0240	0.1985	0.0258	0.0177	20-Feb-94			0.1985		0.0240		0.0258
0.0255	0.1970	0.0243	0.0153	21-Feb-94			0.1970		0.0255		0.0243
0.0216	0.1805	0.0212	0.0139	22-Feb-94			0.1805		0.0216		0.0212
0.0247	0.1974	0.0242	0.0143	23-Feb-94			0.1974		0.0247		0.0242
0.0265	0.2048	0.0259	0.0169	24-Feb-94			0.2048		0.0265		0.0259
0.0245	0.1970	0.0242	0.0165	25-Feb-94			0.1970		0.0245		0.0242
0.0261	0.1981	0.0229	0.0272	26-Feb-94			0.1981		0.0261		0.0229
0.0251	0.1974	0.0223	0.0278	27-Feb-94			0.1974		0.0251		0.0223
0.0292	0.1995	0.0252	0.0462	28-Feb-94	X	0.1995		0.0292		0.0252	
					AVE.	0.2011	0.1988	0.0285	0.0253	0.0268	0.0248
					STD.DEV.	0.0040	0.0066	0.0020	0.0015	0.0021	0.0021

SENSITIVITY ANALYSES

CHANNEL 1								ELIMINATE ZEROS WORST CASE			
	N.D.D.	STD.ERR	N.M.D.	STD.ERR	YR-CUM	STD.ER	YR-PR	N.M.D.	YR-CUM	N.M.D.	YR-CUM
NEUTRON	0.0033	0.0007	0.0488	0.0100	0.069	0.014	0.413	0.0488	0.069	0.1680	0.2748
PHOTON	0.0023	0.0021	0.0343	0.0316	0.053	0.038	0.319	0.0343	0.053	0.3844	0.6001
SUM	0.0055		0.0831		0.122		0.732		0.122		0.8749

SENSITIVITY ANALYSES

CHANNEL 3								ELIMINATE ZEROS WORST CASE			
	N.D.D.	STD.ERR	N.M.D.	STD.ERR	YR-CUM	STD.ER	YR-PR	N.M.D.	YR-CUM	N.M.D.	YR-CUM
NEUTRON	0.0020	0.0007	0.0303	0.0106	0.062	0.015	0.413	0.0303	0.062	0.1412	0.2800
PHOTON	0.0023	0.0077	0.0343	0.1160	0.034	0.143	0.319	0.0343	0.053	0.3844	0.6001
SUM	0.0043		0.0646		0.097		0.732		0.116		0.8800

Figure 2. Spreadsheet Design for on-off dose equivalent calculating model. Month of February is shown. Sensitivity Analyses involve substituting zero in place of negative net monthly dose equivalents. Worst case scenario subtracts the lowest monthly off (background) from the highest on period for the net daily dose equivalent (NDD). This NDD is then multiplied by the number of days on.

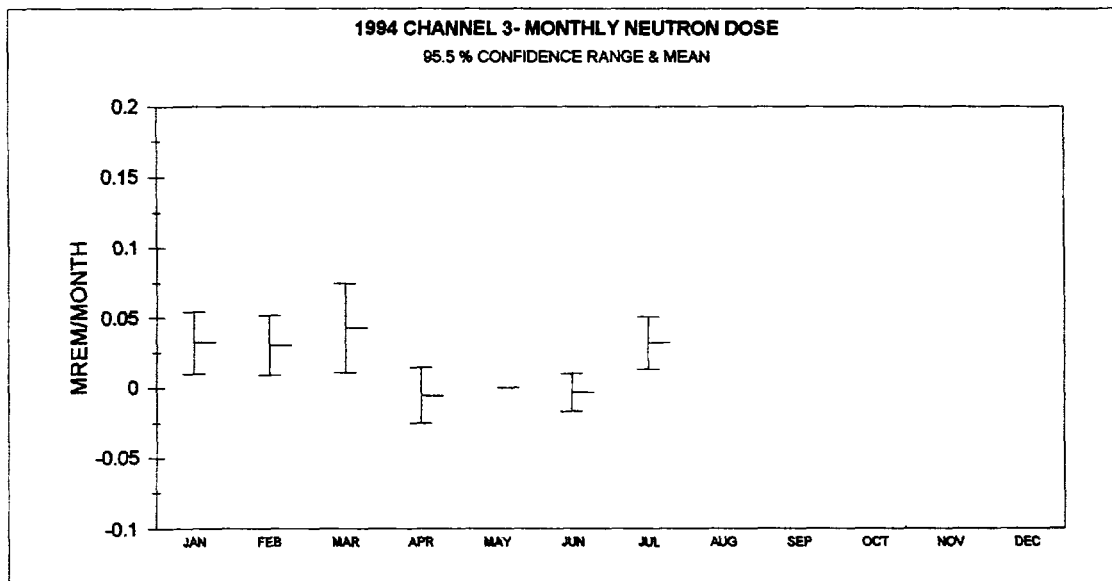
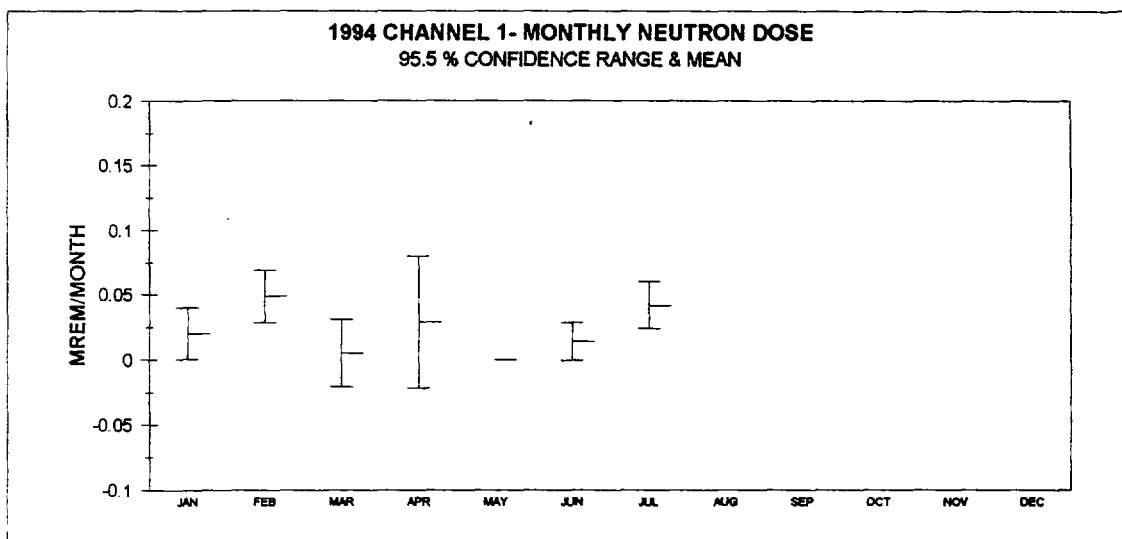
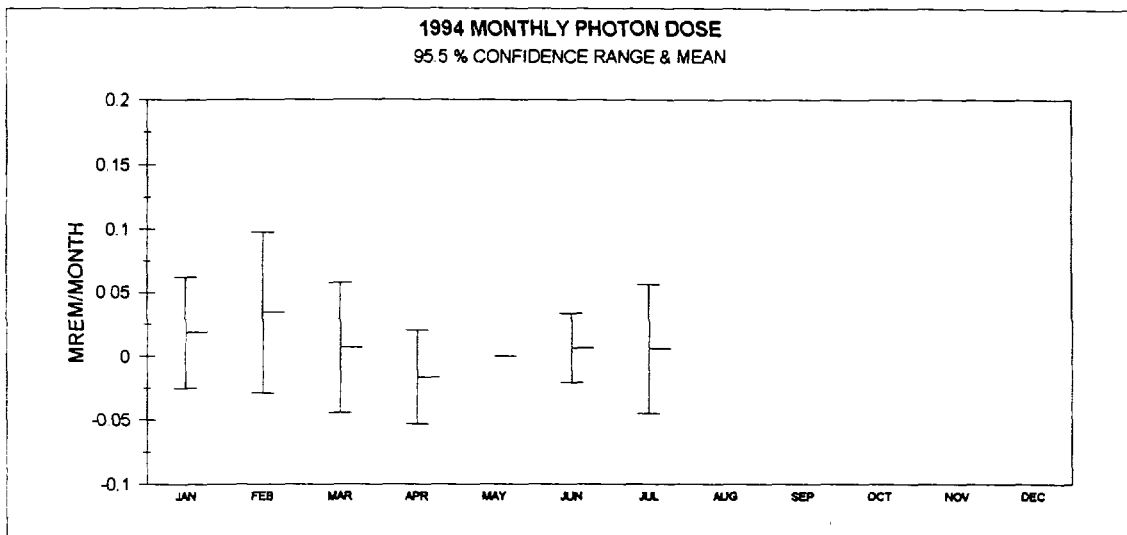


Figure 3. Net monthly mean dose equivalents calculated with standard method. 95.5% confidence intervals (2 standard deviations) are shown.

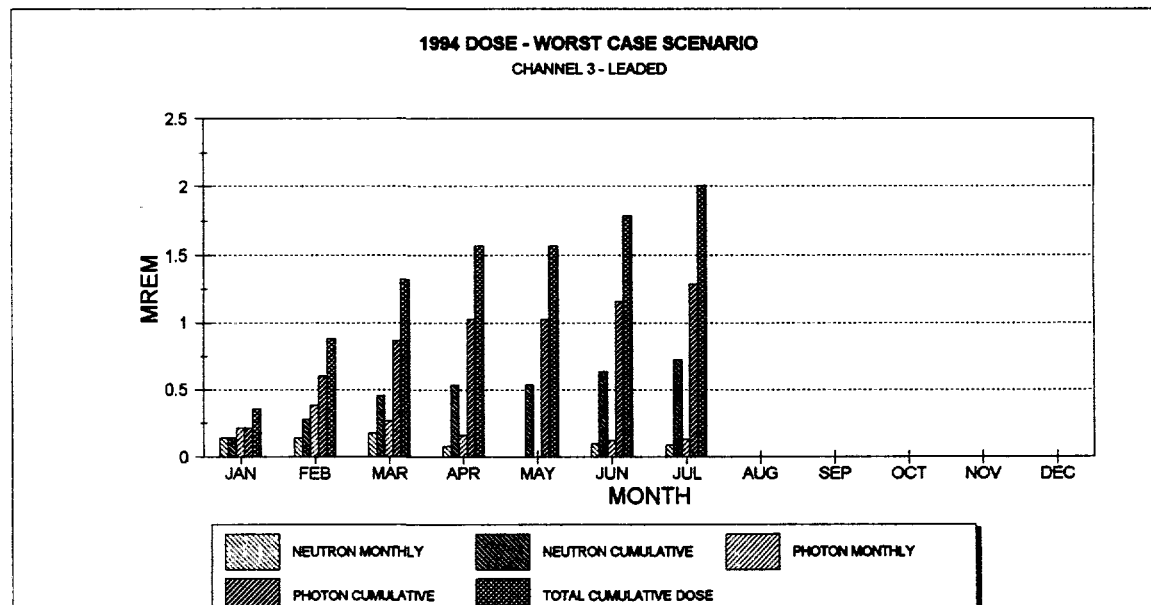
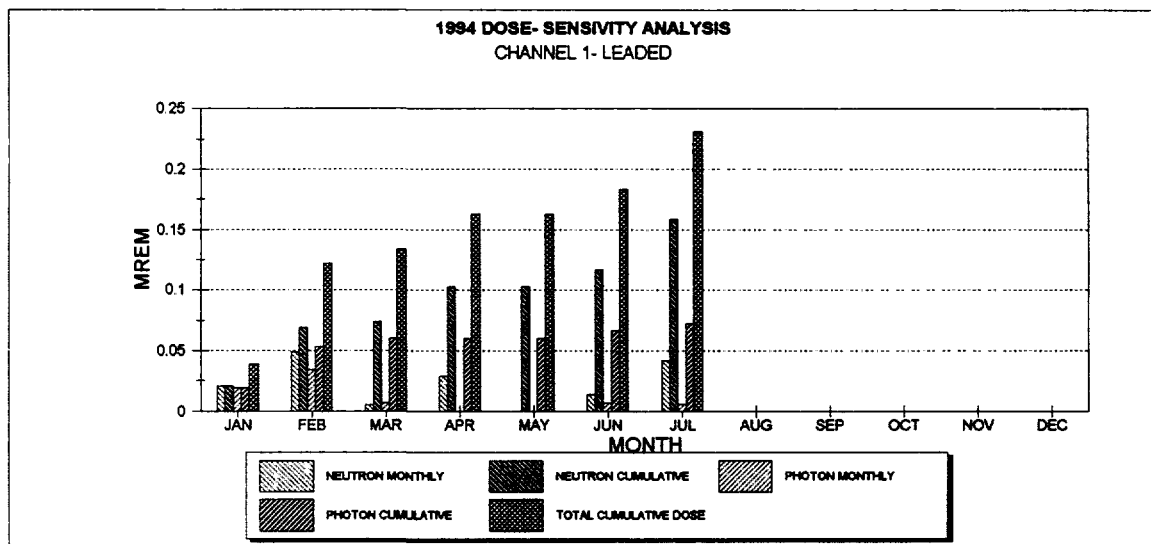
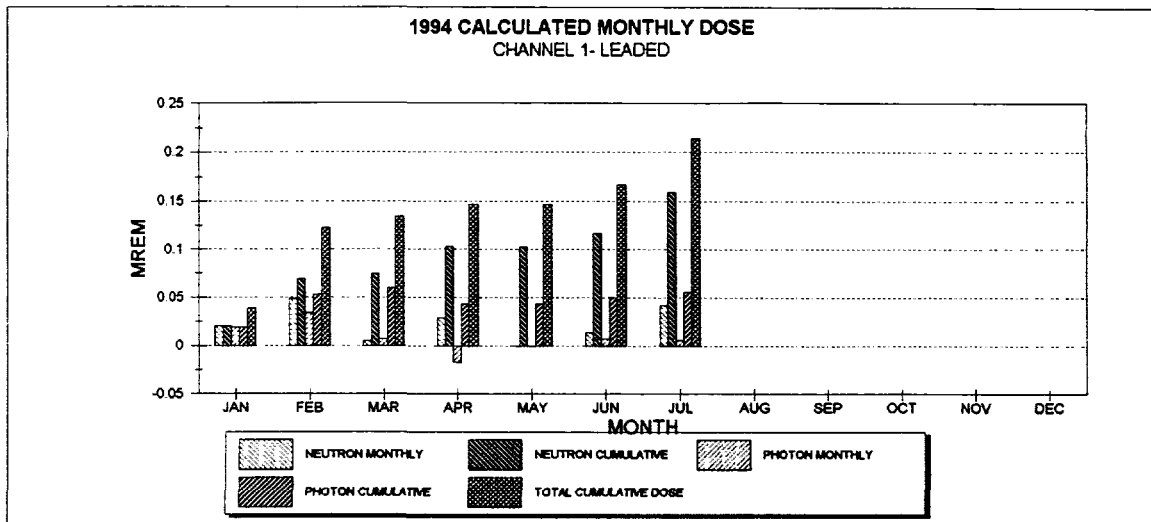


Figure 4. Graphs illustrating monthly total DE through July 1994 at the ALS monitoring shed. The standard calculating method, the sensitivity analysis method (substituting zeros for negative values) and the worst case scenario method are shown.